AD-A126 442 BEHAVIOR OF A HIGH STRENGTH CONCRETE MODEL SUBJECTED TO BIAXIAL COMPRESSION(U) TEXAS UNIV AT AUSTIN DEPT OF CIVIL ENGINEERING J C HERRIN ET AL. DEC 82 1/2

UNCLASSIFIED AFOSR-TR-83-0137 AFOSR-81-0202 F/G 11/2 NL

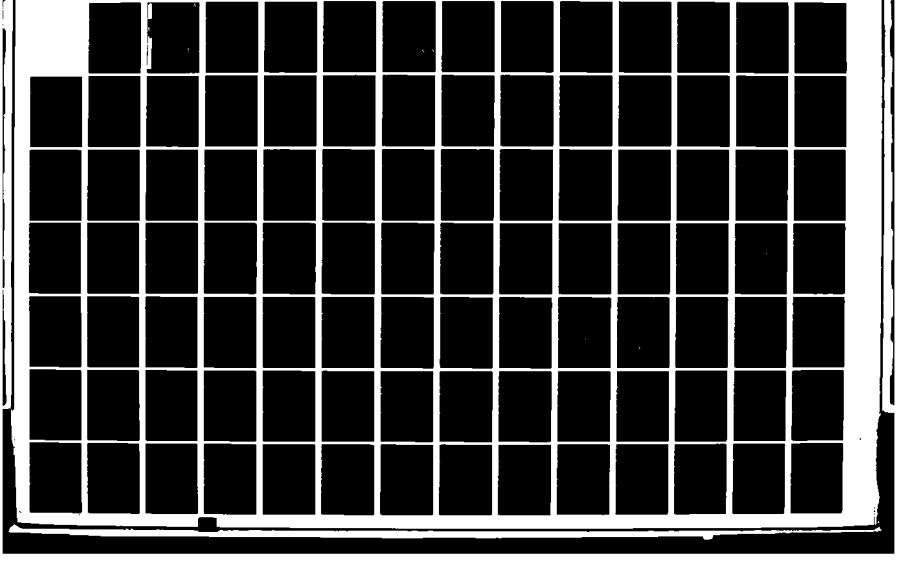

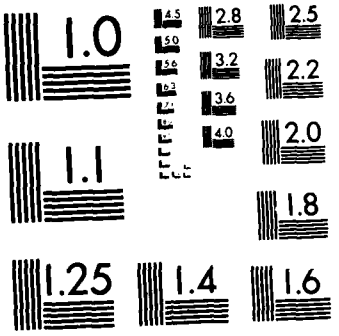

(8)

BEHAVIOR OF A HIGH STRENGTH CONCRETE MODEL SUBJECTED TO BIAXIAL COMPRESSION

BY

JON C. HERRIN

RAMON L. CARRASQUILLO

DAVID W. FOWLER

RESEARCH REPORT AF-1

FOR

UNITED STATES AIR FORCE

OFFICE OF SCIENTIFIC RESEARCH

BOLLING AIR FORCE BASE

CONTRACT NO. AFOSR-81-0202

DEPARTMENT OF CIVIL ENGINEERING

THE UNIVERSITY OF TEXAS AT AUSTIN

DECEMBER 1982

Conditions of Reproduction

SECURITY CLASSIFICATION OF THIS PAGE (When Data Entered)

REPORT DOCUMENTATION PAGE	READ INSTRUCTIONS BEFORE COMPLETING FORM
1. REPORT NUMBER AFOSR-TR- 83-0158 2. GOVT ACCESSION NO. AD-A126442	3. RECIPIENT'S CATALOG NUMBER
4. TITLE (and Subtitle) BEHAVIOR OF A HIGH-STRENGTH CONCRETE MODEL SUBJECTED TO BIAXIAL COMPRESSION	5. TYPE OF REPORT & PERIOD COVERED ANNUAL 15 Jun 81 - 31 Dec 82
	6. PERFORMING ORG. REPORT NUMBER
7. AUTHOR(s) JON C. HERRIN, RAMON L. CARRASQUILLO, AND DAVID W. FOWLER	8. CONTRACT OR GRANT NUMBER(s) AFOSR-81-0202
9. PERFORMING ORGANIZATION NAME AND ADDRESS THE UNIVERSITY OF TEXAS AT AUSTIN DEPARTMENT OF CIVIL ENGINEERING AUSTIN TX 78712	10. PROGRAM ELEMENT, PROJECT, TASK AREA & WORK UNIT NUMBERS 61102F 2307/C2
11. CONTROLLING OFFICE NAME AND ADDRESS AIR FORCE OFFICE OF SCIENTIFIC RESEARCH/NA BOLLING AFB DC 20332	12. REPORT DATE DECEMBER 1982
	13. NUMBER OF PAGES 148
14. MONITORING AGENCY NAME & ADDRESS(if different from Controlling Office)	15. SECURITY CLASS. (of this report) UNCLASSIFIED
	15a. DECLASSIFICATION/DOWNGRADING SCHEDULE

16. DISTRIBUTION STATEMENT (of this Report)

APPROVED FOR PUBLIC RELEASE: DISTRIBUTION UNLIMITED.

17. DISTRIBUTION STATEMENT (of the abstract entered in Block 20, if different from Report)

18. SUPPLEMENTARY NOTES

19. KEY WORDS (Continue on reverse side if necessary and identify by block number)

HIGH-STRENGTH CONCRETE
BIAXIAL LOADING
STRESS-STRAIN BEHAVIOR
FAILURE MODE
DISCONTINUITY
ULTIMATE STRENGTH
PROPORTIONAL LIMIT

20. ABSTRACT (Continue on reverse side if necessary and identify by block number)

The main purpose of the research project reported herein was to determine the stress-strain behavior, ultimate strength, and failure mechanism of high-strength concrete subjected to biaxial compression. Model concrete plate specimens, composed of nine aggregate discs embedded in a mortar matrix, were used. Three different coarse aggregates together with three different mortar mixes having different strength and elastic properties were used in order to determine the effects of material properties on the

DD FORM 1 JAN 73 1473 EDITION OF 1 NOV 65 IS OBSOLETE

SECURITY CLASSIFICATION OF THIS PAGE (When Data Entered)

behavior of high-strength concrete subjected to biaxial compression. The plate specimens were tested using four biaxial stress ratios: 0 (uniaxial), 0.2, 0.5, and 1.0. Deformations in both the major (ε_1) and minor (ε_2) principal directions were measured using Direct Current Differential Transducers. Stress-strain characteristics, discontinuity, ultimate strength and failure modes in biaxial compression as a function of materials properties are discussed.

BEHAVIOR OF A HIGH STRENGTH CONCRETE MODEL SUBJECTED TO BIAXIAL COMPRESSION

BY

JON C. HERRIN

RAMON L. CARRASQUILLO

DAVID W. FOWLER

RESEARCH REPORT AF-1

FOR

UNITED STATES AIR FORCE

OFFICE OF SCIENTIFIC RESEARCH

BOLLING AIR FORCE BASE

CONTRACT NO. AFOSR-81-0202

DEPARTMENT OF CIVIL ENGINEERING

THE UNIVERSITY OF TEXAS AT AUSTIN

DECEMBER 1982

ABSTRACT

The main purpose of the research project reported herein was to determine the stress-strain behavior, ultimate strength, and failure mechanism of high-strength concrete subjected to biaxial compression. Model concrete plate specimens, composed of nine aggregate discs embedded in a mortar matrix, were used. Three different coarse aggregates together with three different mortar mixes having different strength and elastic properties were used in order to determine the effects of material properties on the behavior of high-strength concrete subjected to biaxial compression. The plate specimens were 1.0. Deformations in both the major (ε_1) and minor (ε_2) principal directions were measured using Direct Current Differential Transducers. Stress-strain characteristics, discontinuity, ultimate strength and failure modes in biaxial compression as a function of materials properties are discussed.

ACKNOWLEDGEMENTS

The author wishes to express thanks to his supervising professor, Dr. Ramon Carrasquillo, for his suggestions and encouragement throughout the project. The author is also grateful to Dr. David Fowler for his assistance during the experimental phase, and for his suggestions during the writing of this thesis.

Thanks is due to Mr. David Whitney and Mr. Tom Phillips for their assistance during the experimental work. Special thanks goes to Mr. Robert Chen and Mr. Paullo Castro. Their hard work and dedication to the project is certainly appreciated. Appreciation is expressed to Ms. Charline Grant for the careful typing of the manuscript and to Ms. Jean Gehrke for her assistance with the preparation of the figures.

The present research is part of a larger project on the biaxial properties of high-strength concrete at the University of Texas at Austin sponsored by the United States Air Force Office of Scientific Research, Grant No. 82-NA-136.

TABLE OF CONTENTS

LIST OF TABLES

LIST OF FIGURES

CHAPTER 1
INTRODUCTION

1.1 BACKGROUND

In recent years, new construction materials of vastly improved properties have been developed by material scientists and engineers. In the field of concrete, efforts have been directed into improving the compressive strength of the material.

High strength concrete has been defined as that having a compressive strength in the range of 6000 to 12,000 psi.* Such material is routinely being used in precast plants. It is also being used for certain cast-in-place structures using ready-mixed or site-mixed concrete. Indeed, production of concrete in this strength range, using conventional materials with careful quality control, is technically and economically feasible.

There are distinct advantages in the use of such material. The use of high-strength concrete in columns carrying large axial load will result in smaller, cost saving columns which will allow for increased floor space. The use of prestressing in conjunction with high-strength concrete will result in more efficient flexural members. The useful span of existing types of construction, such as flat plates or standard T- and I-section beams, can be extended through the use of high-strength concrete combined with prestressing.

Applications of high-strength concrete are becoming increasingly common. In the Chicago area, high-strength concrete has been used in many high-rise buildings. In 1972, 9000 psi concrete was used in twenty of the fifty stories of the Mid-Continental Plaza Building.

---

*ACI Committee 363 on High-Strength Concrete, minutes of fall meeting in San Juan, Puerto Rico, on September 22, 1980.

Since then, high-strength concrete has been specified for other Chicago area buildings, including the 200 W. Monroe Building, the Frontier Tower, Water Tower Place Building, and the Marriot Chicago Building (33).

Other applications include the Willows Bridge in Toronto, where strengths of the order of 10,000 psi were obtained, the O'Hare Airport Terminal in Chicago, where 8,000 psi concrete was used in prestressed roof girders, and prestressed concrete containment vessels for nuclear reactors in England and France, which were constructed using 9,000 psi concrete.

Another potential use for high-strength concrete is in underground construction, especially large-span shells. The use of high-strength concrete will result in a thinner, more flexible, stronger underground structure with less cracking.

These types of structures, large shells, containment vessels, and tunnel linings, are subjected to biaxial compression. A knowledge of the behavior of high-strength concrete subjected to biaxial compression is needed to design these structures more efficiently, safely, and economically.

The use of high-strength concrete will increase in the future, as better information about its properties and behavior becomes available due to both technical and economical advantages.

1.2 DEFINITIONS

The following terms are used in this report:

σ_1 = major principal stress

σ_2 = minor principal stress ($\sigma_2 \leq \sigma_1$)

ε_1 = major principal strain (compression = +; tension = -)

ε_2 = minor principal strain (compression = +; tension = -)

f'o = uniaxial strength of model plate specimen

fu = ultimate strength (σ_1) of model specimen in biaxial loading

stress ratio = ratio of minor principal stress to major principal stress ($0 \leq \sigma_2/\sigma_1 \leq 1.0$)

1.3 SCOPE OF RESEARCH

The present research was initiated to determine the stress-strain behavior, strength, and failure mechanism of high-strength concrete subjected to biaxial compression. Model concrete plate specimens, composed of nine aggregate discs embedded in a mortar matrix, were used. Three different coarse aggregates together with three different mortar mixes having different strength and elastic properties were used in order to determine the effects of material properties on the behavior of high-strength concrete subjected to biaxial compression. The plate specimens were tested using four stress ratios: 0 (uniaxial), 0.2, 0.5, and 1.0. Deformations in both the major (ε_1) and minor (ε_2) directions were measured using Direct Current Differential Transducers.

Chapter Two reviews previous studies into the properties of concrete subjected to biaxial compression. Chapter Three includes information on material properties. The experimental program undertaken to determine the mix proportions for the biaxial specimens is summarized.

Chapter Four presents the specimen fabrication procedure, a description of the test apparatus, and the testing procedure. Chapter Five presents the experimental test results. Chapter Six presents an analysis of the test results. Stress-strain characteristics, discontinuity, strength, and failure modes are discussed. Chapter Seven reveals the conclusions of the study and suggests recommendations for future research.

CHAPTER 2

REVIEW OF PREVIOUS BIAXIAL STUDIES

Investigations into the strength of concrete subjected to biaxial compression have been conducted since the beginning of the twentieth century. The different studies can be grouped by type of specimen used: solid cylinders, hollow cylinders, and rectangular specimens (cubes or plates).

2.1 SOLID CYLINDRICAL SPECIMENS

Biaxial compressive stresses can be generated by subjecting a solid cylinder to hydrostatic pressure in the radial directions. Karman (1) and Boker (2) were the first investigators to use this test method. They used 1.57-in. x 3.94-in. (4-cm x 10-cm) marble cylinders.

Several investigators (3-12) have used this method since Karman and Boker's tests in 1911. Richart, et al (3), performed tests on 4-in. x 22-in. (10.2-cm x 55.9-cm) concrete cylinders in 1928 and concluded that the strength of concrete in biaxial compression was at least as great as in uniaxial compression, and, in most cases, it was greater.

There are several disadvantages in testing solid cylindrical specimens. Hydraulic fluid penetrating into the pores of the specimen will induce local tensile stresses at the surface. Therefore, the specimens must be covered with an impermeable membrane. It has been questioned by previous investigators whether this was always done. Also, only one stress ratio, $\sigma_2/\sigma_1 = 1.0$, can be achieved using solid cylindrical specimens. Thus, a complete study of the biaxial strength of concrete is not possible using this type of specimen.

Finally, the specimen is always contained in a pressure vessel during testing, making observation impossible.

2.2 HOLLOW CYLINDRICAL SPECIMENS

Hollow cylindrical specimens have a distinct advantage over solid cylindrical specimens, in that hollow specimens can be used for a general study of the strength of concrete subjected to biaxial stresses. A general state of stress can be generated in hollow cylinders by applying either compressive or tensile axial force while at the same time applying external or internal hydrostatic pressure. The stress ratio, σ_2/σ_1, can vary from -1 to +1, thus allowing for a comprehensive study of biaxial properties.

Hollow cylinders have been used extensively for investigation into the behavior of concrete subjected to biaxial compression-tension. Bellamy (13) and Campbell-Allen (14) used hollow cylinders to investigate biaxial compression. The specimens were 6 in. (15.2 cm) in diameter and 12 in. (30.5 cm) long with a 2.95 in. (7.49 cm) diameter concentric hole. Thus, the wall thickness was just greater than 1.5 in. (3.8 cm). Axial compression was applied using a conventional compression testing machine. Light hydraulic oil was used to apply the external hydrostatic pressure. The specimen was encased in a neoprene sheath to prevent oil from penetrating into the pores of the specimen.

Failure initiated at the inside face of the cylinders where mortar was observed spalling off. Thus, failure was caused by biaxial compression and not triaxial compression, which would be the state of stress at the outside face of the cylinder. The strength of hollow cylinders subjected to biaxial compression were found to be up to 2.69 times the uniaxial compressive strength.

Rosenthal and Glucklich (15) performed biaxial compression tests on hollow cylinders with 12 in. (30.5 cm) diameter, 14 in. (35.6 cm) length, and 1.1 in. (2.8 cm) wall thickness. Axial compression was applied using a universal testing machine. External pressure was applied using hydraulic fluid enclosed in a tubular rubber bag.

Biaxial strengths up to approximately 2.25 times the uniaxial strengths were obtained.

However, a basic problem exists in testing hollow concrete cylinders subjected to a biaxial state of stress. The hoop stress caused by the externally applied pressure has been calculated using conventional elastic equations. Bellamy (13) calculated hoop stress at the inside face using the traditional equation derived for a thick-walled cylinder of an elastic material. Rosenthal and Glucklich (15) assumed the specimens behaved as thin-walled cylinders. Thus, a uniform stress distribution was assumed across the cylinder walls. It is indeed questionable whether these elastic theories can be applied to a heterogeneous material, such as concrete, up to failure.

2.3 RECTANGULAR SPECIMENS

Rectangular specimens, either cubes or plates, seem to be better than solid or hollow cylinders for biaxial testing of concrete or mortar. Any principal stress ratic can be easily achieved using hydraulic rams. The use of rectangular specimens facilitates strain measurements and visual inspection of crack propogation during testing.

However, it is widely recognized that the use of solid steel bearing platens to apply the force to the specimen will cause confinement due to friction. This confinement prevents the existence of a true biaxial state of stress.

Foppl (16) investigated the effect of solid steel bearing platens in 1899, using 2.75-in. (7-cm) mortar cubes. The results showed that frictional confinement by solid platens increased the apparent material strength. Various lubricants were used in order to reduce the confinement. The use of lubricants decreased the apparent strength. Soft lubricants, however, were found to induce lateral tensile stresses, producing an effect just the opposite of the confinement caused by solid platens, and a biaxial strength less than the uniaxial strength was observed.

Mills and Zimmerman (17) used a bearing pad composed of axle grease between two 0.004-in. (0.010-cm) polyethylene sheets to reduce friction between the loading platens and the specimens. Tests on 2.25-in. (5.72-cm) concrete cubes revealed biaxial strengths ranging from 1.44 to 1.88 times the uniaxial strength at a stress ratio of approximately $\sigma_2/\sigma_1 = 0.5$. It was concluded that failure occurred by expansion in the direction of the minimum principle stress.

Weigler and Becker (18) used thin plates, 3.9-in. x 3.9-in. x 1.0-in. (10-cm x 10-cm x 2.5-cm), in order to reduce the effect of frictional confinement. The results showed a 30 to 45 percent strength increase for a biaxial stress ratio between 0.42 and 1.0.

Robinson (19) conducted biaxial compression tests on 10-in. x 10-in. x 4-in. (25-cm x 25-cm x 10-cm) specimens. A special concrete curing compound was used to reduce the confinement. It was concluded that the strength is increased due to the addition of a confining stress (σ_2), and that onset of major microcracking is delayed by the presence of a minor principal stress, σ_2.

Not all investigators have tried to reduce frictional confining stresses. Iyengar (20) used solid steel platens to test 4-in. (10-cm) and 6-in. (15-cm) concrete cubes in biaxial compression. Strengths over 350 percent of the uniaxial strength were found.

The results previously summarized reveal a large scatter in data from biaxial compression tests. These discrepancies can be attributed to the lack of a true biaxial state of stress. Unwanted stresses due to the frictional confinement of solid steel loading platens have been reduced by various lubricating methods. However, these confining stresses probably have not been eliminated.

The use of solid steel platens results in two basic problems. First, due to friction and the differences in lateral displacement of the concrete specimen and the steel platen, lateral stresses are induced near the edge of the specimen. Thus, a triaxial state of stress results near the edge. Second, part of the load in one direction may be transferred by friction to the loading platens in the

other direction. An artificially higher strength will result from this.

Hilsdorf (21) conducted investigations dealing with the problem of confining stresses. After determining that solid steel platens do indeed create extremely high confining stresses, Hilsdorf developed a special loading platen designed to induce no confining stresses. These loading platens consist of closely spaced steel bars. Each bar is essentially a column; each one is designed to transmit the required force without buckling. However, the bars, or brushes, are flexible enough to follow the concrete specimen as it expands under load. Thus, no lateral stresses are induced.

Kupfer, et al (22), used Hilsdorf's brush bearing platens to test in biaxial compression 7.9-in. x 7.9-in. x 2-in. (20-cm x 20-cm x 5-cm) concrete plates. The platens consisted of individual steel filaments with a 0.2-in. x 0.12-in. (5-mm x 3-mm) cross-section. The length of the filaments varied from 3.94 in. (100 mm) to 5.51 in. (140 mm), depending on the expected maximum stress in the specimen. The length is calculated based upon Euler's theory of buckling. The filaments were spaced 0.2 mm apart.

The effectiveness of the brush bearing platens was verified by Kupfer. Concrete specimens with various aspect ratios, including cubes and 7.9-in. x 7.9-in. x 2-in. (20-cm x 20-cm x 5-cm) plates, were tested in uniaxial compression, using both solid platens and brush platens. The strengths obtained using brush platens were independent of the shape of the specimen. "This appears to provide sufficient proof that end restraint of concrete specimens can be eliminated by brush bearing platens"(22).

Kupfer, et al (22), found that the strength of concrete subjected to biaxial compression is higher than the uniaxial strength. However, the strength increase was not as much as previously reported when using solid platens or cylindrical specimens. The highest strength increase was 27 percent at $\sigma_2/\sigma_1 = 0.5$. For equal compression in both directions ($\sigma_2/\sigma_1 = 1.0$), the strength increase was

sixteen percent. To further verify the effect of the brush bearing platens, additional biaxial tests were made using solid platens. The apparent strength increase at $\sigma_2/\sigma_1 = 0.5$ was 48 percent. At $\sigma_2/\sigma_1 = 1.0$, the apparent strength was 45 percent higher than the uniaxial strength. These apparently higher strengths were due only to the confinement produced by the solid platens.

Buyukozturk, et al (23), performed biaxial compression tests as part of the study of internal microcracking of concrete conducted at Cornell University. Brush bearing platens similar to those used by Kupfer, et al (22), were used. The specimens were proportioned according to the following considerations:

1) the wish to obtain as nearly as possible a state of plane stress
2) the need to produce compression without the specimen buckling
3) the wish to obtain a concrete model which could be studied analytically

The resulting specimens were 5-in. x 5-in. x 1/2-in. (12.7-cm x 12.7-cm x 12.7-cm) thick plates consisting of nine aggregate discs embedded in a mortar matrix.

Buyukozturk (23) tested the models at four different stress ratios (σ_2/σ_1): zero (uniaxial load), 0.2, 0.5, and 1.0. Gross deformations over the length of the specimens were measured, as well as local deformations at critical locations, such as aggregate-mortar interfaces. The specimens were inspected during testing using x-ray techniques to gather information on microcracking.

The following conclusions were made as a result of these tests:

1) Significantly higher strength is attainable for a given material in biaxial loading than in uniaxial loading. The strength increase is dependent on the ratio of the principal stresses, and appears to be a maximum at a stress ratio of about 0.5, diminishing somewhat as the ratio is increased to unity. The strength increase was 32 percent

at a stress ratio of 0.5 and decreased to a 24 percent increase at a stress ratio of unity (23).

2) The stiffness in that first principal direction is significantly increased by the introduction of principal stress in the perpendicular direction; i.e., compressive deformation in the first direction is substantially reduced by compressive stress in the second direction (23).
3) In the uniaxial case, failure occurs by progressive microcracking, starting at the aggregate-mortar interfaces and later extending as tensile cracks through the mortar. In the biaxial case, cracks perpendicular to the plane of the specimen were neither observed by experiment nor predicted by analysis (23).
4) In the uniaxial case, ultimate failure occurs by splitting in planes perpendicular to the face of the specimen and parallel to the load. In the biaxial case, ultimate failure occurs by splitting along a plane parallel to the face of the specimen. The results indicate the possibility that fracture occurs whenever limiting tensile deformations perpendicular to planes of loading have been exceeded (23).

The studies at Cornell were continued by Liu, et al (24). Real concrete specimens with the same dimensions as the models were tested in biaxial compression. The same brush bearing platens used by Buyukozturk (23) were used by Liu.

Microcracking information was again gathered using x-ray. It was found that bond cracks exist due to shrinkage and bleeding before load is applied. These bond cracks increase in length and width at a load of 65 percent of ultimate. At about 85 percent of ultimate, mortar cracks are initiated, and finally combine with the bond cracks to cause failure.

The tests on real concrete specimens led to the following conclusions:

1) Test results show that the strength of concrete under biaxial compression is higher than under uniaxial loading. The strength increase under biaxial compression is dependent on the principal stress ratio (24).
2) In biaxial loading, strains are significantly less than predicted by theoretical elastic analysis, presumably because microcracks are prevented from occurring (24).
3) Prediction of initiation and propogation of microcracks by theoretical analysis of Buyukozturk, based on a simple model, was found to apply also to both complex models and real concrete (24).
4) The principal strain ratio for uniaxial compression remains practically constant up to sixty percent of the ultimate load. At higher stress levels, the principal strain ratio increases owing to the cracking within the specimen. In the biaxial compression case, the principal strain ratios remain practically constant throughout the range of loading (24).
5) In uniaxial loading, for the flat specimens tested, ultimate failure occurs by splitting in the plane parallel to the load and perpendicular to the face of the specimen. In the biaxial compression case, ultimate failure occurs by splitting along planes parallel to the load and parallel to the face of the specimen. The modes of failure suggest that tensile deformation is vital in the failure mechanism of concrete (24).

Further studies at Cornell were conducted by Tasuji (25). Real concrete specimens, such as those used by Lui (24), were tested in biaxial compression, biaxial tension, and compression-tension. The same loading platens were again used.

Tasuji (25) reached the following conclusions:

1) The ultimate strength of concrete subjected to biaxial compression is greater than the uniaxial strength, and is

dependent upon the principle stress ratio. The maximum strength increase was found to be 22 percent at σ_2/σ_1 = 0.5.

2) Under biaxial compression, failure occurred by cracking along a plane parallel to the unloaded surface of the specimen. Under uniaxial compression, failure took place by the formation of cracks parallel to the applied load and perpendicular to the face of the specimen.

3) The discontinuity point, which represents the onset of major microcracking in concrete, was found to be at about 76 percent of the ultimate load in uniaxial and biaxial compression tests.

Biaxial compression tests have been made using brush bearing platens on lightweight aggregate concrete (26, 27). In general, the strength increase due to biaxial loading is in good agreement with the results reported by Kupfer, et al (22), and the researchers at Cornell (23, 24, 25) for normal weight concrete.

Recent biaxial compression tests have been conducted on polymer-impregnated concrete (PIC) at the University of Texas at Austin by Khana (28) and Park (29). Model plate specimens similar to those previously used by Buyukozturk, et al (23), were used as well as real PIC plate specimens. Brush bearing platens were used to transmit the load to the specimens. The shape of the strength envelope was found to be similar to that for plain concrete. Maximum strength increases ranged from thirty percent to 52 percent, depending on the type of PIC tested.

2.4 SUMMARY OF PREVIOUS STUDIES

Studies of the behavior of concrete subjected to biaxial compression have been conducted since the beginning of the twentieth century. Several types of specimens and loading methods have been used. The experimental test results have varied greatly. For instance, strength values under equal biaxial compression (σ_2/σ_1 = 1.0)

vary from 110 to 350 percent of the uniaxial strength. Such differences can be attributed to an unintended lack of a true biaxial state of stress.

A true biaxial state of stress appears to be achievable using plate specimens and brush-type loading platens. Also, deformations can be easily measured using plate specimens. At Cornell University, tests on concrete plate specimens using brush-type platens revealed that the strength of concrete in biaxial compression is about 130 percent of the uniaxial strength at a stress ratio of 0.5 ($\sigma_2/\sigma_1 = 0.5$).

CHAPTER 3

MATERIAL PROPERTIES

3.1 INTRODUCTION

In order to develop a general knowledge of the properties and behavior of high strength concrete subjected to biaxial compression, it is necessary to test specimens containing all possible combinations of mortar and aggregate strength and elastic properties. A rather extensive experimental program was conducted in order to determine the properties of mortar and aggregate which could be used in the production of high-strength concrete. The composition of the biaxial specimens was determined as a result of this preliminary experimental program.

3.2 MORTAR TESTS

A series of tests were made to determine the proper selection and optimum proportions of materials for producing mortars with the desired strength and elastic properties. Water-cement ratio and fine aggregate-cement ratio were varied to determine their effects on the desired properties. Several different types of fine aggregate and cement were used. All materials used are commercially available in Texas.

3.2.1 Sand

Three types of sand were used during the mortar tests: Local sand, cemix sand, and ferro boat sand.

1) Local concrete sand - this sand is widely used as a local concrete sand. It is an alluvial deposit obtained locally from the Colorado River.

2) Cemix sand - a bagged, all-purpose sand, also obtained locally from the Colorado River.

3) Ferro boat sand - an alluvial deposit obtained from Maryland.

Standard ASTM tests were performed on each type of sand to determine gradation, fineness modulus, absorption, and specific gravity. Standard ASTM sieve analysis results are given in Table 3.1. Other properties are shown in Table 3.2.

3.2.2 Cement

Two brands of commercially available ASTM Type I portland cement produced in Texas were used.

3.2.3 Mix Proportions

Water-cement (weight) ratios of 0.30, 0.35, and 0.40 were used. Sand-cement (weight) ratios ranging from zero (cement-water paste) to 3.0 were used with each type of sand and cement combination.

3.2.4 Mixing, Casting, and Curing

Materials were weighed using a balance having an accuracy of $\pm$0.5 g. Mixing was done by hand in a small metal pan using a steel trowel. The sand and cement were thoroughly mixed dry prior to adding the water.

The fresh mortar was cast into 3-in. x 6-in. cylinder molds. Due to the low water content needed for producing high strength mortar, the cylinders were vibrated using a vibrating table to ensure good compaction.

The cylinders were covered with wet burlap for one day. The molds were then removed, and the cylinders were cured at 100 percent relative humidity and 73 $\pm$ 3^{o}F until testing at 28 days.

TABLE 3.1 STANDARD SIEVE ANALYSIS AND FINENESS MODULUS FOR SANDS[a]

Sieve No.	Percent Passing		
	Local Sand	Cemix Sand	Ferro Boat Sand
4	99	100	100
8	94	100	100
16	86	79	92
30	65	65	79
50	31	39	47
100	5	5	6
200	1	0	0
Fineness Modulus	3.19	3.14	2.75

[a]based on ASTM C136-80

TABLE 3.2 SPECIFIC GRAVITY[a] AND ABSORPTION[a] FOR SANDS

Sand	Specific Gravity at SSD (ASTM C127-80)	Absorption (ASTM C127-80), percent
Local	2.61	0.6
Cemix	2.63	0.7
Ferry boat	2.62	1.2

[a]based on ASTM C127-80

3.2.5 Testing Procedure

The cylinders were tested at 28 days. The specimens were capped with a sulphur-based capping compound the day of the test. A standard Baldwin 400 kip (1780 kN) compression testing machine was used to test the cylinders to failure. A loading rate of sixty psi per second (414 kN/m^2 per second) was used.

Deformations were measured using a compressometer equipped with two dial gauges capable of reading deflections to $\pm$ 1/10,000 in. Readings were taken at each 4000 lb (17.8 kN) load increment, up to 32,000 lb (142 kN). The 32,000 lb (142 kN) load corresponds to about fifty percent of the ultimate load of the highest strength mortar.

3.2.6 Test Results

Compressive strengths reported herein represent the average of three cylinders tested for each mix. Strengths ranging from 3300 to 14,000 psi (22.8 to 96.5 MN/m^2) were obtained as shown in Figs. 3.1 through 3.5.

Modulus of elasticity values, calculated using the secant method to forty percent of ultimate, varied from 3×10^6 to 6×10^6 psi (21×10^3 to 41×10^3 MN/m^2). Average values for all mortars tested are shown graphically in Figs. 3.6 through 3.8. Complete test results are tabulated in Appendix A (Tables A-1 through A-5) for all mortar specimens tested.

Based on the test data, the following observations were made:

1) Regardless of the mix proportions, local sand and brand A cement consistently produced the highest strength.
2) The optimum sand-cement ratio for highest strength decreased as the water-cement ratio decreased for all sands and cements tested.
3) Compressive strength increased with decreasing water-cement ratio for all sands and cements tested. The highest strength obtained was 13,990 psi with a water-cement ratio of 0.30 and a sand-cement ratio of 0.2.

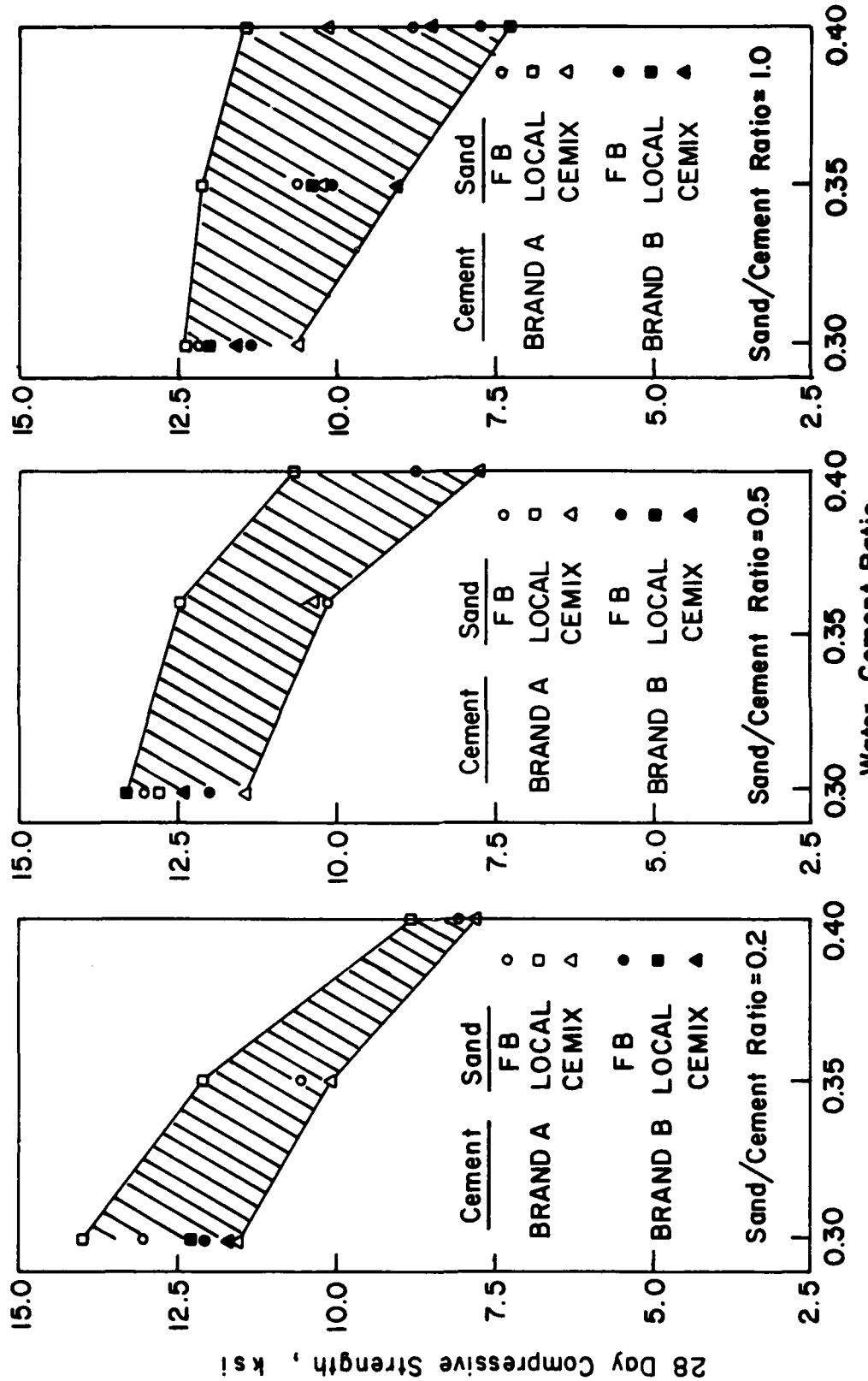

Figure 3.1 Effect of Water-Cement Ratio on Compressive Strength of Mortar for Sand/Cement Ratios of 0.2, 0.5, and 1.0

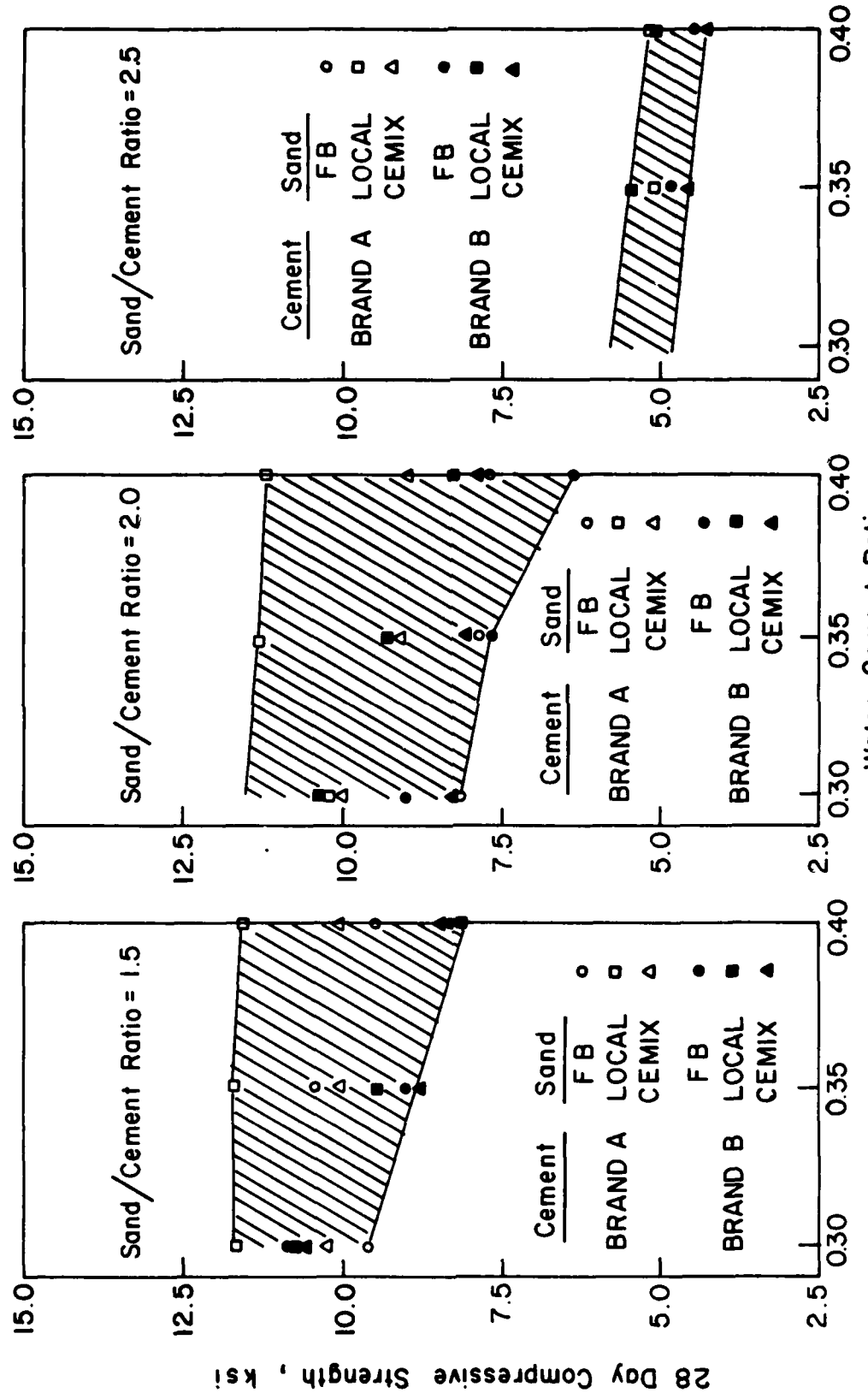

Figure 3.2 Effect of Water-Cement Ratio on Compressive Strength of Mortar for Sand/Cement Ratios of 1.5, 2.0, and 2.5

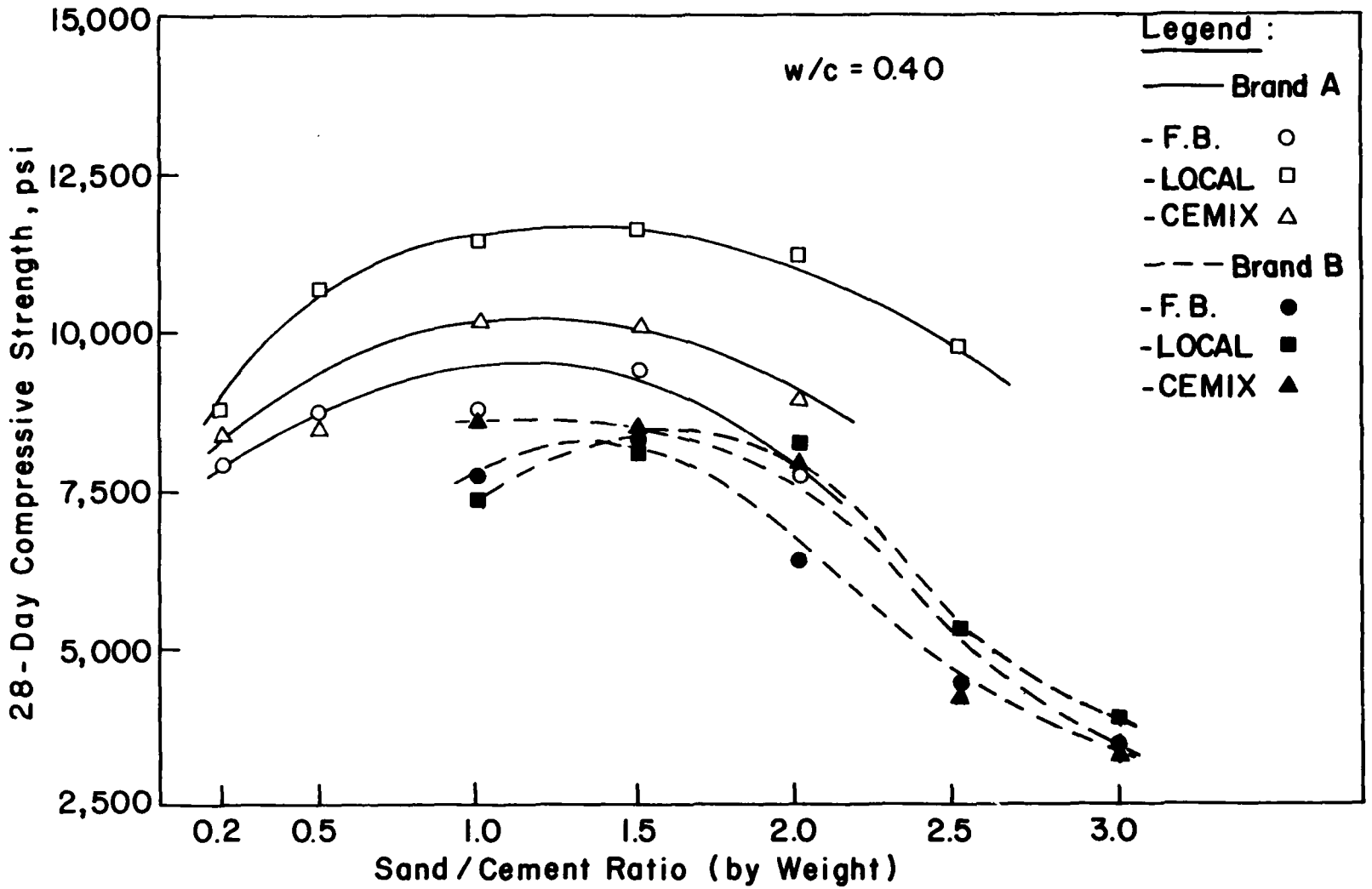

Figure 3.3 Effect of Sand-Cement Ratio on Compressive Strength of Mortar for Water/Cement Ratio of 0.40

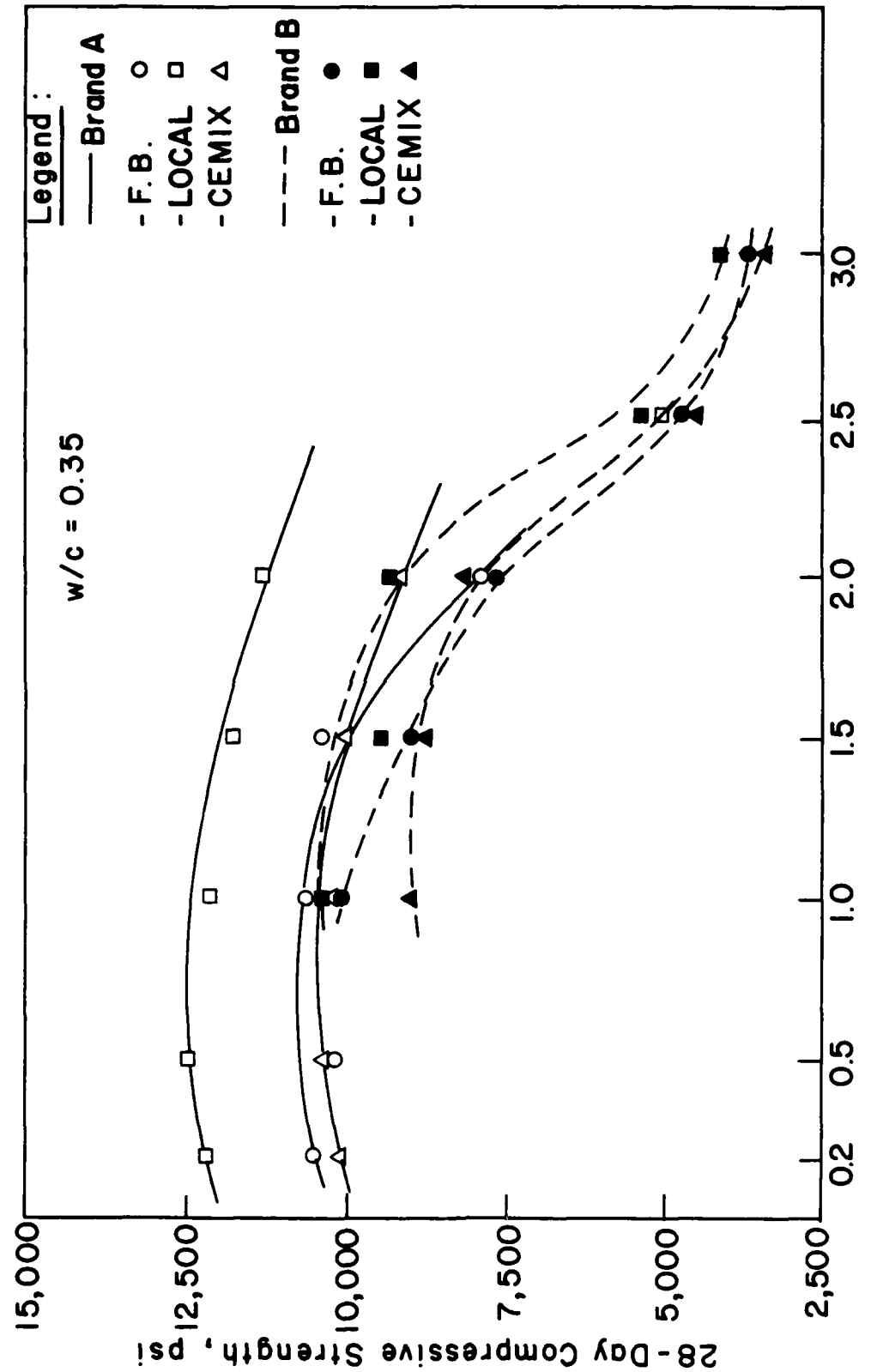

Figure 3.4 Effect of Sand-Cement Ratio on Compressive Strength of Mortar for Water/Cement Ratio of 0.35

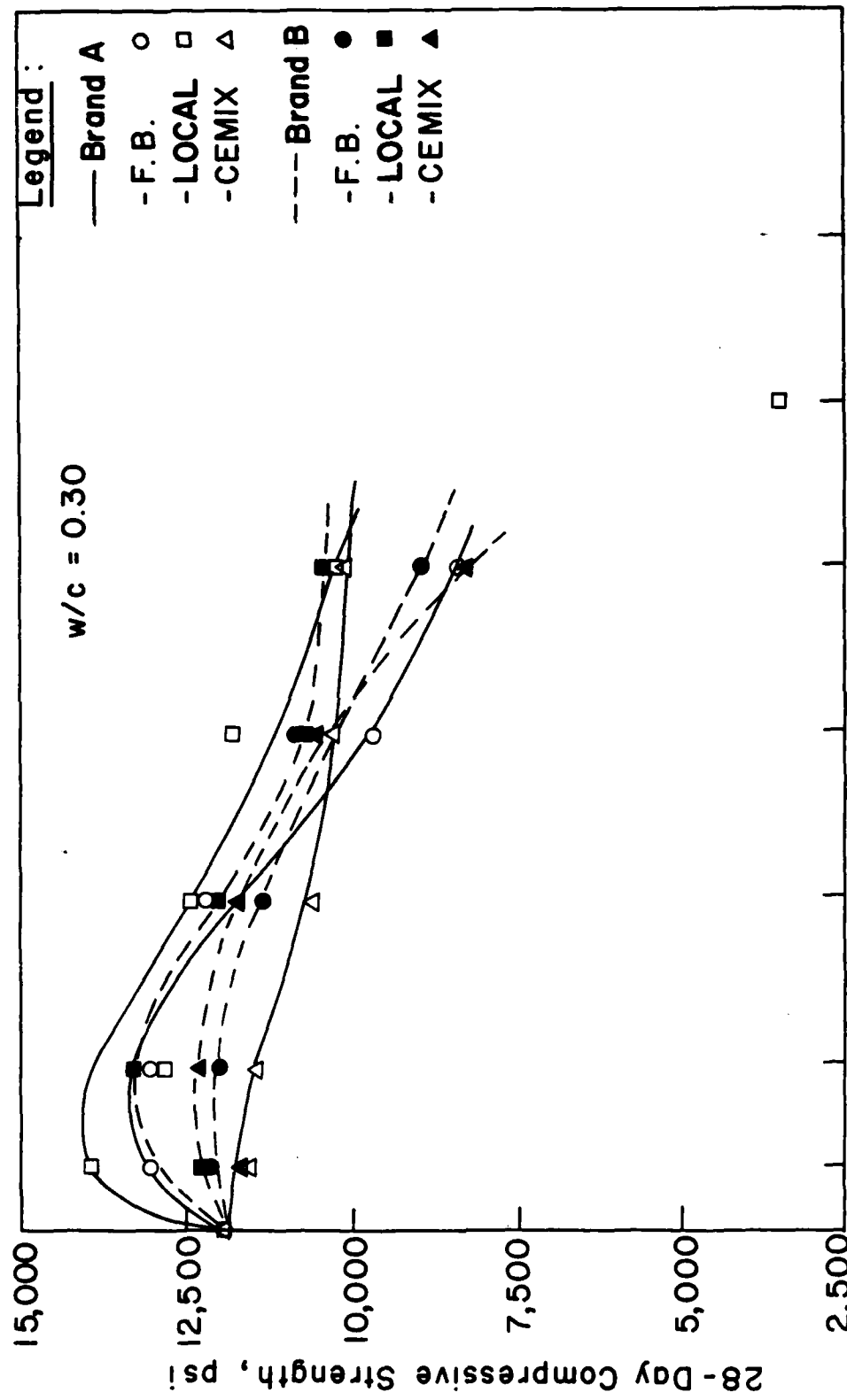

Figure 3.5 Effect of Sand-Cement Ratio on Compressive Strength of Mortar for Water/Cement Ratio of 0.30

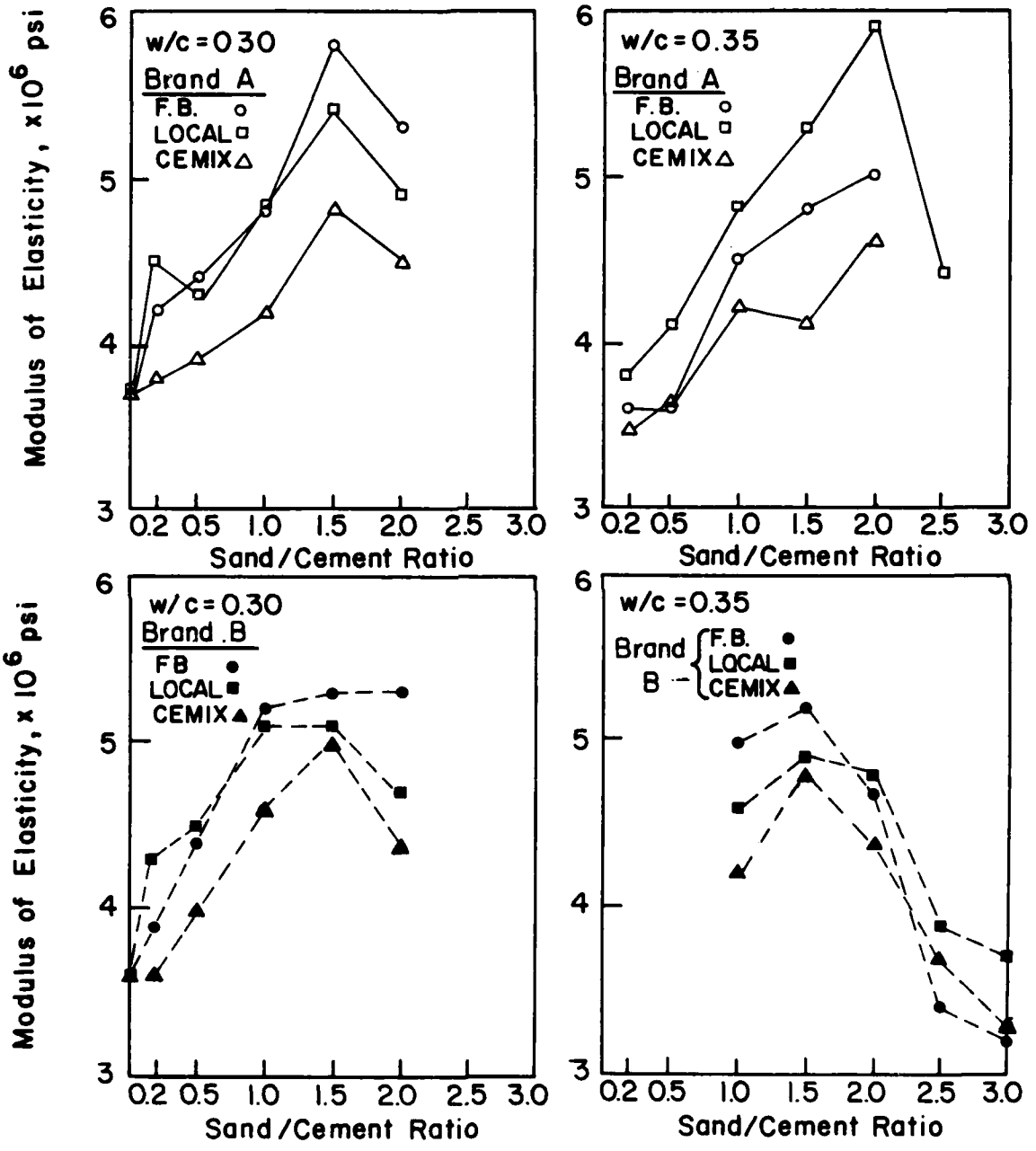

Figure 3.6 Relationship between Modulus of Elasticity and Sand/Cement Ratio for Mortar Specimens with a Water/Cement Ratio of 0.30 and 0.35

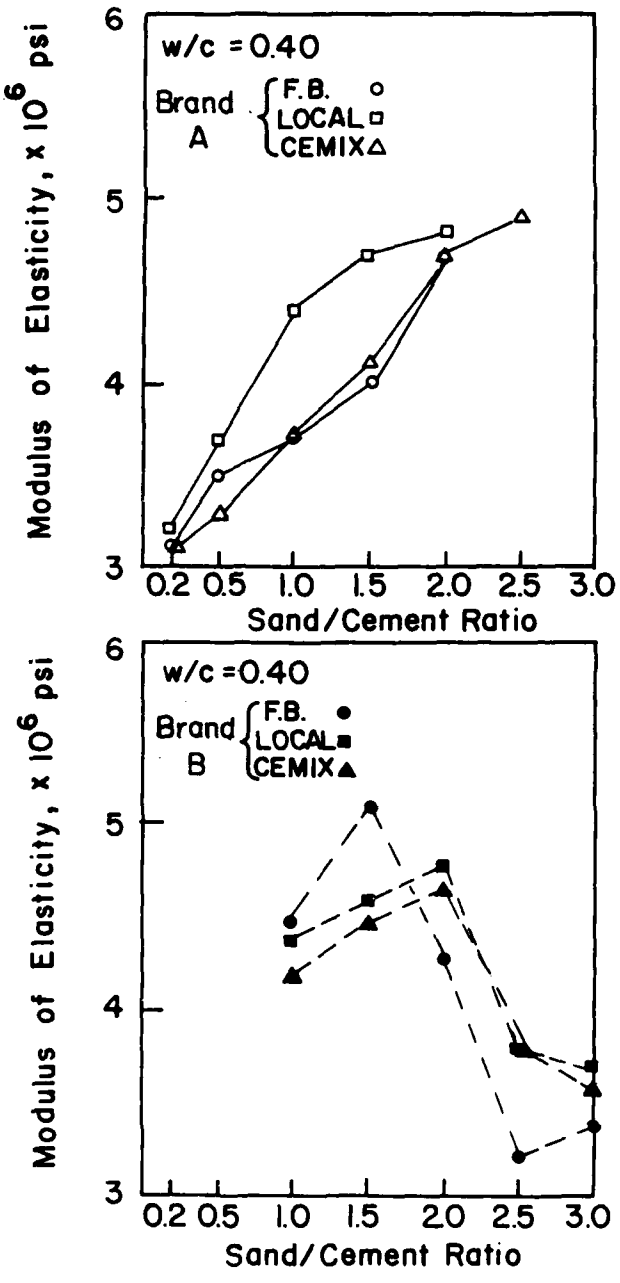

Figure 3.7 Relationship between Modulus of Elasticity and Sand/Cement Ratio for Mortar Specimens with a Water/Cement Ratio of 0.40

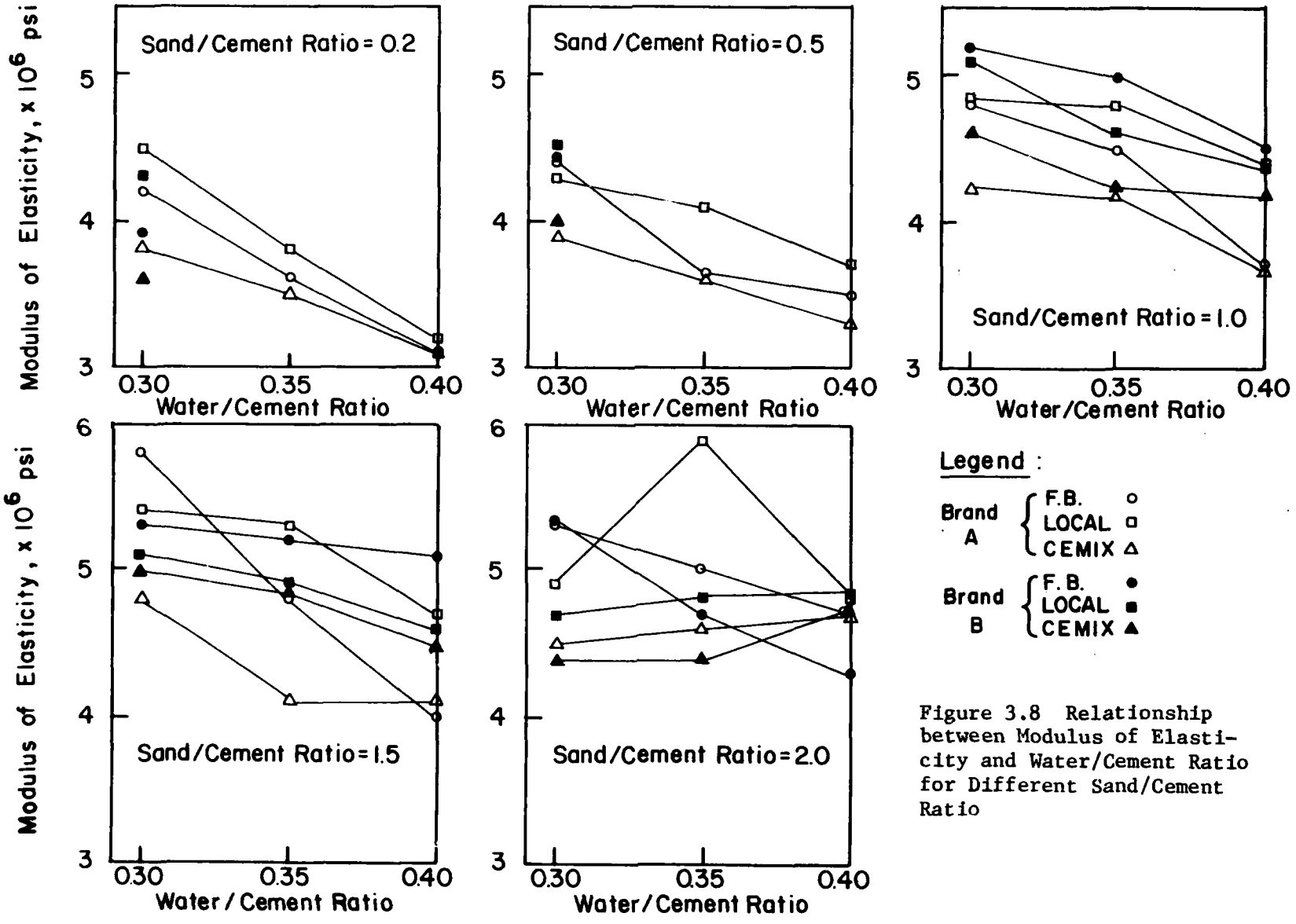

Figure 3.8 Relationship between Modulus of Elasticity and Water/Cement Ratio for Different Sand/Cement Ratio

4) Modulus of elasticity values increased with increasing sand-cement ratios, up to an optimum value. The optimum sand-cement ratios for modulus of elasticity decreased with decreasing water-cement ratio. Optimum ratios varied from about 2.0 to 2.5 for a water-cement ratio of 0.40 to 1.0 to 1.5 for a water-cement ratio of 0.30.
5) High strength mortar was produced with modulus of elasticity values from 3×10^6 to 6×10^6 psi (21×10^3 to 41×10^3 MN/m^2). Strengths were produced from 3300 to 14,000 psi (22.8 to 96.5 MN/m^2).

3.3 COARSE AGGREGATE

Coarse aggregates with distinctively different elastic properties were obtained for use with the different mortars developed. Three different types of rock were available within 150 miles of Austin: limestone, granite, and traprock. Tests were performed to determine the strength and the elastic properties of each of these three types of rock.

3.3.1 Types of Coarse Aggregate

3.3.1.1 Limestone. The limestone was obtained in nearby Georgetown, Texas. It is a biogenic limestone sedimentary rock composed almost entirely of calcium carbonate ($CaCO_3$) with only a trace of silica in the form of chert and quartz.

3.3.1.2 Granite. The samples of pink granite were located near Granite Shoals, Texas. The granite is an intrusive igneous rock. The coarse crystalline structure of the granite is composed of approximately sixty percent pink orthoclase feldspar ($KAl_2Si_3O_8$), 25 percent quartz (SiO_2), and fifteen percent mica, hornblend, and other minor minerals.

3.3.1.3 Traprock. Traprock is the common name for a basalt which is mined in Knippa, Texas. The black rock is a very fine grained crystalline igneous rock. It is an extrusive rock, indicating that it was formed from fast cooling molten lava. Its composition is approximately 85 percent plagioclase feldspar ($NaAl_2Si_3O_8$ or $CaAl_2Si_3O_8$) and fifteen percent magnetite and other minor minerals.

3.3.2 Specimen Preparation

Each type of rock was cored using a 2-in. (5.1-cm) diameter diamond tipped surface-set coring barrel. The coring barrel was attached to a standard drill press which had been modified for rock coring. Kerosene was continuously pumped into the cutting area for cooling and lubrication. The cores were then cut to a 4-in. length using a diamond tipped blade rock saw. A lightweight oil was used for cooling and lubrication. They were then soaked in acetone for a minimum of one hour to remove the oil. The cores were capped using gypsum mortar (hydrostone).

Strain gauges were bonded to the surface using a rapid setting epoxy at least 24 hours prior to testing. Four strain gauges were used on each core; two, with a 2.4-in. (6.1-cm) gauge length, were applied in the longitudinal direction, and two, with a 0.64-in. (1.6-cm) gauge length, were applied horizontally in order to measure transverse strain.

3.3.3 Testing Procedure

Three cores from each rock type were tested in the same compression testing machine used for the mortar tests. A loading rate of 125 psi per second (862 kN/m^2 per second) was used.

The use of strain gauges allowed the entire stress-strain curve to be obtained. Test data was obtained in the form of graphs showing compressive force versus longitudinal and transverse deformations, which were plotted during testing using x-y recorders.

3.3.4 Test Results

Typical stress-strain curves for each type of rock are shown in Fig. 3.9. Curves for each specimen are given in Appendix A (Figs. A-1 through A-3).

Modulus of elasticity values were calculated using the chord method outlined in ASTM C469-65. Average values were 4.49×10^6 psi 31.0×10^3 MN/m^2) for limestone, 3.22×10^6 psi (22.2×10^3 MN/m^2) for granite, and 8.43×10^6 psi (58.1×10^3 MN/m^2) for traprock. Ultimate compressive strengths were 12,850 psi (88.6 MN/m^2) for limestone, 18,600 psi (128 MN/m^2) for granite, and 39,390 psi (272 MN/m^2) for traprock. Poisson's ratio, calculated as outlined in ASTM C469-65, was 5.83 percent for limestone, 3.11 for granite, and 5.50 percent for traprock. Modulus of elasticity values, ultimate compressive strengths, and Poisson's ratios are given in Table 3.3 for each specimen.

3.4 CHOICE OF BIAXIAL SPECIMEN MIX PROPORTIONS

High-strength mortar can be produced possessing a wide range of elastic properties. By varying water-cement ratios and sand-cement ratios, high-strength mortar can be made with modulus of elasticity values varying from 3×10^6 to 6×10^6 psi (21×10^3 to 41×10^3 MN/m^2) with compressive strengths up to 14,000 psi (96.5 MN/m^2).

The biaxial compression experimental program consisted of three mortar mixes combined with all three types of coarse aggregate, resulting in nine different mixes. The three mortar mixes were chosen based upon their high strength combined with widely varying modulus of elasticity values. Mix proportions for the three mortar mixes used in the present biaxial study are presented in Table 3.4.

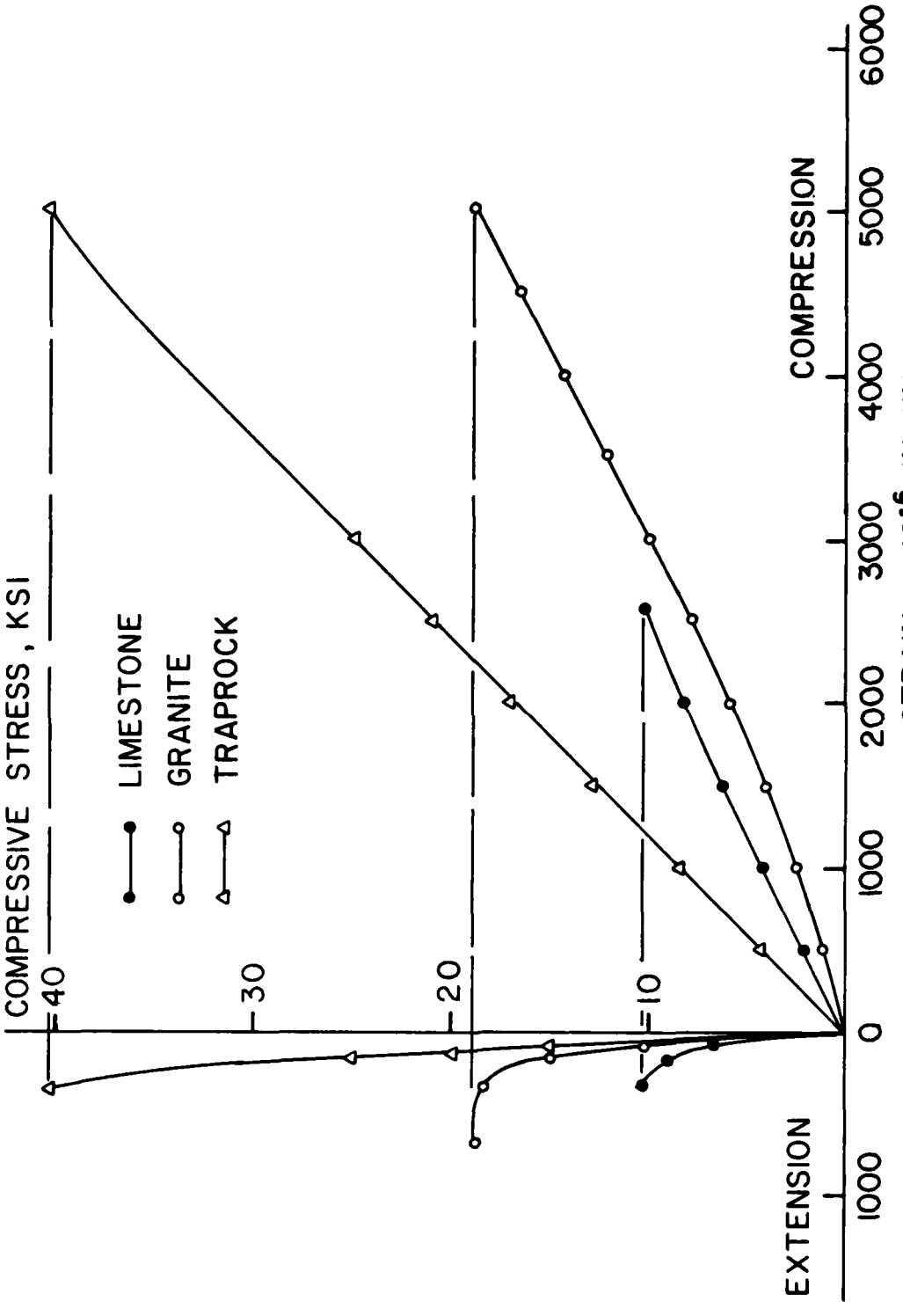

Figure 3.9 Typical Longitudinal and Transverse Stress-Strain Curves for Limestone, Granite, and Traprock

TABLE 3.3 UNIAXIAL COMPRESSIVE STRENGTH, MODULUS OF ELASTICITY, AND POISSON'S RATIO FOR EACH TYPE OF ROCK

Type of Rock	Test No.	Ultimate Compressive Strength (psi)	Modulus of Elasticity (x 10^6 psi)	Poisson's Ratio (percent)
Limestone	L1	12,130	4.68	N/A[a]
	L2	10,240	4.28	6.12
	L3	16,190	4.50	5.54
	Ave.	(12,850)	(4.49)	(5.83)
Granite	G1	18,920	3.16	2.28
	G2	17,640	3.13	4.00
	G3	19,250	3.36	3.06
	Ave.	(18,600)	(3.22)	(3.11)
Traprock	T1	41,110	8.46	5.1
	T2	40,500	8.44	5.7
	T3	36,550	8.40	5.6
	Ave.	(39,390)	(8.43)	(5.5)

[a]Faulty strain gauge did not permit transverse strain measurement.

TABLE 3.4 MORTAR MIX PROPORTIONS FOR BIAXIAL SPECIMENS

Mix No.	Sand	Type I Cement	Water-Cement (by weight)	Fine Aggregate-Cement (by weight)	28 day Compressive Strength (psi)	Modulus of Elasticity (x 10^6 psi)
1	Local	Brand A	0.40	0.2	8,710	3.2
2	Local	Brand A	0.40	1.5	11,600	4.7
3	Local	Brand A	0.35	2.0	11,320	5.9

CHAPTER 4

SPECIMEN PREPARATION AND TESTING PROCEDURE

4.1 DESCRIPTION OF MODEL SPECIMEN

The model specimen used in the study was developed by Buyukozturk as part of the internal microcracking research performed at Cornell (23). The model consists of a mortar matrix, in which were embedded nine circular discs of aggregate as shown in Fig. 4.1. The aggregate discs were 1 1/4 in. (3.18 cm) in diameter and were arranged in a square array with a clear distance between aggregate discs of 5/16 in. (0.79 cm)(d = 0.5r). Buyukozturk (23) also studied a model with d = 0.2r. Reducing the clear distance, however, had little or no effect on the strength properties of the model.

The model specimen was used in order to reduce the complexity of concrete due to its heterogenous composition, allowing for an analytical study using finite element techniques. Moreover, the model maintained the appearance and properties of real concrete, as determined by Liu (24).

Plate specimens 5-in. x 5-in. x 1/2-in. (12.7-cm x 12.7-cm x 1.27-cm) thick were used because, as shown in earlier studies at Cornell, this shape specimen produces a state of plane stress within the specimen, and no buckling of the specimen occurs due to concentric compression loading.

4.2 SPECIMEN FABRICATION

4.2.1 Material Preparation

Two different methods were used in the fabrication of the aggregate discs. Traprock and granite rocks were first trimmed using

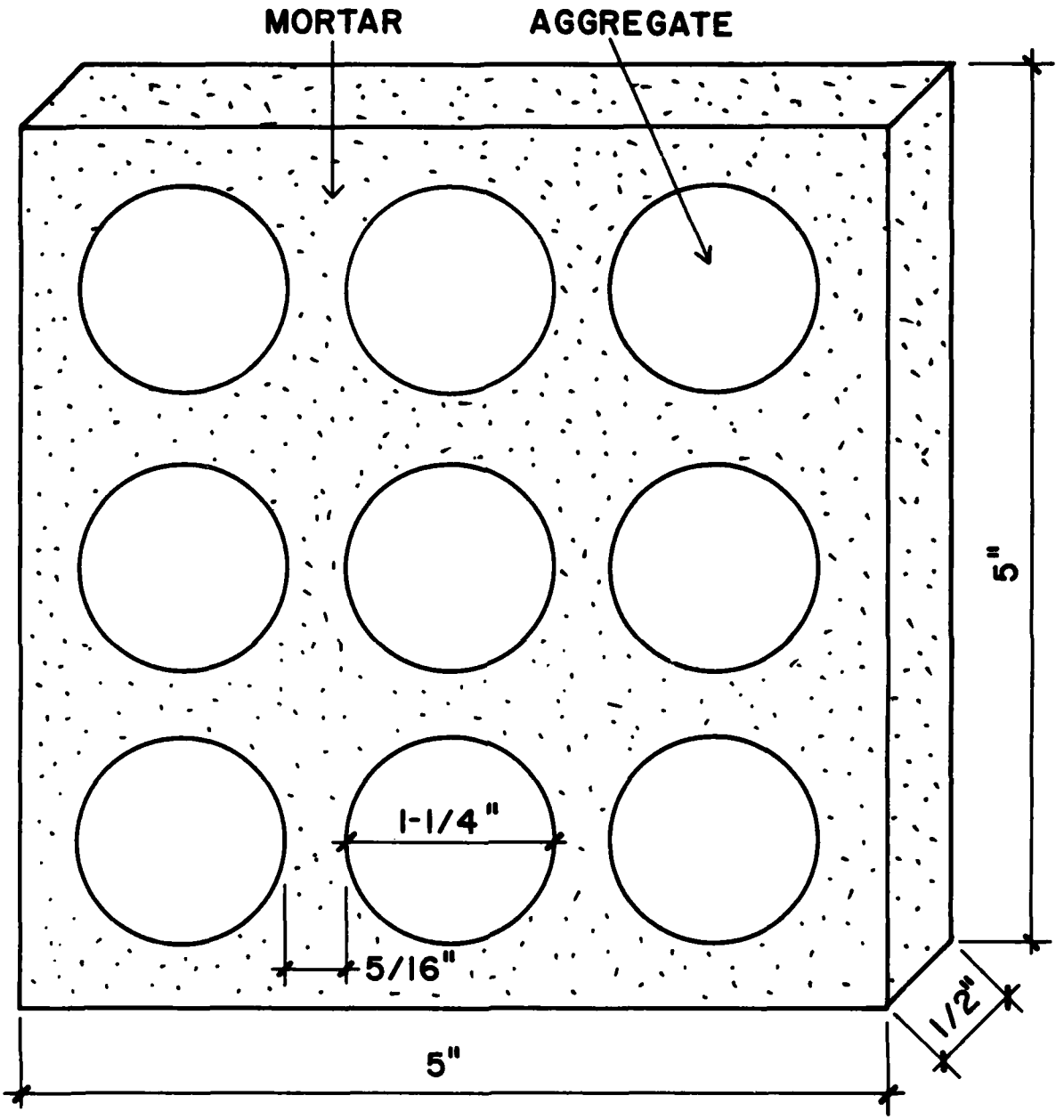

Figure 4.1 Model Concrete Plate Specimen

a water-cooled masonry saw. A cross-section with a maximum dimension of six inches was needed to enable the pieces to fit into a slow-feeding, diamond-tipped blade rock saw. The saw, which is cooled and lubricated with a mixture of light-weight motor oil and kerosene, was used to slice the rock samples into 1/2-in. (1.27-cm) thick slabs. The slabs were examined for proper thickness. Those slabs with a thickness less than 1/2 in. (1.27 cm) were used and later ground to the proper thickness after casting.

The aggregate discs were then made by coring the slabs using a 1 1/4-in. (3.18-cm) diameter diamond-tipped coring barrel. The coring barrel was attached to a small drill press. Water was used for cooling when coring the rock slabs. After drying, the discs were immersed in acetone for a minimum of one hour in order to remove any oil residue the rock may have absorbed during the slab slicing procedure.

Due to a limited supply of limestone, it was necessary to fabricate the limestone discs differently. The rough limestone rocks were first cored using a 1 1/4-in. (3.18-cm) diameter diamond-tipped coring barrel. The resulting 6-in. (15.2-cm) long cores were sliced into 1/2-in. (1.27-cm) thick discs using a small, hand-operated, water-cooled rock saw. These discs were also soaked in acetone in order to remove the oil residue from the coring process.

4.2.2 Mixing, Casting, and Curing

The plate specimens were cast in steel molds which were designed especially to accommodate the models. The molds consisted of a 1/4-in. (0.64-cm) thick by 8-in. (20.3-cm) square base plate, to which four 1/2-in. (1.27-cm) square bars were attached to form the 5-in. x 5-in. x 1/2-in. (12.7-cm x 12.7-cm x 1.27-cm) mold as shown in Fig. 4.2. Circles showing the location of the nine aggregate discs were etched into the base plate. The aggregate discs were glued to the base plate using a very small amount of epoxy one day prior to casting.

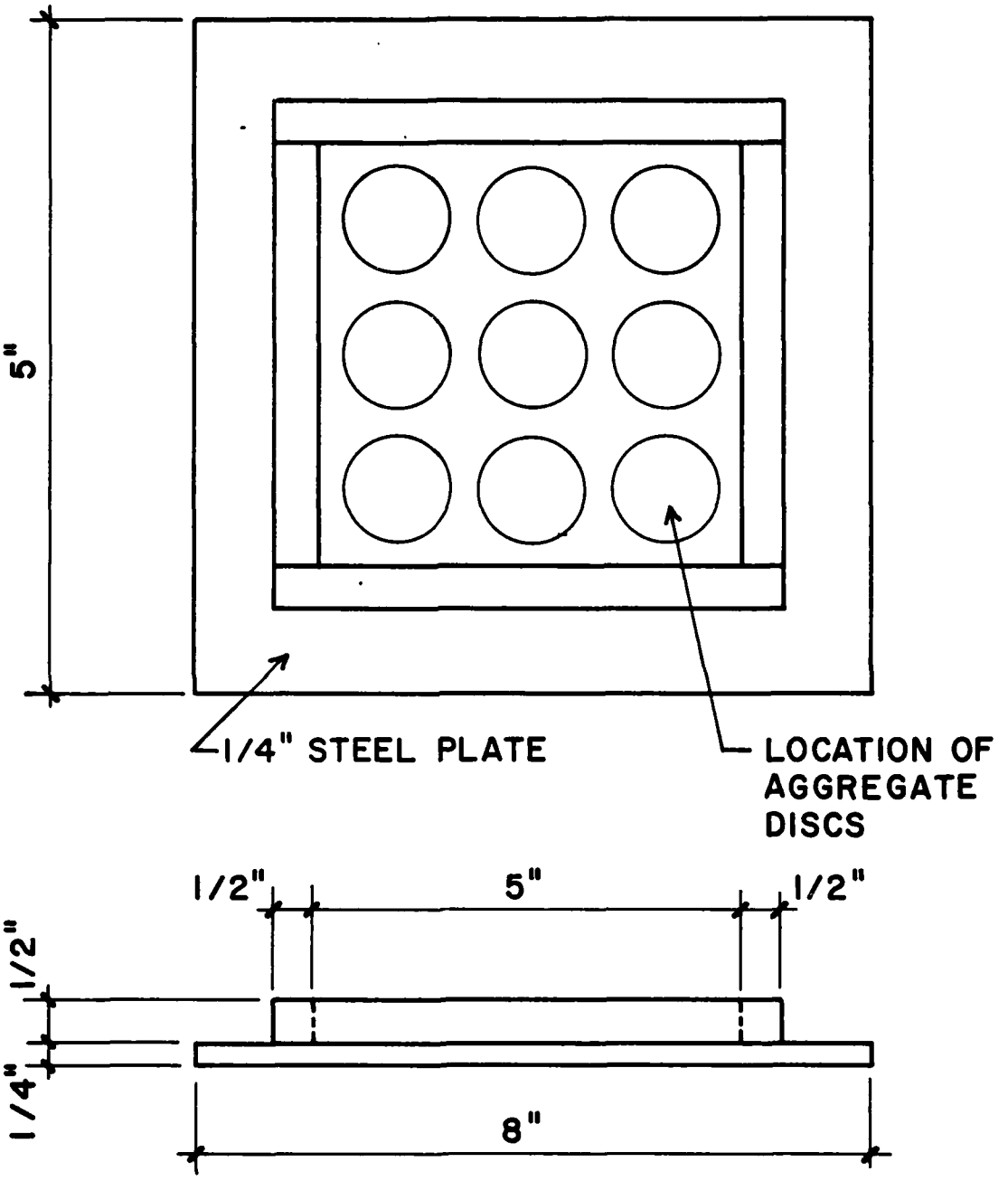

Figure 4.2 Mold for Casting Model Specimen

Materials for the mortar were weighed using a balance with an accuracy of ± 0.5 g. The materials were mixed by hand in a metal pan using a steel trowel. The cement and sand were thoroughly mixed dry prior to adding the mixing water

The mortar was placed into the molds by hand, sometimes using a small trowel. The molds were fastened to a vibrating table where the specimens were vibrated in order to achieve good consolidation. The specimens were vibrated at a medium frequency until the surface appeared free of air voids. Vibrating times ranged from three to ten minutes depending on the workability of the mortar mix.

The specimens were covered with wet burlap for 24 hours. The forms were then removed, and the specimens were cured at 73 ± 3°F and 100 percent humidity until testing. A total of twelve plate specimens and three 3-in. x 6-in. mortar cylinders were cast from each mortar batch.

4.2.3 Grinding

After curing for at least 34 days, the plate specimens were ground to achieve a uniform thickness and to obtain a smooth specimen surface. A tabletop disc grinding wheel was used with #90 grit silicon carbide grinding powder. The specimen was rotated opposite to the direction of the rotating wheel in order to produce an evenly ground specimen. Periodically, the specimen was washed and measured to ensure the thickness was not reduced to less than 1/2 in. (1.27 cm). The specimens were ground one day prior to testing.

4.3 TEST APPARATUS

4.3.1 Loading Frame

The loading frame, shown in Fig. 4.3, used in the present study was designed especially for biaxial compression testing. Two hydraulic rams mounted in orthogonal directions are used to produce the required biaxial forces. Loads are measured using two 100-kip (445-kN) capacity load cells, mounted opposite of the rams.

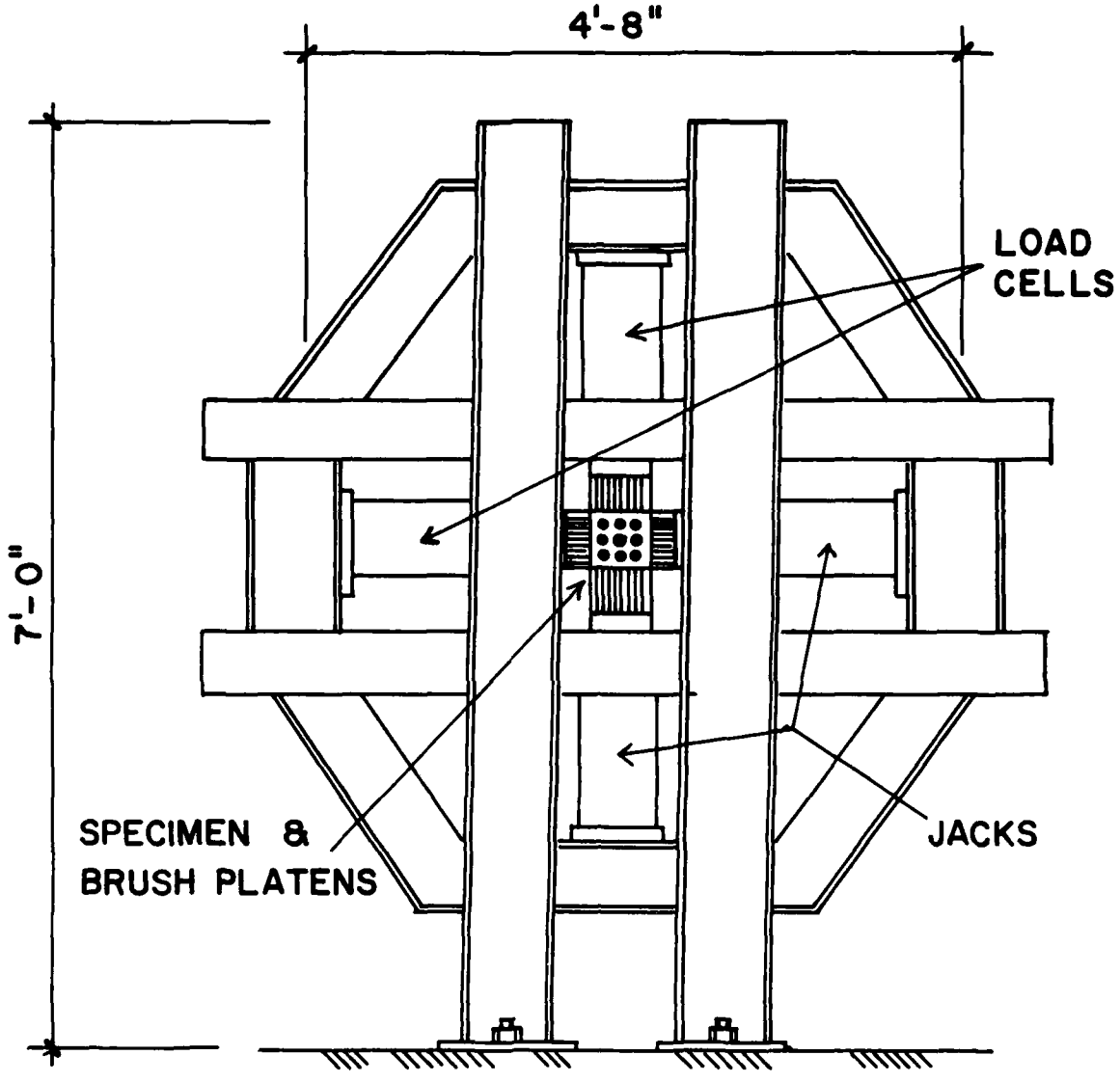

Figure 4.3 Biaxial Loading Frame

4.3.2 Loading Platens

It has been shown that the use of solid steel bearing platens induces confining stresses due to the friction between the platen and the concrete specimen (16, 21, 22). In this study, brush bearing platens similar to those developed by Hilsdorf (21) were used. The brush bearing platens allow the compressive load to be transferred to the specimen without producing any significant confining stresses.

The brush bearing platens were used previously at the University of Texas at Austin during studies on polymer impregnated concrete. A detailed review of the platens design is given by Khanna (28) and Park (29). The platens are shown in Fig. 4.4.

4.3.3 Loading

The biaxial tests were controlled by two material testing system (MTS) units. The servo controlled system allowed for load to be applied in the major principal load direction (horizontal) at a constant strain rate of 500 microstrain per minute. The specimens failed approximately three minutes after beginning the test. Loads in the minor principal load direction (vertical) were applied at a constant ratio of the horizontal load equal to the biaxial stress ratio desired for the test.

4.3.4 Deflection Measuring Apparatus

Deflections in both principal directions were measured using Direct Current Differential Transducers (DCDT's). Two DCDT's, one on each side of the specimen, were used in each direction. The values recorded from each pair were averaged to obtain the deflection in each direction.

The DCDT's were held in place by a system of U-clamps which were attached to the specimen with contact pins. A gauge length of 3.75 in. between contact pins was used so that the pins could be tightened into the aggregate discs as opposed to the mortar matrix. The reason for this is that cracking is less likely to occur in the discs than in the mortar matrix.

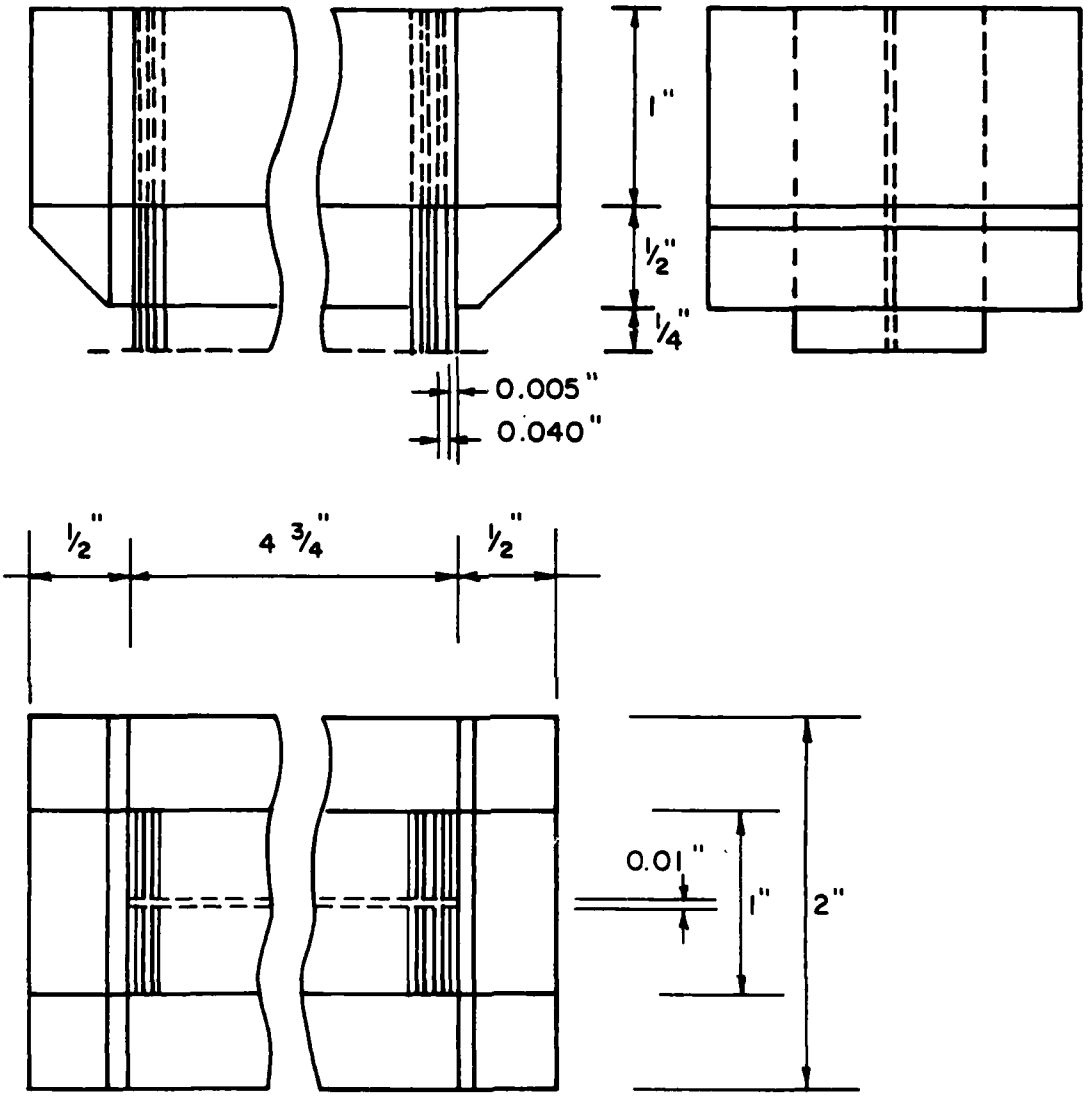

Figure 4.4 Dimensions of Loading Brush Platen

4.4 TESTING PROCEDURE

4.4.1 Specimen Mounting

After marking the points on the specimen where the contact pins of the U-clamps were to be located, the specimen was ready for mounting in the loading frame. The two horizontal brush bearing platens were aligned with respect to the horizontal ram and load cell, and the bottom vertical brush was positioned on the vertical load cell. The ends of the specimen were coated with a thin layer of gypsum mortar (hydrostone) to provide for a flat loading surface. The specimen was then lowered into place and aligned. A confining load of about 400 lb (181 kg) was applied in the horizontal direction while the upper vertical brush was aligned. The same confining load was then applied in the vertical direction for about thirty minutes, until the hydrostone hardened.

4.4.2 Testing Procedure

The U-clamps were positioned during the time required for the hydrostone to set. The eight contact pins were screwed tightly onto the specimen to prevent slip.

The DCDT's were mounted onto the U-clamps after the hydrostone had fully hardened. The confining loads were removed, and the DCDT's were zeroed. After zeroing the DCDT's, the hydraulic rams were brought in contact with the specimen at approximately 400 lbs (181 kg) contact load and then the test was started. For uniaxial tests, load was applied in the horizontal direction only.

Load-deflection curves, one for each direction, were plotted during testing using x-y recorders, omnigraphic model 2000R. The test was stopped immediately after failure. The specimen was then removed from the test frame, marked, and stored for future analysis.

CHAPTER 5

EXPERIMENTAL RESULTS

Model high-strength concrete plate specimens were tested in uniaxial and biaxial compression. Three types of coarse aggregate, limestone, traprock, and granite, were combined with three different mortar mixes to make nine total batches. Each batch consisted of twelve specimens, three for testing at each stress ratio (0.0, 0.2, 0.5, and 1.0). Each batch was designated by a letter, either L (limestone), T (traprock), or G (granite), followed by a number, 1 through 3. The letter indicates the type of coarse aggregate used in the specimen while the number identifies the mortar mix used (1 - low modulus mortar, 2 - medium modulus mortar, 3 - high modulus mortar).

5.1 TYPICAL STRESS-STRAIN CURVES

Typical stress-strain curves for each mix are shown in Figs. 5.1 through 5.9 for all stress ratios. Stress-strain curves for each specimen tested are included in Appendix B (Figs. B-1 through B-36). Each graph consists of average strains in both principal directions, ε_1 and ε_2. Typical curves for each stress ratio, 0.0, 0.2, 0.5, and 1.0, are shown for each of the nine mixes. Due to the sudden nature of the failure of the specimens and large variability in the recorded measurement of strains past ultimate strength, the post-peak behavior of the stress-strain curves of the specimens is not shown in Figs. 5.1 throdgh 5.9 and Figs. B-1 through B-36.

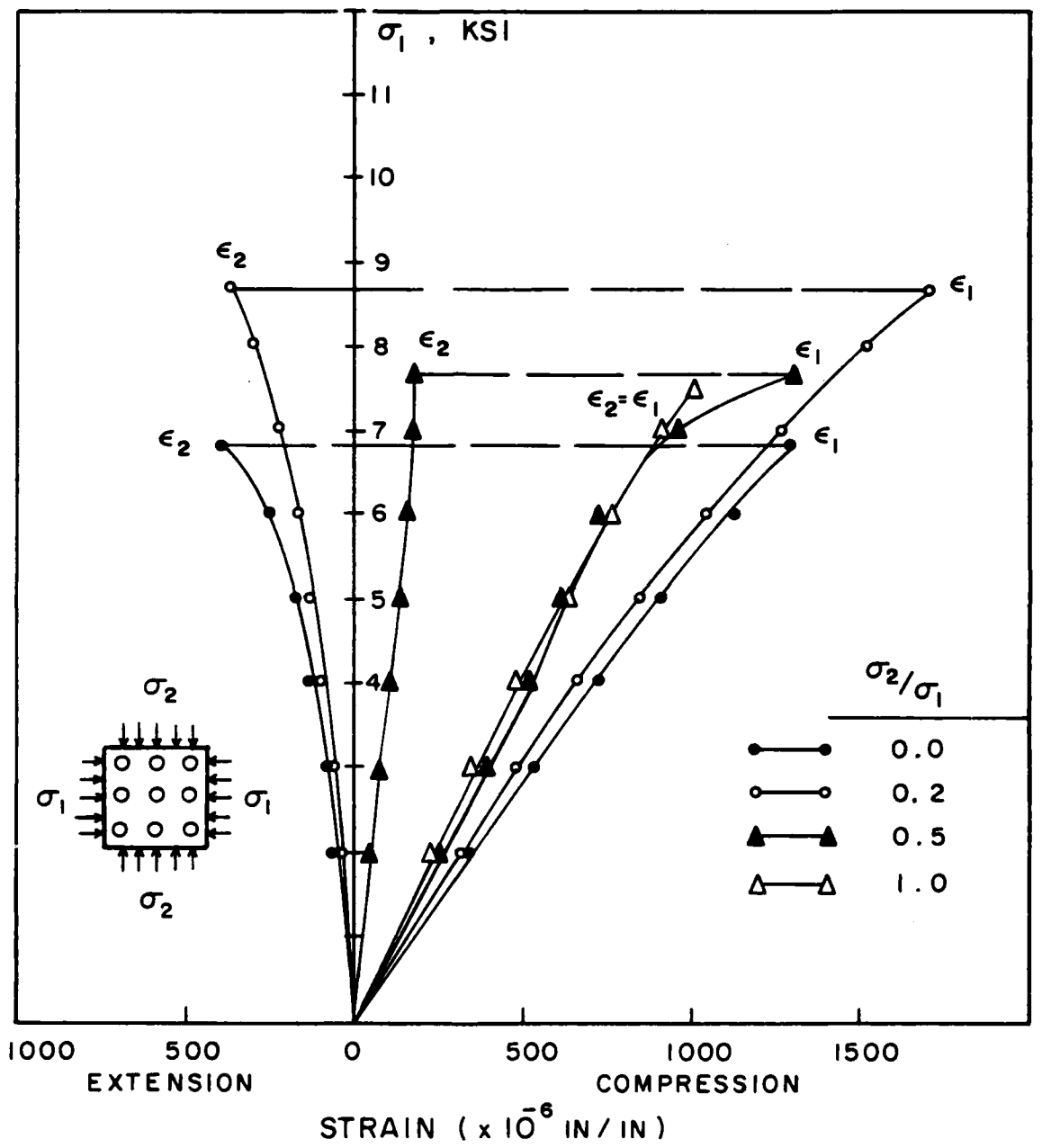

Figure 5.1 Typical Stress-Strain Curves for Model Specimens L1 for all Biaxial Stress Ratios

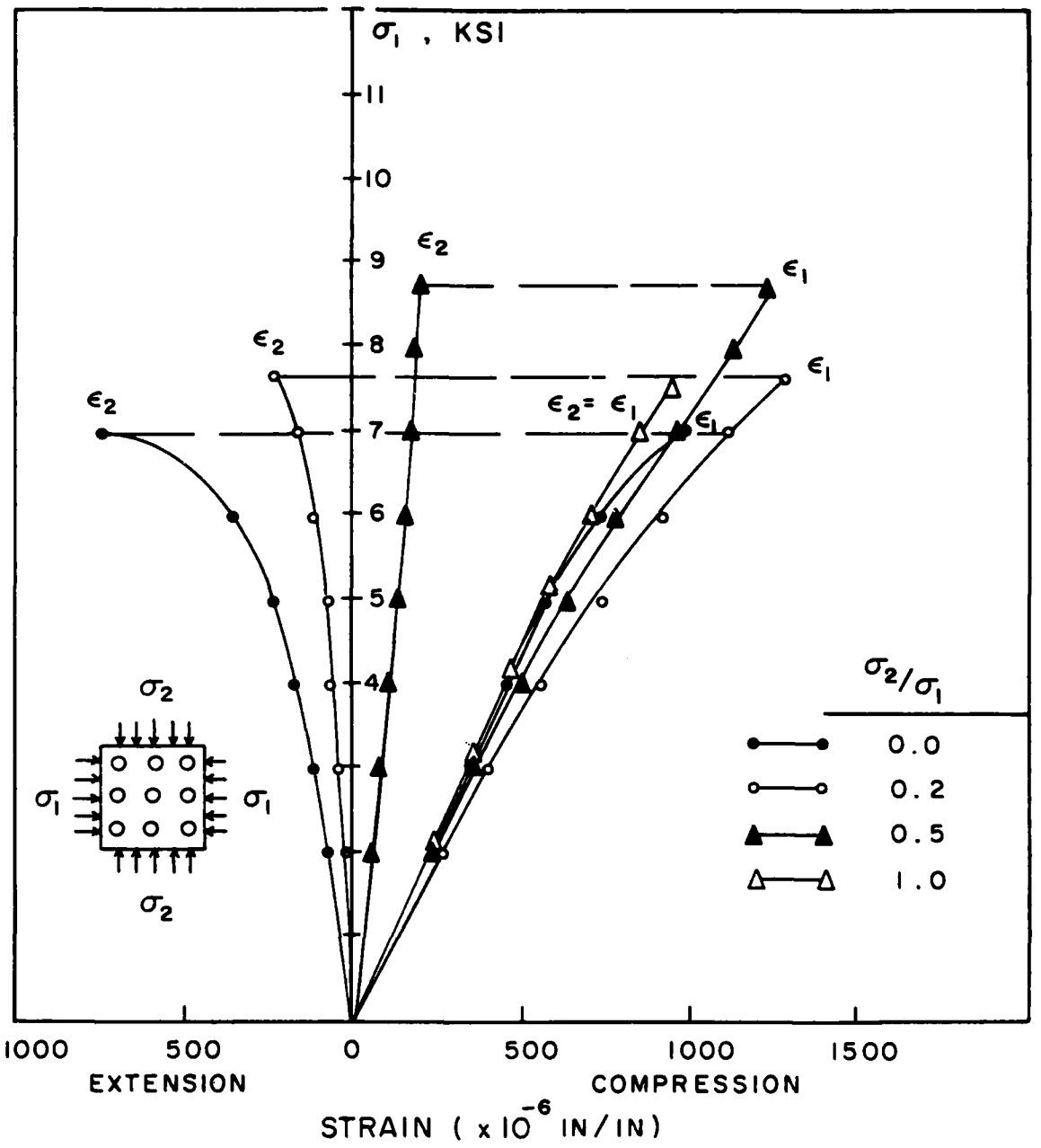

Figure 5.2 Typical Biaxial Stress-Strain Curves for Model Specimens L2 for all Biaxial Stress Ratios

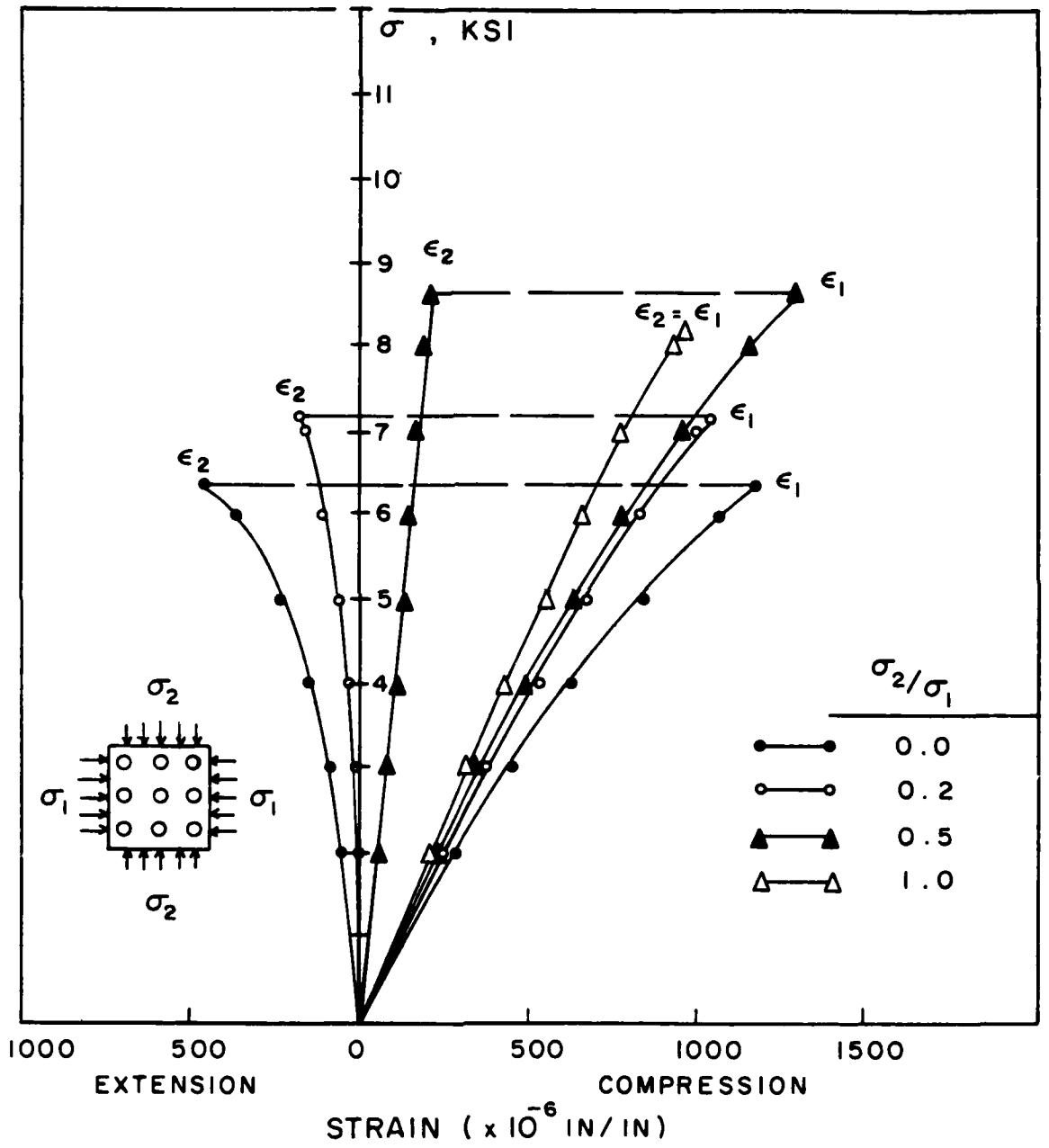

Figure 5.3 Typical Biaxial Stress-Strain Curves for Model Specimens L3 for all Biaxial Stress Ratios

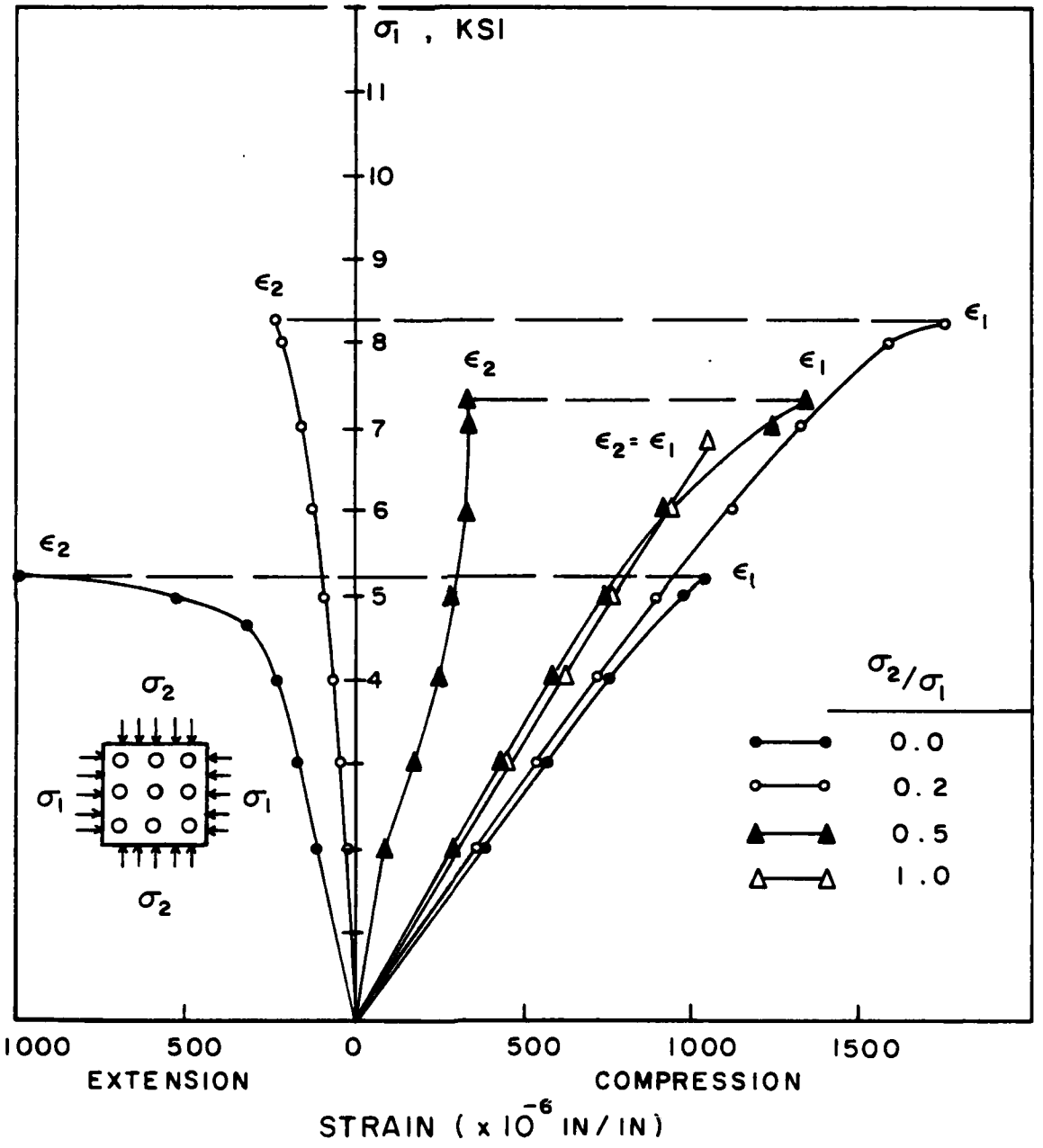

Figure 5.4 Typical Biaxial Stress-Strain Curves for Model Specimens G1 for all Biaxial Stress Ratios

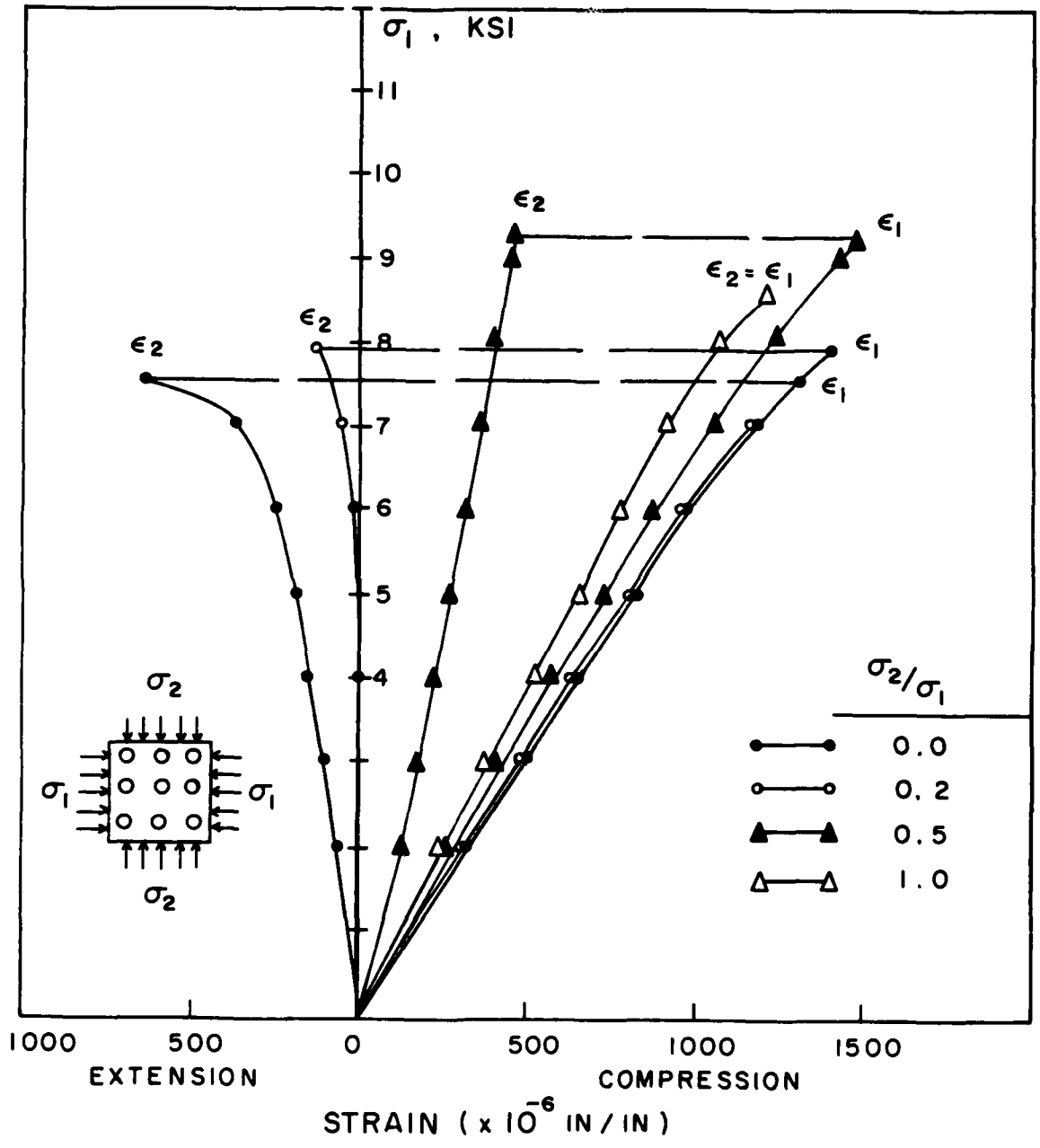

Figure 5.5 Typical Biaxial Stress-Strain Curves for Model Specimens G2 for all Biaxial Stress Ratios

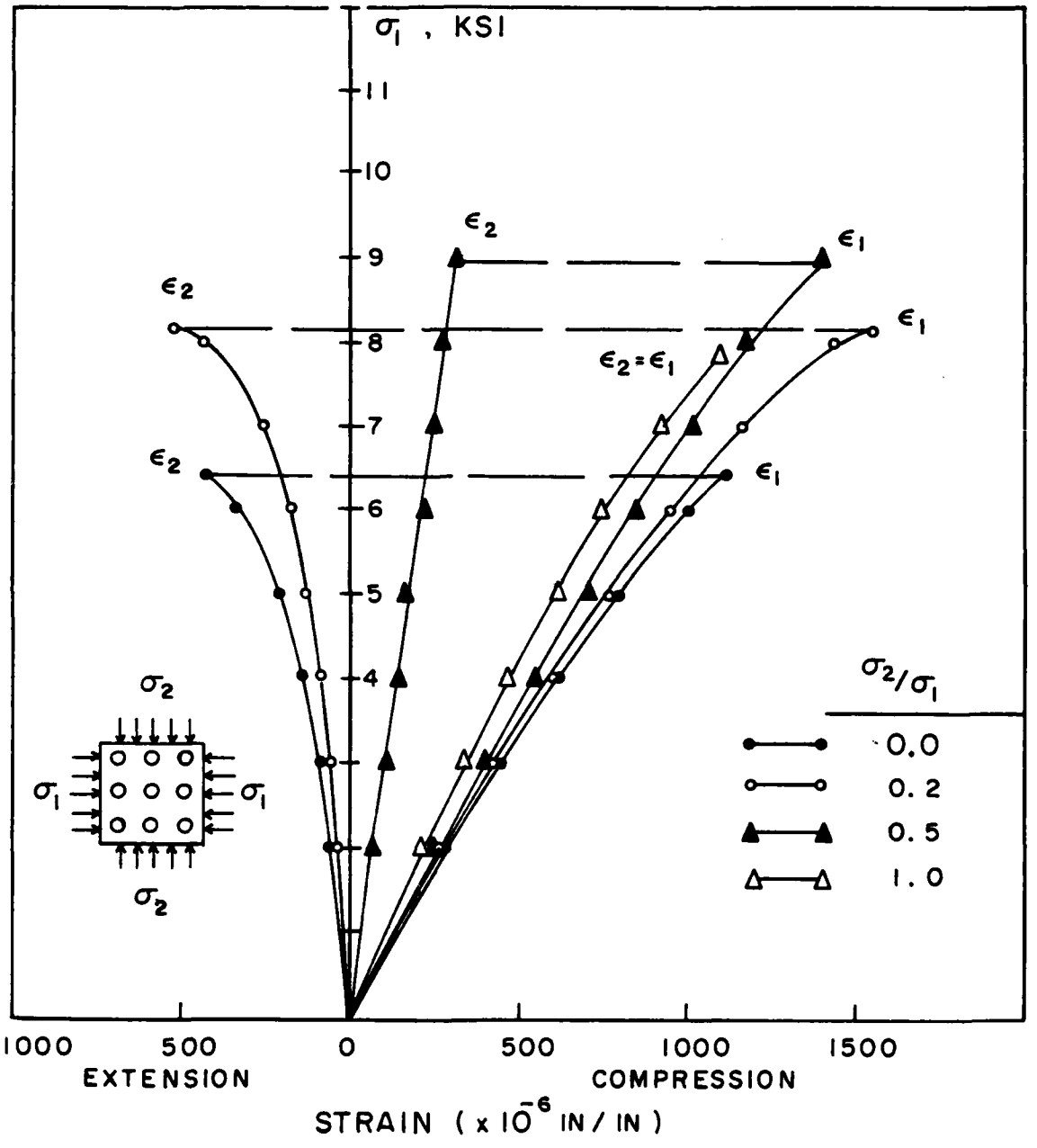

Figure 5.6 Typical Biaxial Stress-Strain Curves for Model Specimens G3 for all Biaxial Stress Ratios

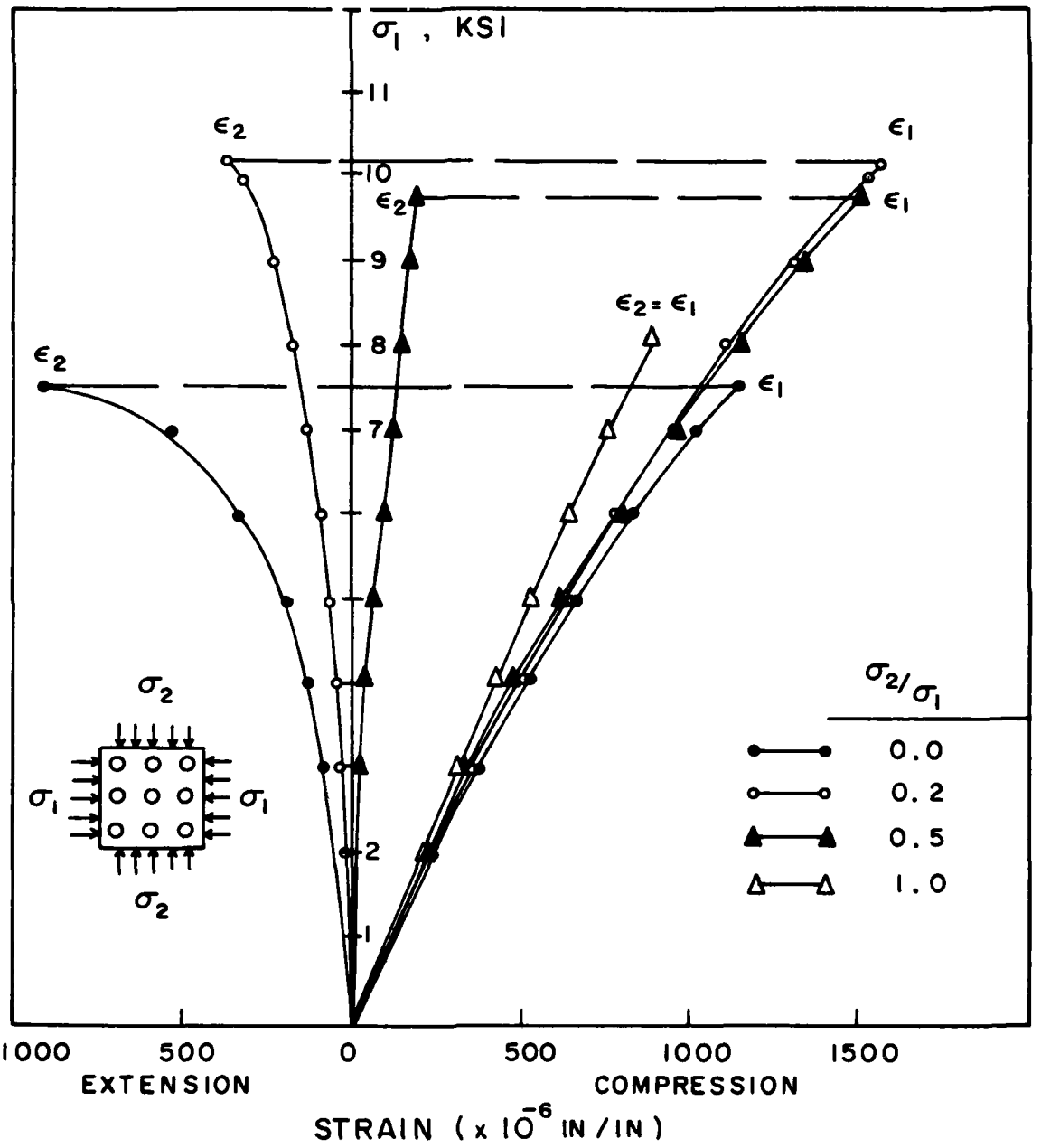

Figure 5.7 Typical Biaxial Stress-Strain Curves for Model Specimens T1 for all Biaxial Stress Ratios

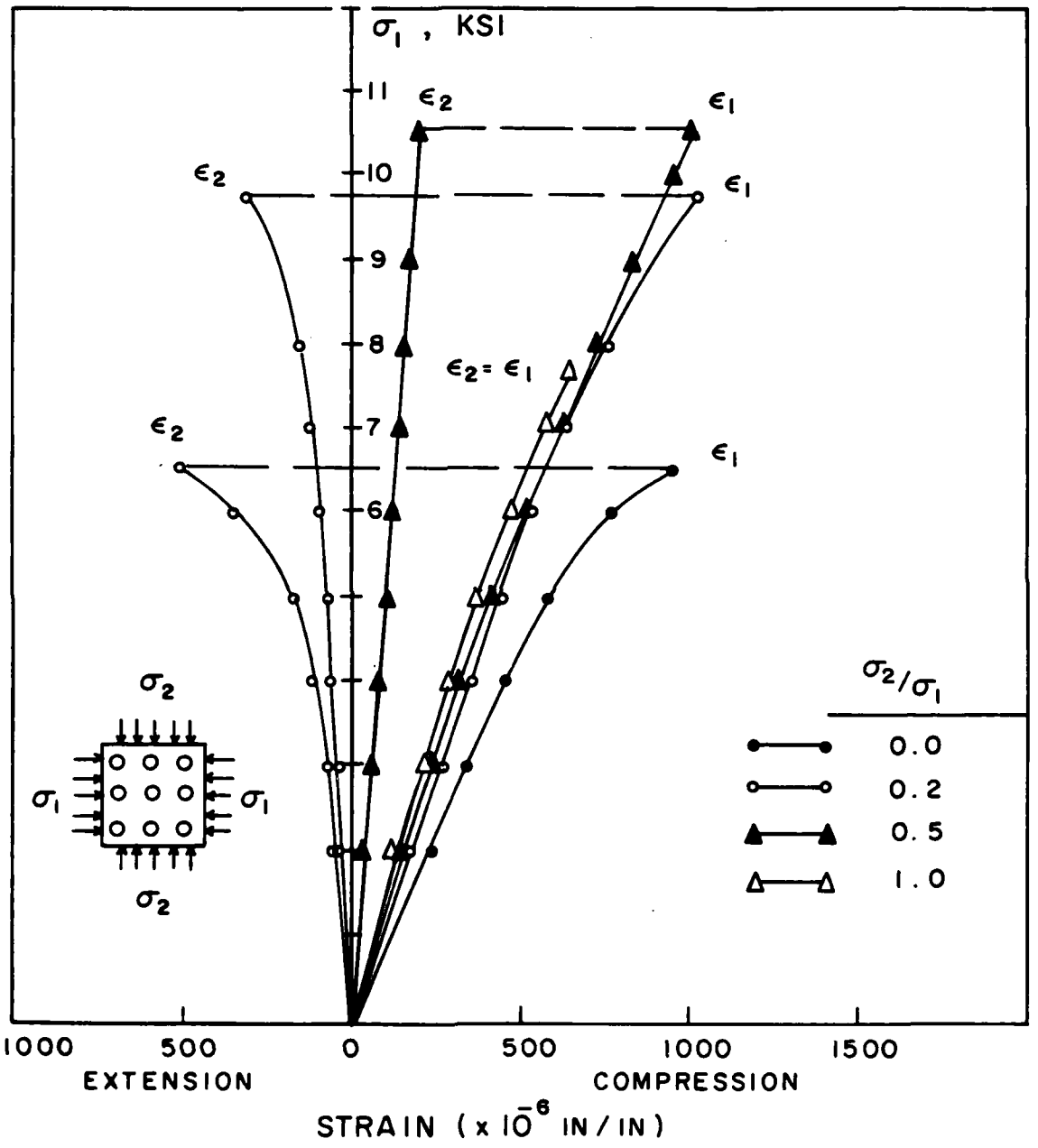

Figure 5.8 Typical Biaxial Stress-Strain Curves for Model Specimens T2 for all Biaxial Stress Ratios

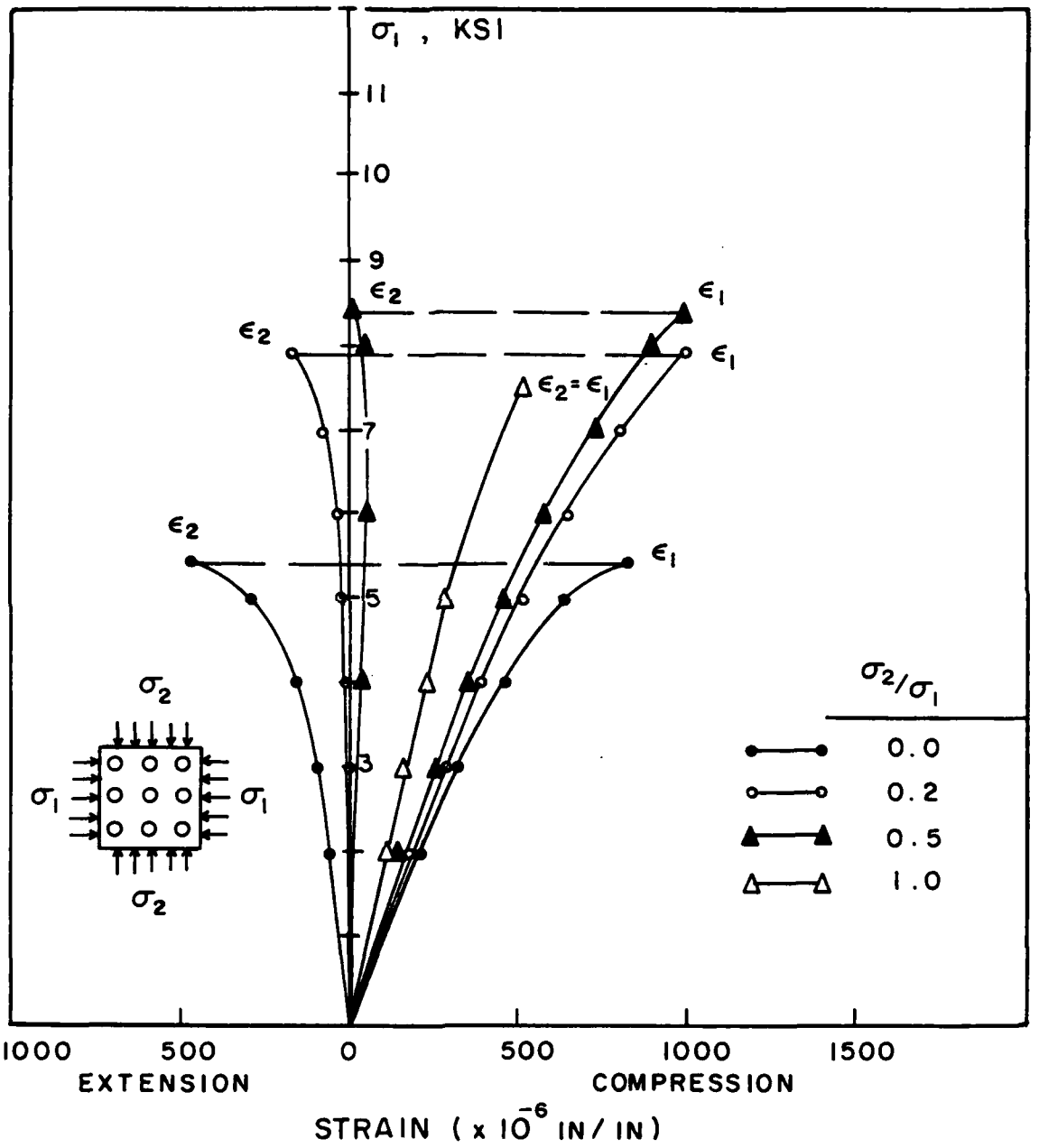

Figure 5.9 Typical Biaxial Stress-Strain Curves for Model Specimens T3 for all Biaxial Stress Ratios

5.2 STRENGTH DATA

Ultimate strengths for each model specimen tested are presented in Tables 5.1 through 5.3 for all biaxial stress ratios.

5.3 PROPERTIES OF MORTAR USED IN BIAXIAL PLATE SPECIMENS

Three mortar cylinders were made with each of the nine mortar batches used in the biaxial model specimens. Average compressive strength, modulus of elasticity, and Poisson's ratio of the mortar are presented in Table 5.4.

TABLE 5.1 ULTIMATE STRENGTH VALUES FOR MODEL SPECIMENS WITH LIMESTONE COARSE AGGREGATE

Stress Ratio		Specimen Designation		
		L1	L2	L3
$\sigma_2/\sigma_1 = 0.0$		-[a]	6700	6550
		6950	7000	5650
		6300	6975	6400
	Av.	(6625)	(6892)	(6200)
$\sigma_2/\sigma_1 = 0.2$		-[a]	8750	7150
		8650	7700	6500
		8400	7300	11,000
	Av.	(8525)	(7917)	(8217)
$\sigma_2/\sigma_1 = 0.5$		-[a]	8400	-[a]
		7700	8800	8750
		8325	9500	8700
	Av.	(8025)	(8900)	(8725)
$\sigma_2/\sigma_1 = 1.0$		-[a]	-[a]	6450
		7650	7550	6300
		6800	7350	8200
	Av.	(7225)	(7450)	(6983)

[a]Specimen was damaged prior to testing.

TABLE 5.2 ULTIMATE STRENGTH VALUES FOR SPECIMENS WITH GRANITE COARSE AGGREGATE

Stress Ratio	Specimen Designation		
	G1	G2	G3
$\sigma_2/\sigma_1 = 0.0$	5300	5750	6575
	6500	7450	5900
	4600	5100	6350
	Av. (5467)	(6100)	(6275)
$\sigma_2/\sigma_1 = 0.2$		7100	8100
	7900	9750	8150
	8200	7900	10,500
	Av. (8050)	(8250)	(8917)
$\sigma_2/\sigma_1 = 0.5$	6400	8900	-[a]
	7300	9250	9250
	10,200	8400	9000
	Av. (7967)	(8850)	(9125)
$\sigma_2/\sigma_1 = 1.0$	5300		
	7500	6600	7400
	6000	8500	7800
	6850	6950	8450
	Av. (6413)	(7350)	(7883)

[a]Specimen was damaged prior to testing.

TABLE 5.3 ULTIMATE STRENGTH VALUES FOR SPECIMENS WITH TRAPROCK COARSE AGGREGATE

Stress Ratio	Specimen Designation		
	T1	T2	T3
$\sigma_2/\sigma_1 = 0.0$	7500	6500	6800
	6800	5800	6600
	7100	8000	5400
	Av. (7133)	(6767)	(6267)
$\sigma_2/\sigma_1 = 0.2$	9100	9300	8400
	8600	7100	7900
	10,200	9700	8500
	Av. (9300)	(8700)	(8267)
$\sigma_2/\sigma_1 = 0.5$	-[a]	10,600	8400
	10,500	6700	8800
	9850	9200	8000
	Av. (10,175)	(8833)	(8400)
$\sigma_2/\sigma_1 = 1.0$	7200	7200	7500
	8150	6000	7200
	8400	7600	7200
	Av. (7917)	(6933)	(7300)

[a]Specimen was damaged prior to testing.

TABLE 5.4 AVERAGE COMPRESSIVE STRENGTH, MODULUS OF ELASTICITY, AND POISSON'S RATIO FOR MORTAR USED IN THE BIAXIAL MODEL SPECIMENS

Specimen[a] Designation	Compressive Strength (psi)	Modulus of Elasticity (x 10^{-6} psi)	Poisson's Ratio
L1	11,220	2.64	0.23
G1	10,430	3.65	0.27
T1	9,506	3.31	0.23
L2	12,280	3.69	0.20
G2	10,420	5.36	0.21
T2	12,350	5.61	0.24
L3	10,970	6.74	0.25
G3	11,930	5.26	0.20
T3	12,490	5.82	0.23

[a] L = limestone coarse aggregate; G = granite coarse aggregate; T = traprock coarse aggregate

CHAPTER 6

ANALYSIS AND DISCUSSION OF EXPERIMENTAL RESULTS

6.1 ULTIMATE STRENGTH

6.1.1 Uniaxial Strength

The ultimate compressive strength of the model plate specimens is presented in Tables 5.1 through 5.3 for all specimens tested. Average uniaxial strength, f'o, ranged from 5467 to 6275 psi (37.7 to 43.3 MN/m^2) for specimens using granite coarse aggregate, 6200 to 6892 psi (42.7 to 47.5 MN/m^2) for limestone, and 6267 to 7133 psi (43.2 to 49.2 MN/m^2) for traprock.

6.1.2 Biaxial Strength

Biaxial ultimate strength envelopes for each specimen tested are shown in Figs. 6.1 through 6.9. A comparison of the biaxial ultimate strength envelopes for specimens having the same coarse aggregate is shown in Figs. 6.10 through 6.12 for limestone, granite, and traprock aggregates. All data are shown normalized in terms of the uniaxial strength, f'o, of the plate specimens.

The ultimate strength under biaxial compression shows a significant increase over the uniaxial strength for all specimens tested. Maximum biaxial strength occurs at a biaxial stress ratio between 2.0 and 0.5 for all specimens. Maximum strength increases ranged from 29 to 41 percent for specimens using limestone coarse aggregate, 45 to 47 percent for granite, and 31 to 43 percent for traprock. At equal biaxial compression ($\sigma_2/\sigma_1 = 1.0$), strength increases ranged from eight to thirteen percent for specimens with limestone coarse aggregate, seventeen to 26 percent for granite, and two to sixteen percent for traprock. Average biaxial strengths are presented in Tables 6.1 through 6.3 for all specimens tested.

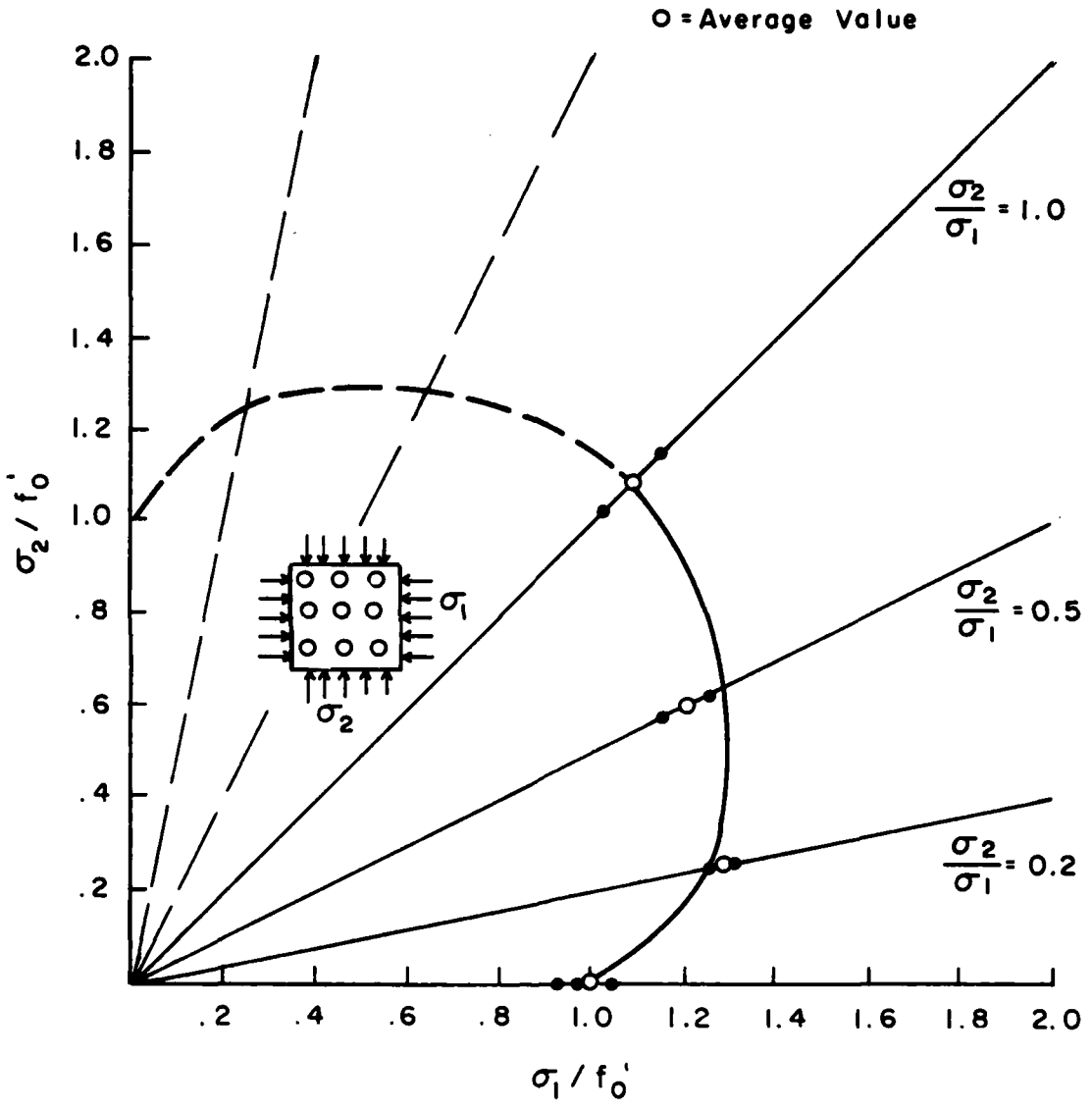

Figure 6.1 Biaxial Ultimate Strength Envelope for Model Specimen L1 Containing Limestone Aggregate and Low Modulus Mortar

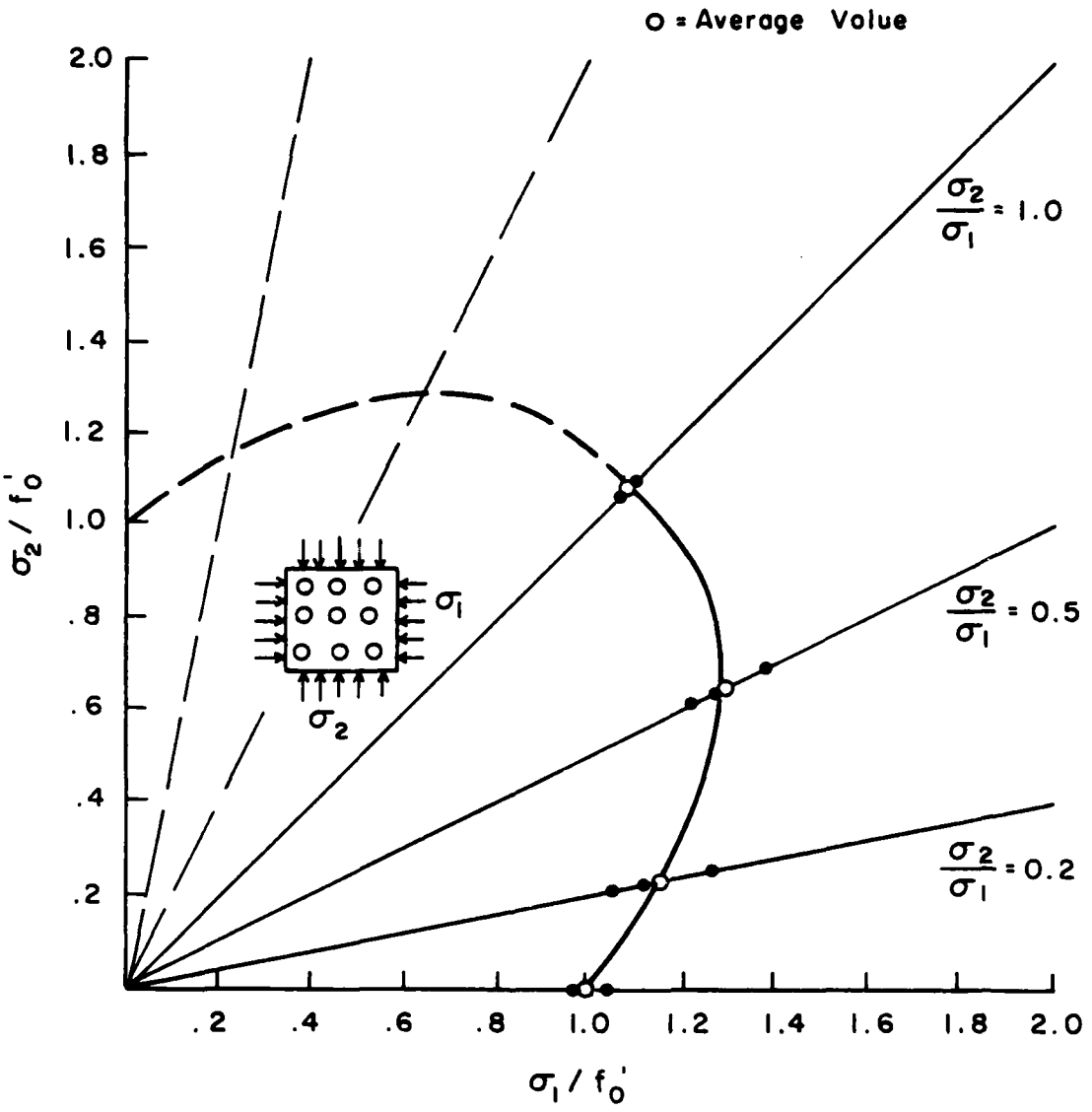

Figure 6.2 Biaxial Ultimate Strength Envelope for Model Specimen L2 Containing Limestone Aggregate and Medium Modulus Mortar

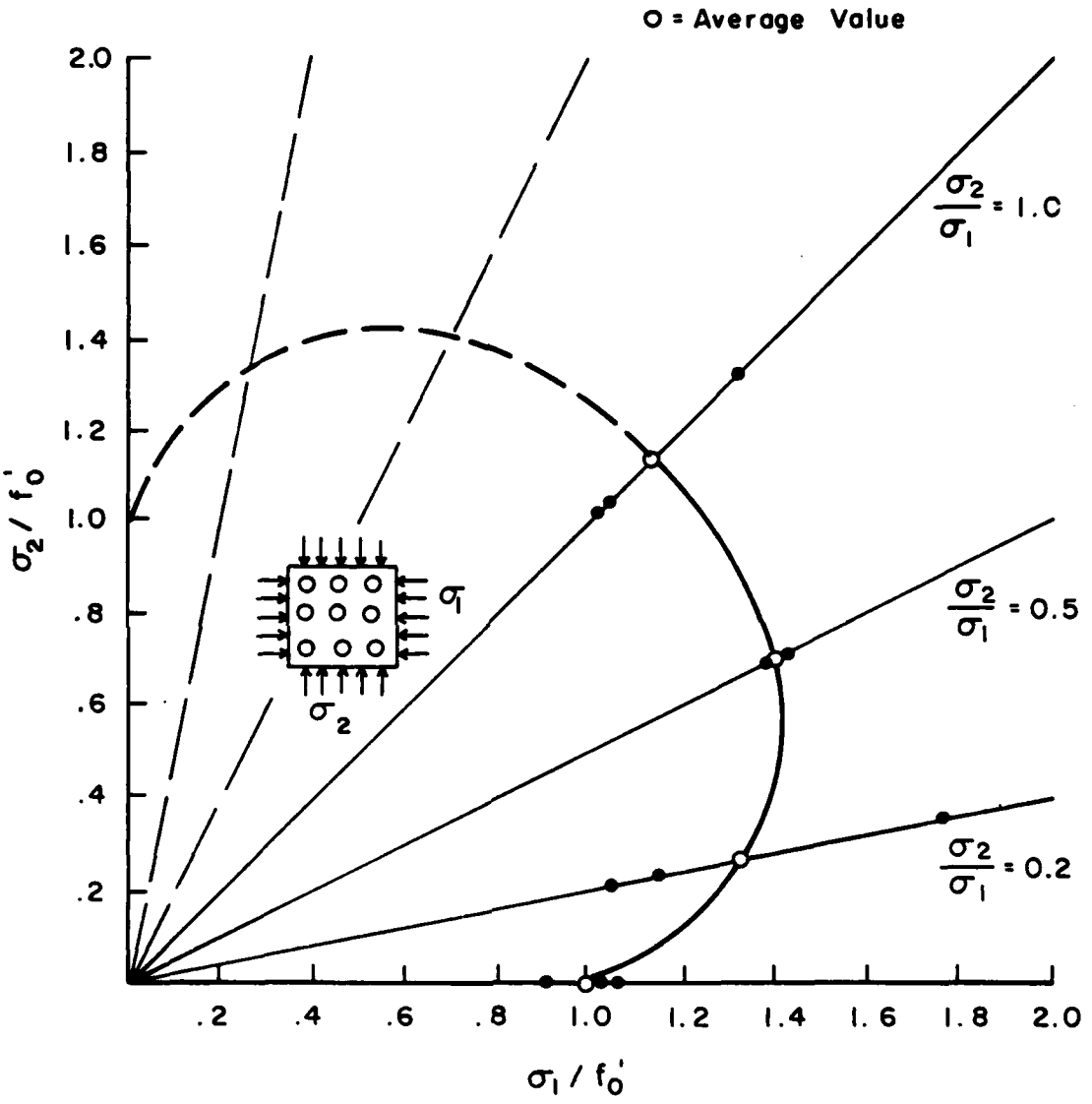

Figure 6.3 Biaxial Ultimate Strength Envelope for Model Specimen L3 Containing Limestone Aggregate and High Modulus Mortar

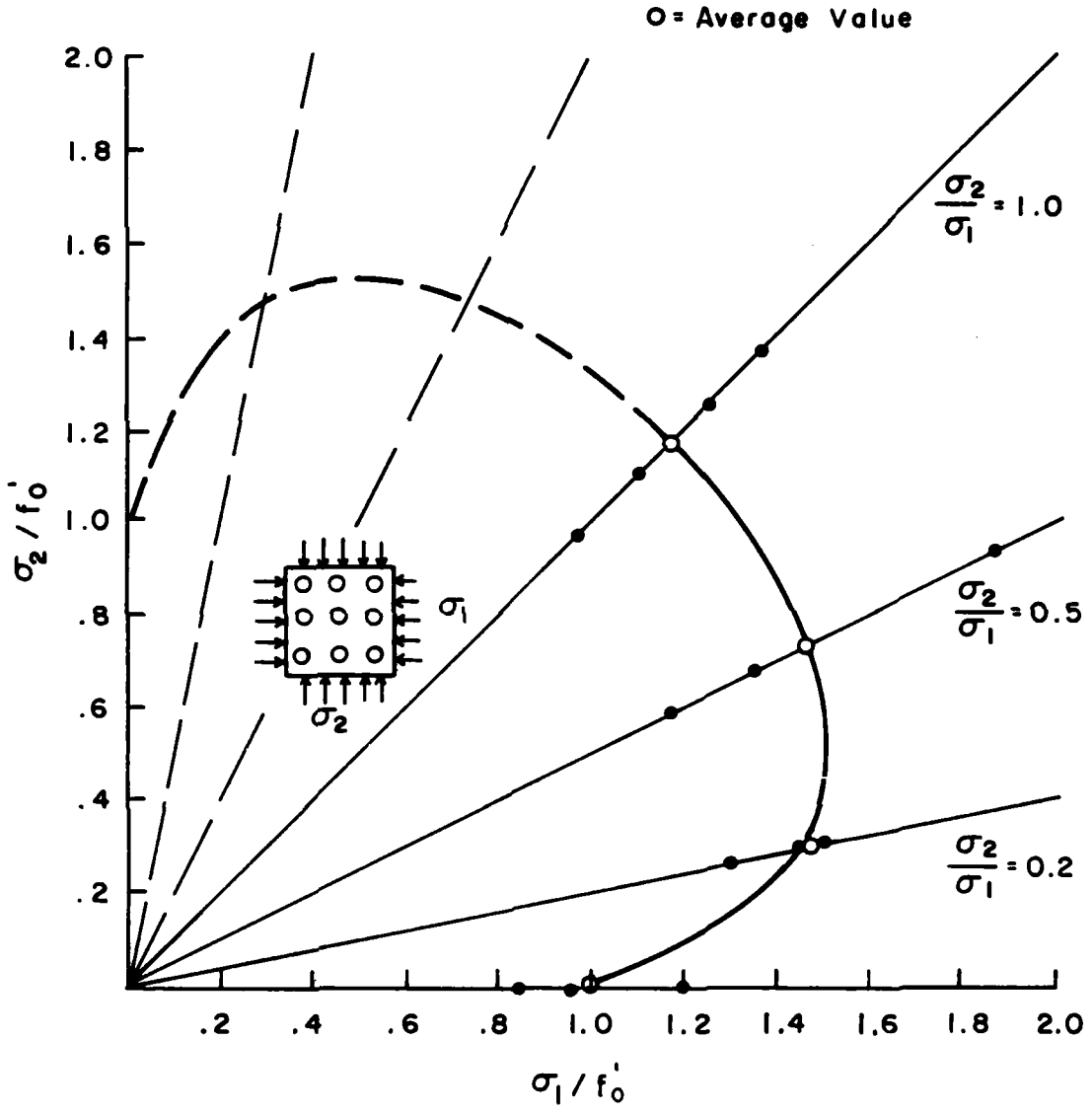

Figure 6.4 Biaxial Ultimate Strength Envelope for Model Specimen G1 Containing Granite Aggregate and Low Modulus Mortar

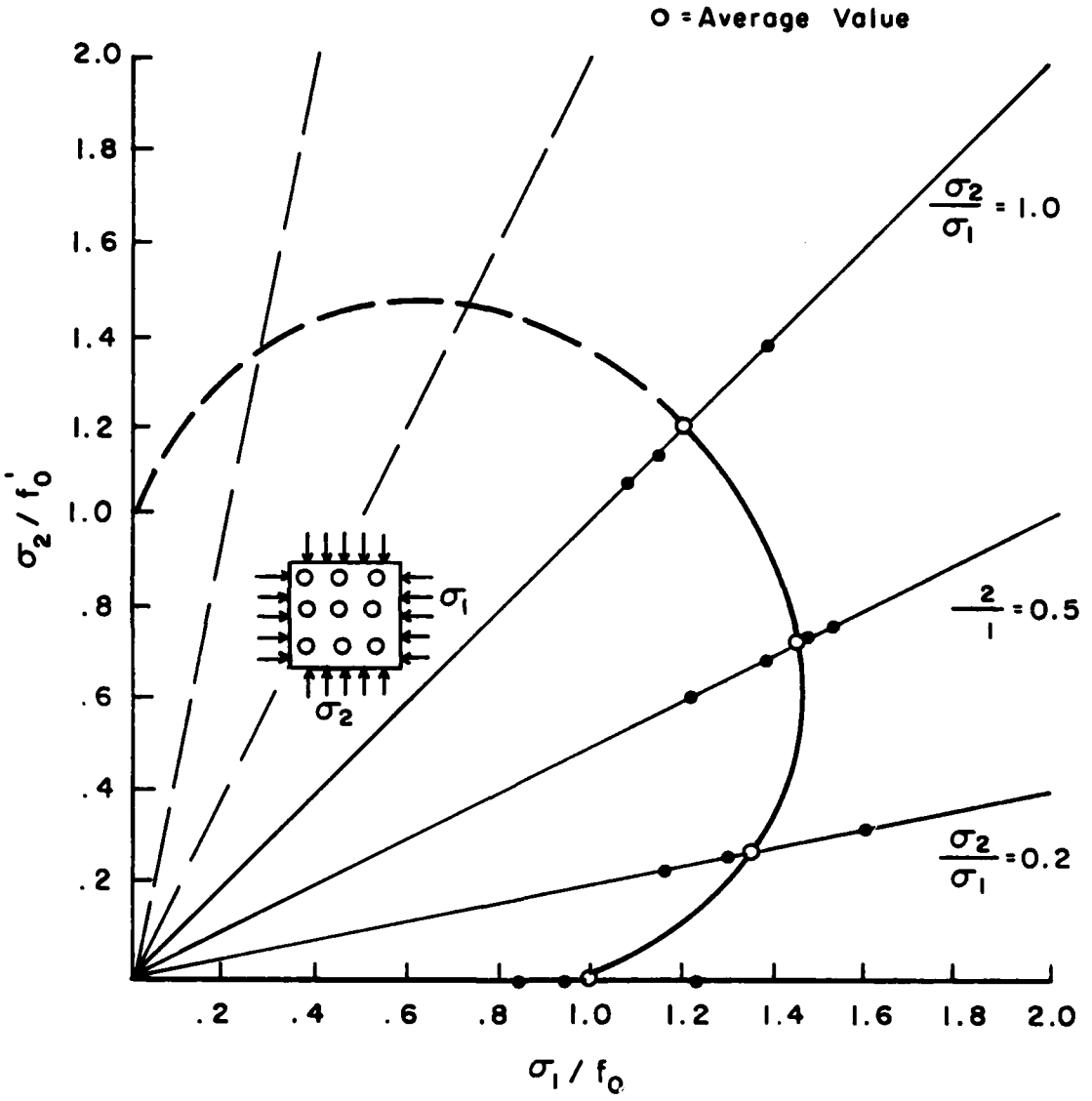

Figure 6.5 Biaxial Ultimate Strength Envelope for Model Specimen G2 Containing Granite Aggregate and Medium Modulus Mortar

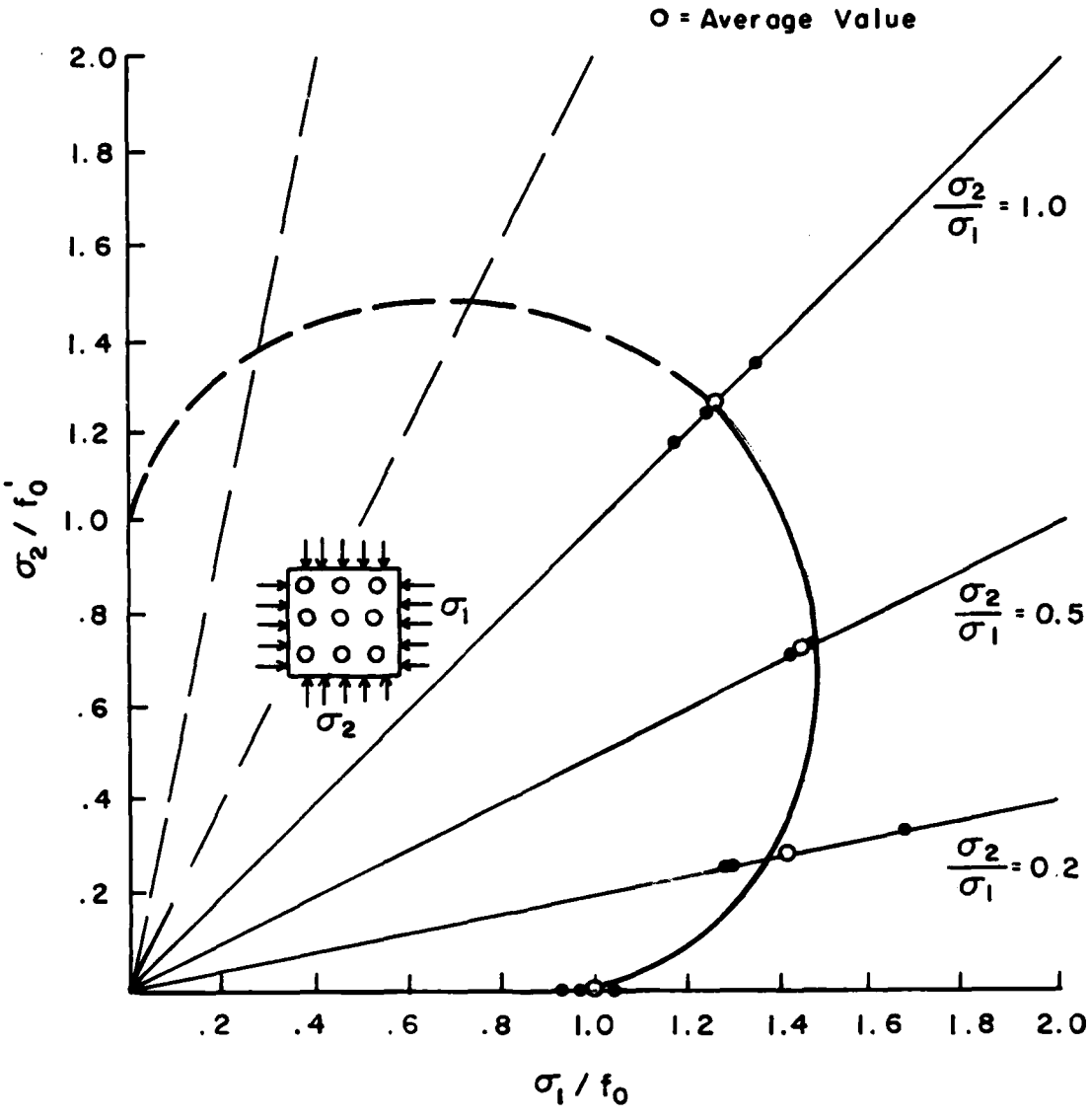

Figure 6.6 Biaxial Ultimate Strength Envelope for Model Specimen G3 Containing Granite Aggregate and High Modulus Mortar

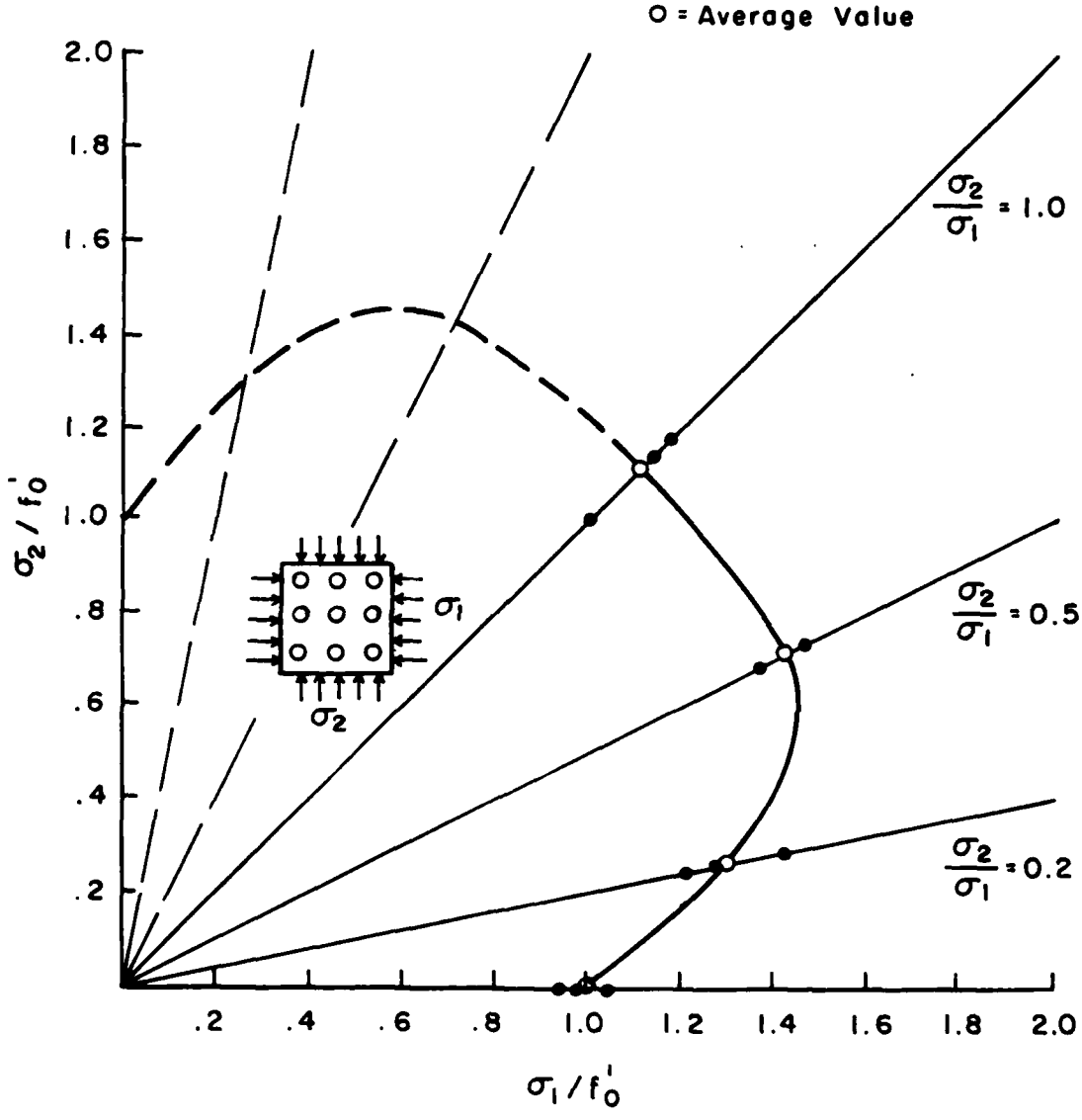

Figure 6.7 Biaxial Ultimate Strength Envelope for Model Specimen T1 Containing Traprock Aggregate and Low Modulus Mortar

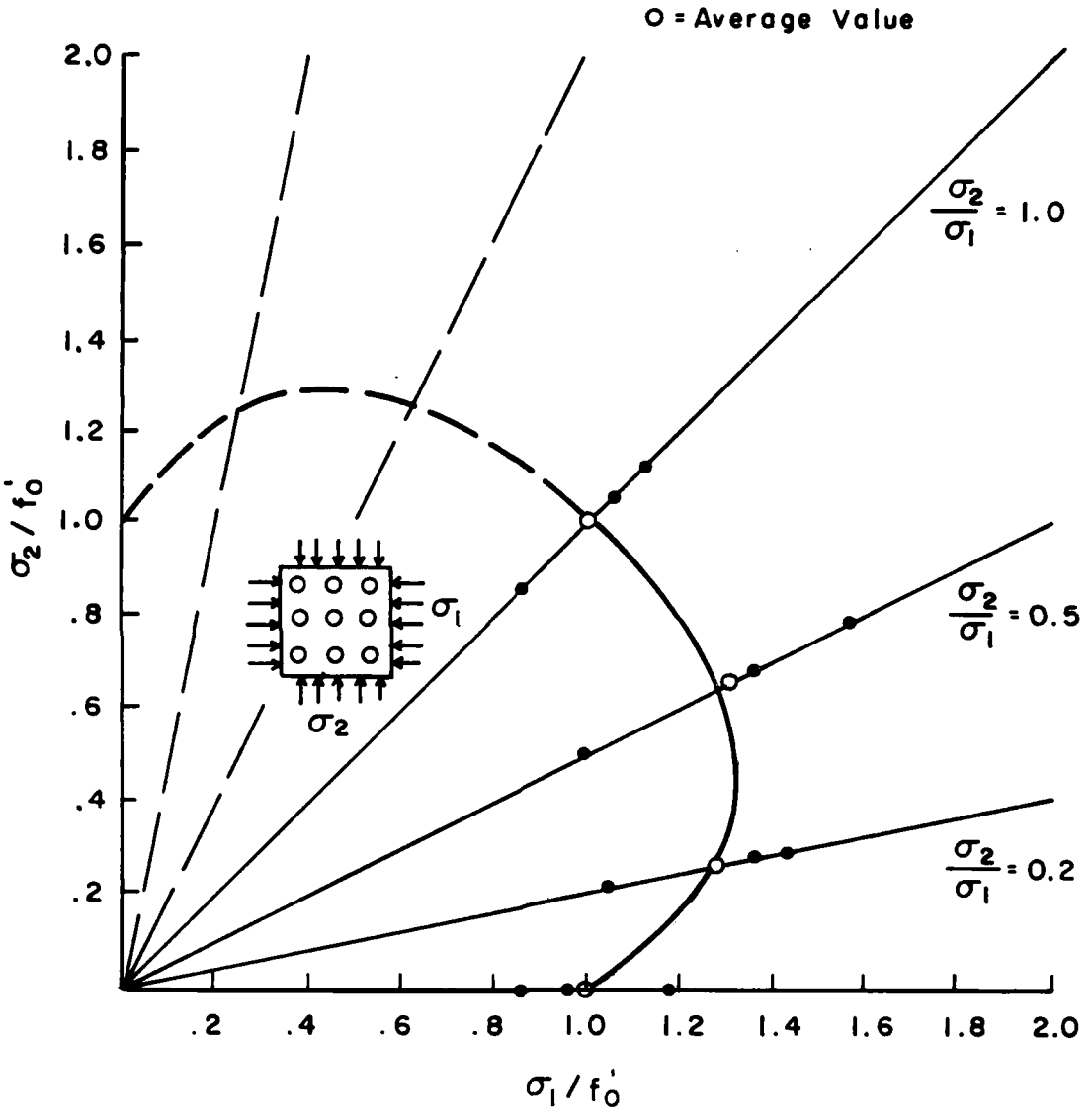

Figure 6.8 Biaxial Ultimate Strength Envelope for Model Specimen T2 Containing Traprock Aggregate and Medium Modulus Mortar

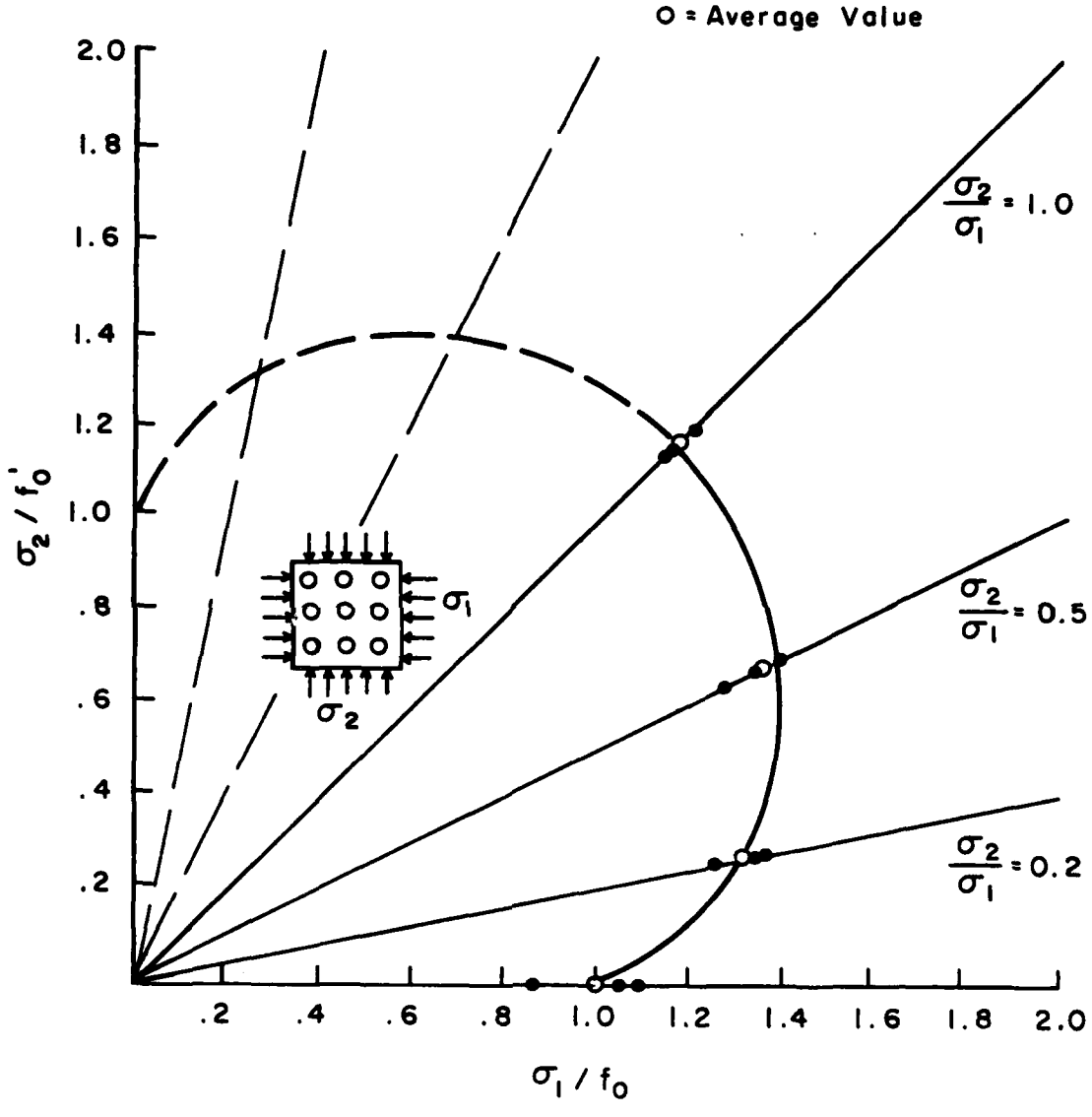

Figure 6.9 Biaxial Ultimate Strength Envelope for Model Specimen T3 Containing Traprock Aggregate and High Modulus Mortar

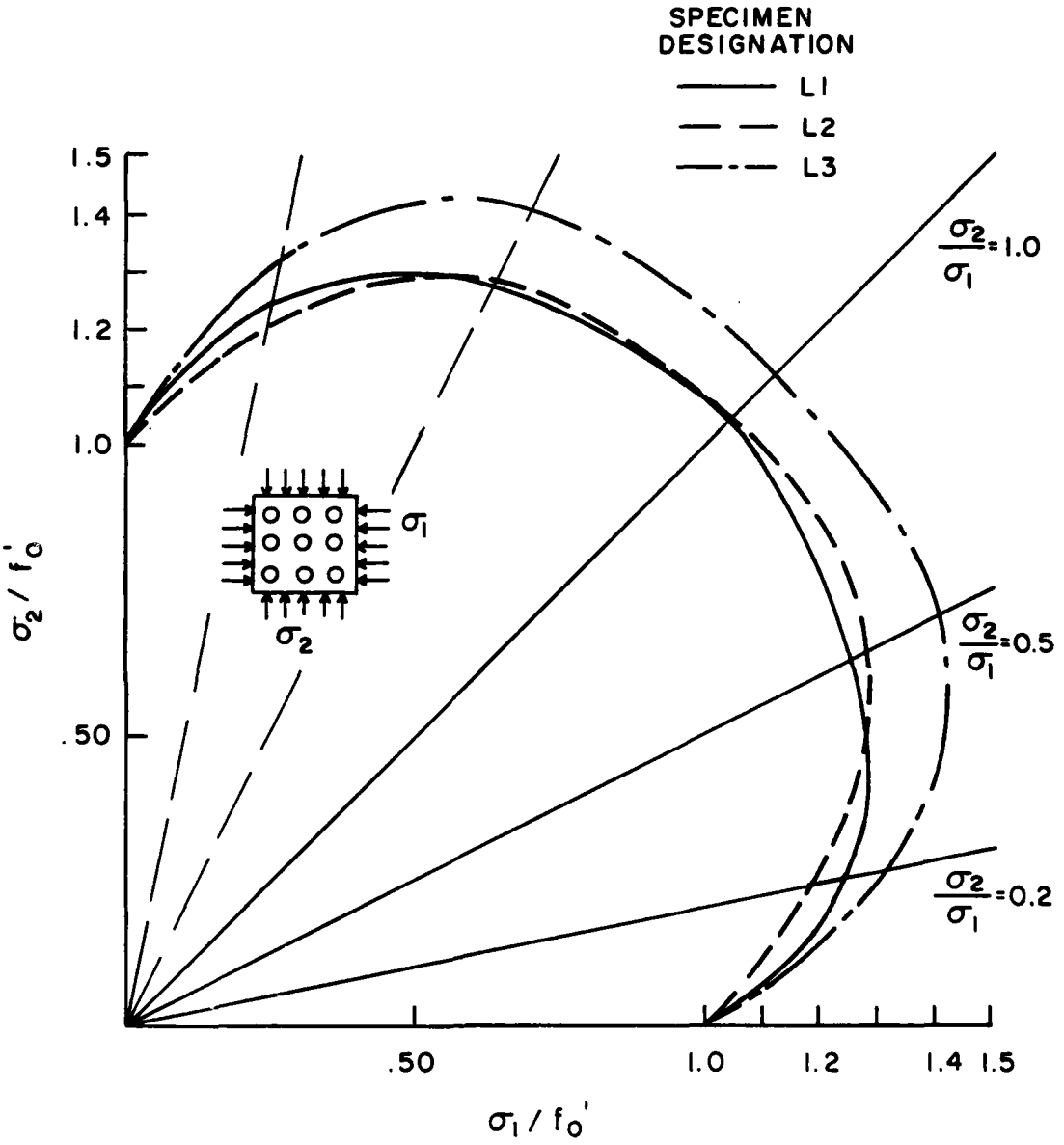

Figure 6.10 Biaxial Ultimate Strength Envelopes for Model Specimens with Limestone Aggregate

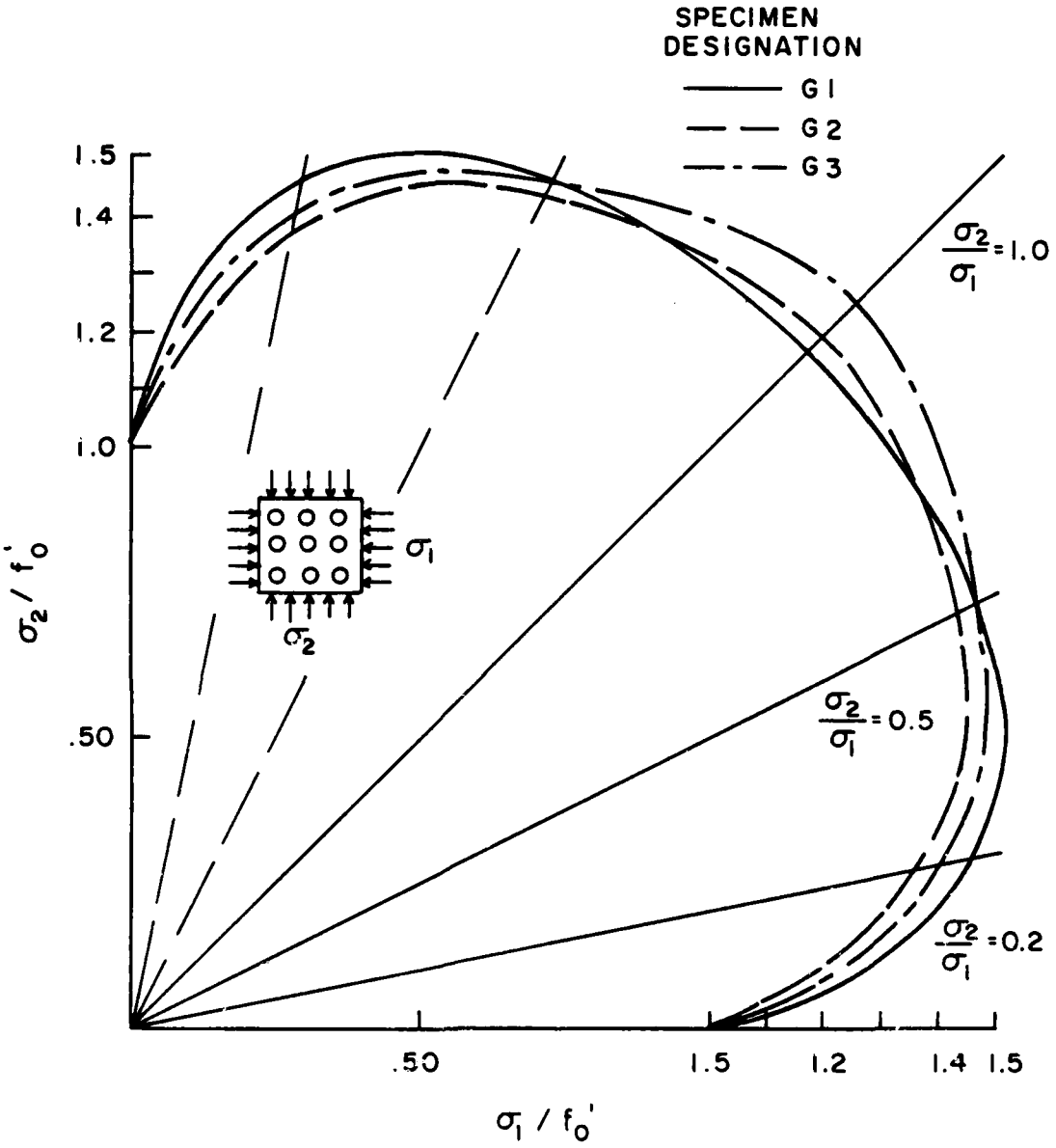

Figure 6.11 Biaxial Ultimate Strength Envelopes for Model Specimens with Granite Aggregate

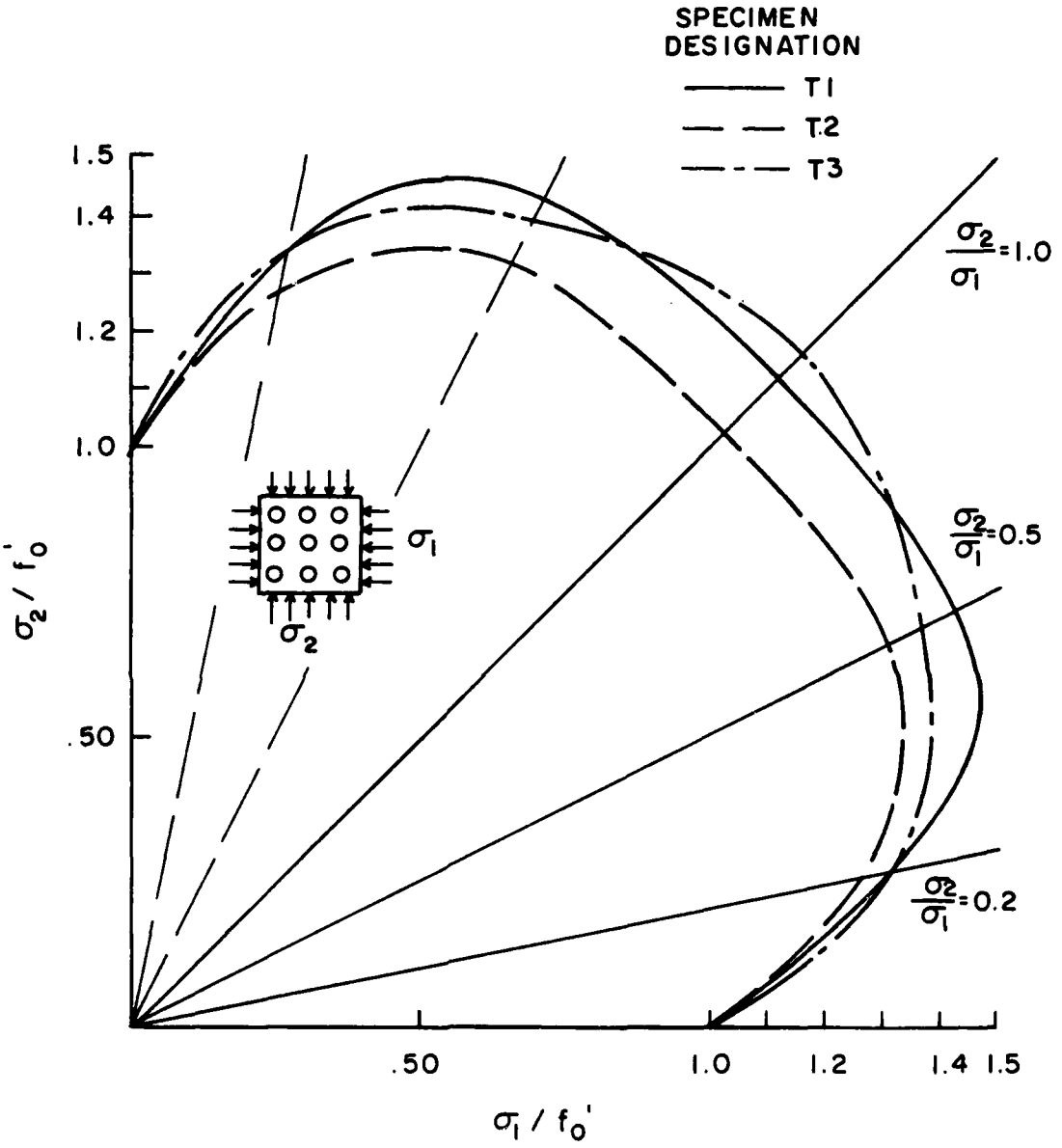

Figure 6.12 Biaxial Ultimate Strength Envelopes for Model Specimens with Traprock Aggregate

TABLE 6.1 AVERAGE RATIO OF ULTIMATE BIAXIAL TO ULTIMATE UNIAXIAL STRENGTH FOR SPECIMENS WITH LIMESTONE COARSE AGGREGATE

Stress Ratio	Specimen Designation		
	L1	L2	L3
$\sigma_2/\sigma_1 = 0.0$	1.0	1.0	1.0
$\sigma_2/\sigma_1 = 0.2$	1.29	1.15	1.33
$\sigma_2/\sigma_1 = 0.5$	1.21	1.29	1.41
$\sigma_2/\sigma_1 = 1.0$	1.09	1.08	1.13

TABLE 6.2 AVERAGE RATIO OF ULTIMATE BIAXIAL TO ULTIMATE UNIAXIAL STRENGTH FOR SPECIMENS WITH GRANITE COARSE AGGREGATE

Stress Ratio	Specimen Designation		
	G1	G2	G3
$\sigma_2/\sigma_1 = 0.0$	1.0	1.0	1.0
$\sigma_2/\sigma_1 = 0.2$	1.47	1.35	1.42
$\sigma_2/\sigma_1 = 0.5$	1.46	1.45	1.45
$\sigma_2/\sigma_1 = 1.0$	1.17	1.20	1.26

TABLE 6.3 AVERAGE RATIO OF ULTIMATE BIAXIAL TO ULTIMATE UNIAXIAL STRENGTH FOR SPECIMENS WITH TRAPROCK COARSE AGGREGATE

Stress Ratio	Specimen Designation		
	T1	T2	T3
$\sigma_2/\sigma_1 = 0.0$	1.0	1.0	1.0
$\sigma_2/\sigma_1 = 0.2$	1.30	1.28	1.32
$\sigma_2/\sigma_1 = 0.5$	1.43	1.31	1.34
$\sigma_2/\sigma_1 = 1.0$	1.11	1.02	1.16

6.1.3 Effect of Coarse Aggregate and Mortar Properties on Uniaxial Strength

Figure 6.13 presents a plot of average uniaxial strength of the model specimens, f'o, versus the compressive cylinder strength of the mortar used in the particular specimen. Overall, the uniaxial strength, f'o, of the model specimens remains practically constant as the strength of the mortar increases from 9500 to 12,500 psi (65.5 to 86.2 MN/m^2). As long as the mortar has a relatively high-strength, slight fluctuations in the mortar strength has only a minor effect on the uniaxial strength of the model specimens.

The uniaxial strength of the model specimens is plotted versus the ratio of modulus of elasticity of coarse aggregate to mortar in Fig. 6.14. There is a definite reduction in uniaxial strength as the E_a/E_m ratio drops below unity. This would seem to be the reason that the uniaxial strength of each mix using granite coarse aggregate was among the lowest observed, since the granite had a very low modulus of elasticity.

In general, the higher the modulus of elasticity of the aggregate, the higher the uniaxial strength that can be obtained. Also, the optimum E_a/E_m ratio increases as the modulus of the aggregate increases. It can be seen in Fig. 6.14 that the optimum E_a/E_m ratio is 0.61 for specimens using granite coarse aggregate, 1.22 for limestone, and 2.55 or greater for traprock.

6.1.4 Effect of Coarse Aggregate and Mortar Properties on Biaxial Strength

Figure 6.15 presents the relationship between the average maximum strength increase under biaxial compression and the modulus of elasticity ratio, E_a/E_m. With the exception of one mix using traprock coarse aggregate, there is a definite trend. The maximum strength increase becomes larger as E_a/E_m becomes smaller. This trend, when combined with the uniaxial results presented in the previous section, results in an almost constant maximum strength in biaxial compression

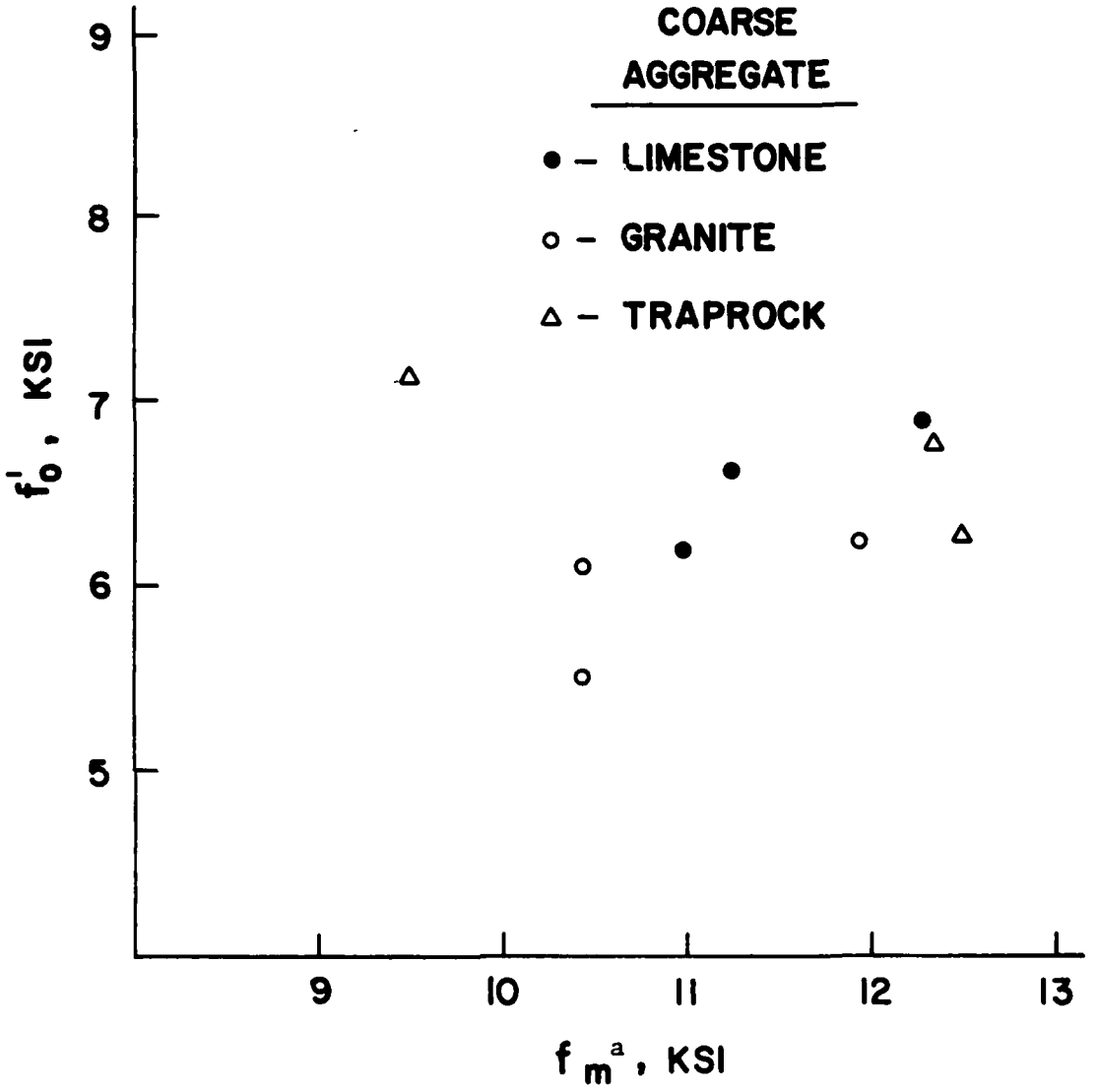

Figure 6.13 Average Uniaxial Compressive Strength of Model Specimens, f'o, versus Average Compressive Strength of Mortar

$^{a}f_{m}$ = average cylinder compressive strength of mortar

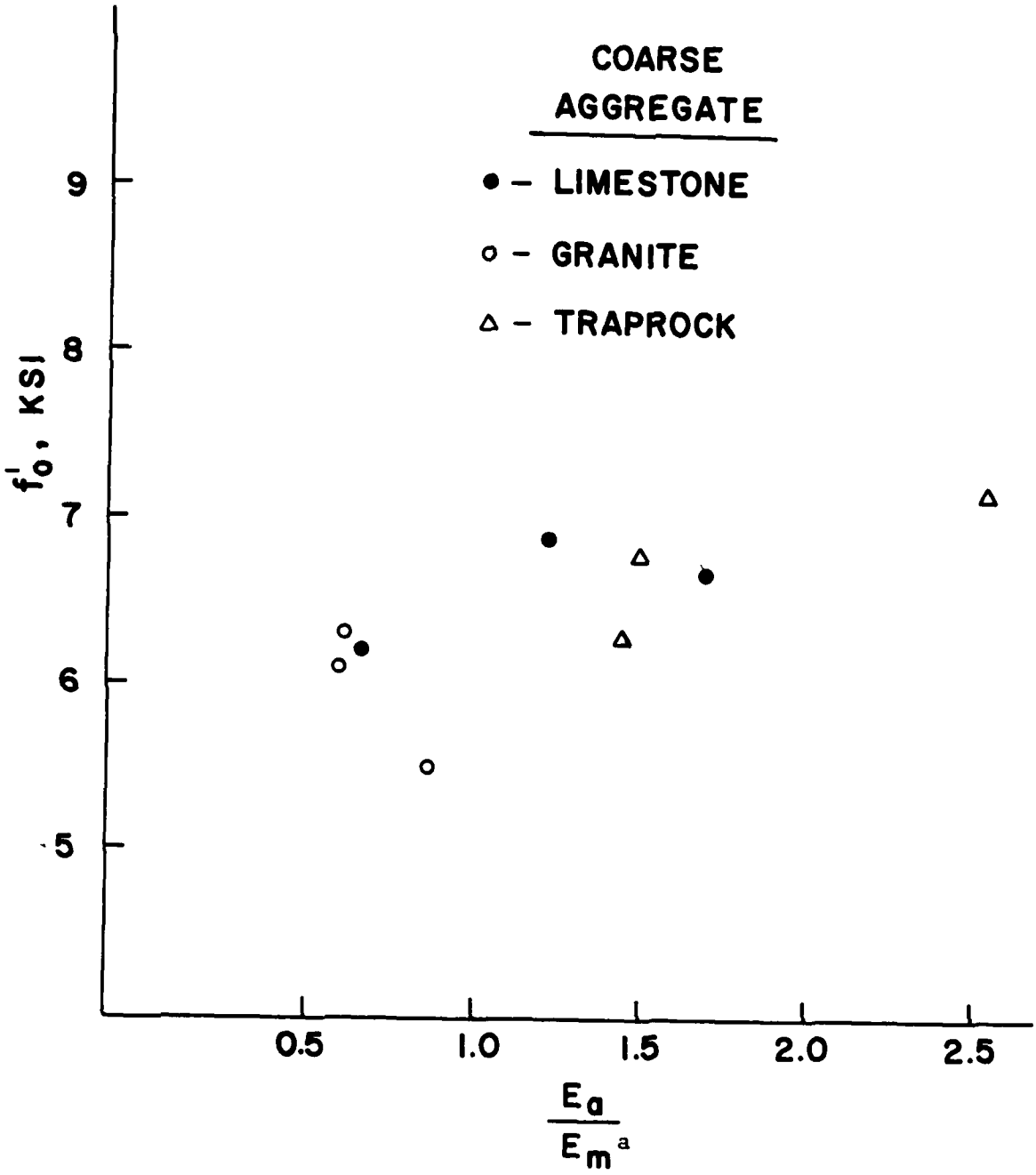

Figure 6.14 Average Uniaxial Strength of Model Specimens, f'o, versus Modulus of Elasticity Ratio of Coarse Aggregate to Mortar

$^{a}E_a$ = modulus of elasticity of coarse aggregate

E_m = modulus of elasticity of mortar

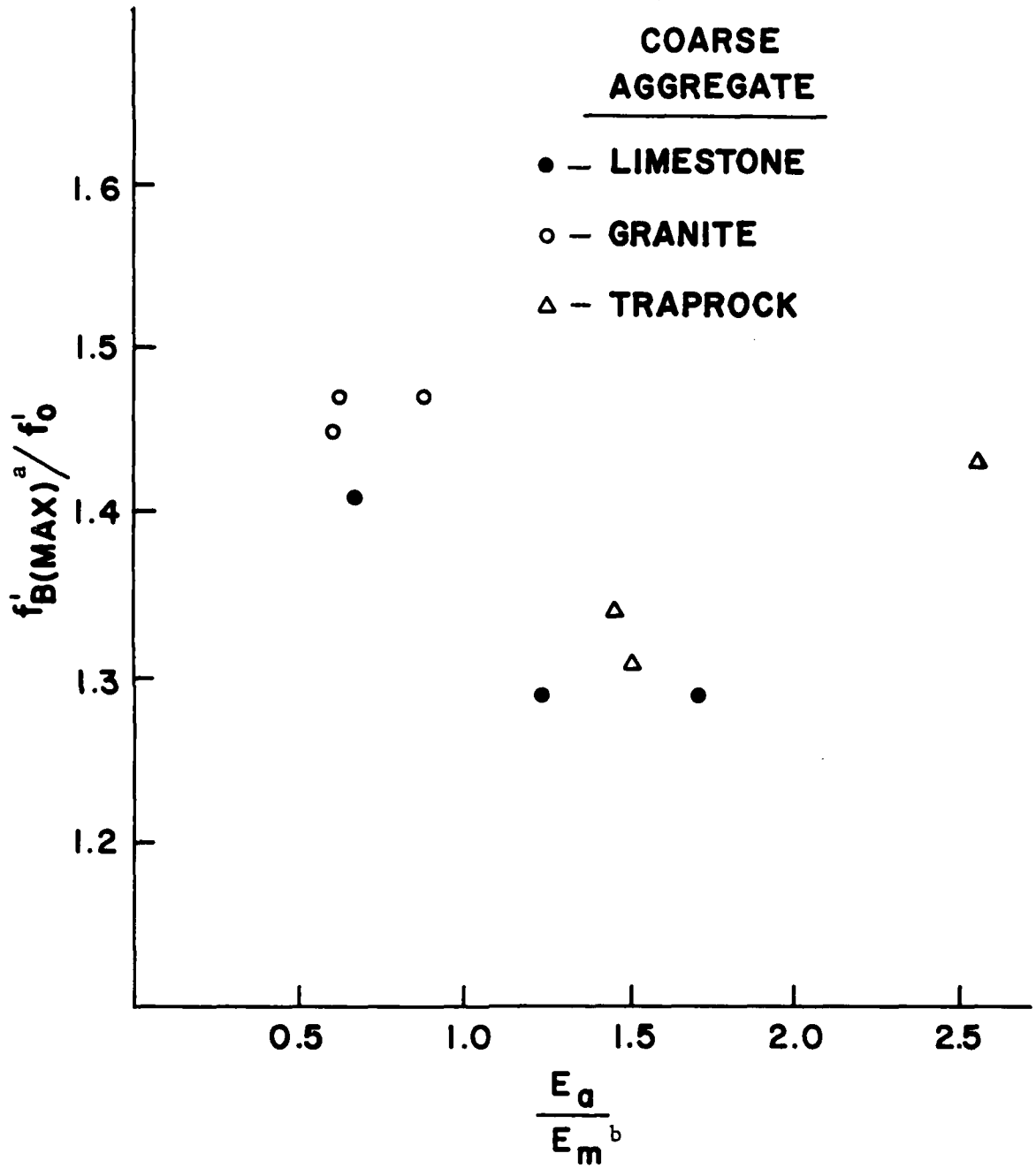

Figure 6.15 Ratio of Average Maximum Biaxial Strength to Average Uniaxial Strength, f'o, versus Modulus of Elasticity Ratio of Coarse Aggregate to Mortar

[a] $f'_{B(MAX)}$ = average maximum strength under biaxial compression

[b] E_a = modulus of elasticity of coarse aggregate

E_m = modulus of elasticity of mortar

in the range of 8050 to 9125 psi (55.5 to 62.9 MN/m^2), with the exception of the one traprock mix mentioned above. This is illustrated in Fig. 6.16.

The mixes using granite coarse aggregate, which has a low modulus of elasticity and, therefore, a relatively low E_a/E_m ratio, had the highest strength increase over the uniaxial strength, f'o, when subjected to biaxial stress. Even though the specimens using limestone and traprock coarse aggregate had higher uniaxial strengths, all of the specimens showed about the same biaxial compressive strengths since the granite specimens showed a higher increase in strength when subjected to biaxial stress.

6.2 STRESS-STRAIN CHARACTERISTICS

Typical stress-strain curves for all specimens tested are shown in Figs. 5.1 through 5.9.

6.2.1 Stiffness

The addition of a minor principal stress, σ_2, generally increases the stiffness of the model specimen in the major principal stress direction. A comparison of stiffnesses at different stress ratios for all specimens is presented in Table 6.4. Modulus of elasticity values were calculated as the secant modulus of elasticity up to forty percent of ultimate stress.

6.2.2 Effect of Coarse Aggregate and Mortar Properties on Stiffness

It can be observed from Table 6.4 that the average increase in stiffness in the major principal stress direction due to the minor principal stress is less for specimens with granite coarse aggregate than for either limestone or traprock. This behavior is due to the small Poisson's ratio and modulus of elasticity of the granite, as shown in Table 3.3.

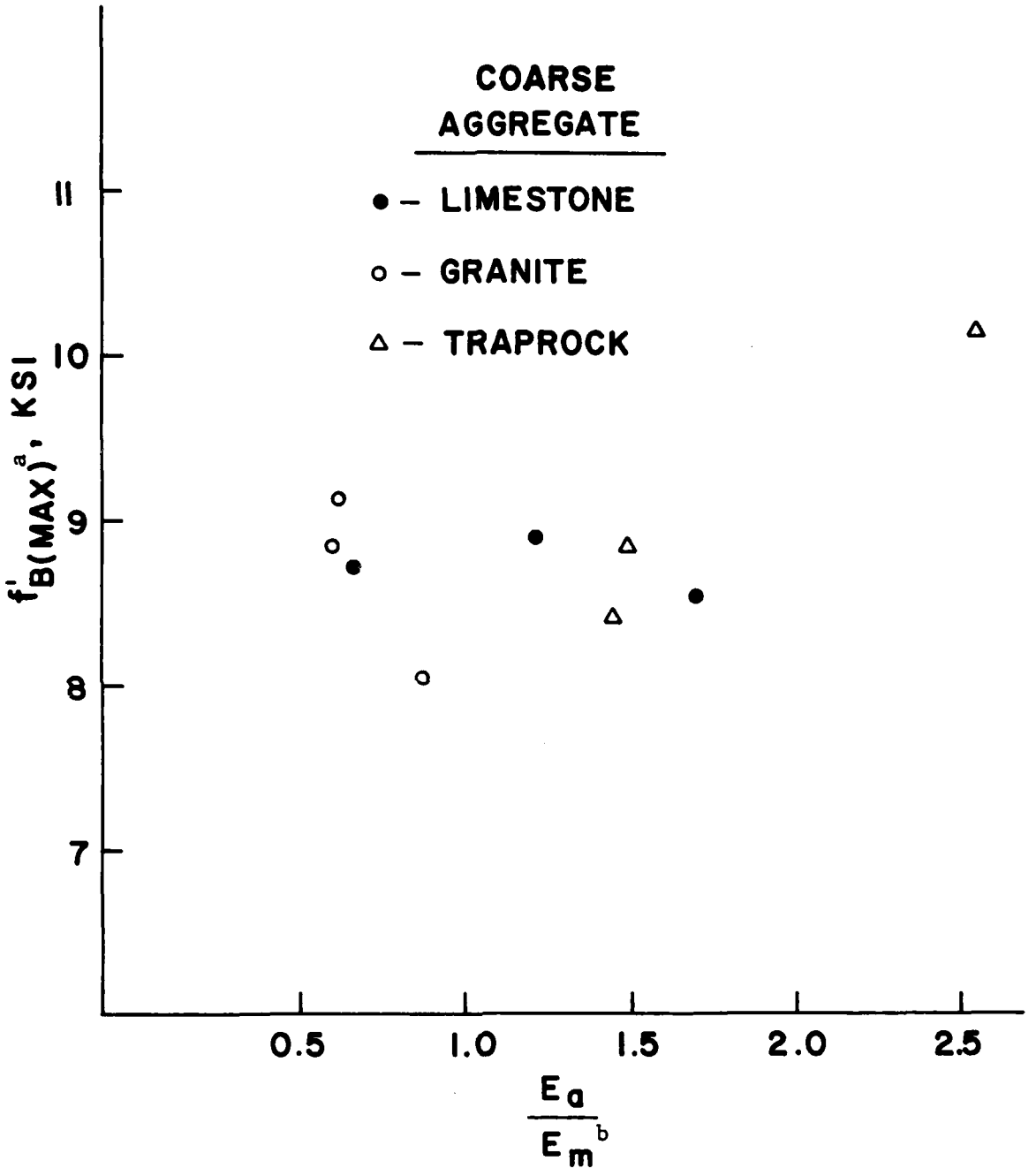

Figure 6.16 Average Maximum Strength under Biaxial Loading versus Modulus of Elasticity Ratio of Coarse Aggregate to Mortar

[a] $f'_{B(MAX)}$ = average maximum strength under biaxial compression

[b] E_a = modulus of elasticity of coarse aggregate

E_m = modulus of elasticity of mortar

TABLE 6.4 AVERAGE STIFFNESS RATIO[a] IN THE MAJOR PRINCIPAL STRESS DIRECTION FOR ALL SPECIMENS TESTED

Specimen Designation		Stress Ratio, σ_2/σ_1			
Coarse Aggregate	Mortar Mix	0.0	0.2	0.5	1.0
Limestone	1	1.0	1.19	1.45	1.57
	2	1.0	0.93	1.01	1.17
	3	1.0	1.05	1.06	1.32
Granite	1	1.0	1.00	1.07	1.14
	2	1.0	0.88	0.95	1.03
	3	1.0	0.95	1.09	1.27
Traprock	1	1.0	1.01	1.05	1.21
	2	1.0	1.15	1.25	1.54
	3	1.0	1.00	1.02	1.48

[a]ratio of modulus of elasticity in the major principal stress direction under biaxial state of stress to that under uniaxial compression

6.2.3 Proportional Limit

The addition of a stress in the minor principal stress direction, σ_2, affects the shape of the stress-strain curve in the major principal stress direction. Proportional limit values were calculated for each test, defined as the point at which the stress-strain curve deviates by three percent from the initial tangent line. The average proportional limit stress for all specimens is given in Table 6.5. As the σ_2 stress is increased the proportional limit stress is also increased. Therefore, as the principal stress ratio (σ_2/σ_1) is increased, the stress-strain curve in the major principal stress direction becomes linear up to a higher stress-strength ratio.

A major cause for the non-linearity of the stress-strain curve for concrete is internal microcracking. It was observed in previous studies at Cornell University that, under uniaxial loading, microcracks were formed parallel to the major principal stress, σ_1, and perpendicular to the face of the specimen (23, 24). The microcracks begin as bond cracks at the aggregate-mortar interface, and ultimately propogate through the mortar matrix to cause failure. The addition of a stress in the minor principal stress direction, σ_2, prevents these microcracks from propogating. Adding a stress in the minor principal stress direction results in a stiffer, more linear stress-strain response in the major principal stress direction.

The proportional limit is given as a percentage of the ultimate strength for the uniaxial loading case in Table 6.6 for all specimens. Values range from 54 to 66 percent for the concrete models using limestone, 68 to 84 percent for granite, and 57 to 62 percent for traprock. Previous tests at the University of Texas at Austin on normal strength concrete model specimens indicate that the proportional limit under uniaxial load was between forty and 43 percent of the ultimate load (28). The high-strength concrete model specimens behave elastically to a higher percentage of ultimate stress than the normal strength concrete models. This agrees with the findings of Carrasquillo, et al (35), who stated, "The stress-strain curve for

TABLE 6.5 AVERAGE PROPORTIONAL LIMIT STRESS (PSI)
FOR ALL SPECIMENS TESTED

Specimen Designation		Stress Ratio, σ_2/σ_1			
Coarse Aggregate	Mortar Mix	0.0	0.2	0.5	1.0
Limestone	1	4350 (1.0)	5450 (1.25)	-[a]	6250 (1.44)
	2	-[a]	4950	5550	6700
	3	3367 (1.0)	4967 (1.48)	5200 (1.54)	5250 (1.56)
Granite	1	4633 (1.0)	5250 (1.13)	5667 (1.22)	5813 (1.25)
	2	4900 (1.0)	6983 (1.43)	7633 (1.56)	6683 (1.36)
	3	4425 (1.0)	6200 (1.40)	6675 (1.51)	7600 (1.72)
Traprock	1	4067 (1.0)	5483 (1.35)	5775 (1.42)	7350 (1.81)
	2	4133 (1.0)	5033 (1.22)	4667 (1.13)	4250 (1.03)
	3	3850 (1.0)	5600 (1.46)	5867 (1.52)	6600 (1.71)

[a] proportional limit not obtained

NOTE: Value in parentheses refers to the ratio of biaxial proportional limit to the uniaxial proportional limit

TABLE 6.6 AVERAGE RATIO OF PROPORTIONAL LIMIT STRESS TO ULTIMATE STRENGTH FOR MODEL SPECIMENS TESTED UNDER UNIAXIAL COMPRESSION ($\sigma_2/\sigma_1 = 0.0$)

Specimen Designation		$\sigma_{PL}/f'o^a$, percent
Coarse Aggregate	Mortar Mix	
Limestone	1	65.9
	2	-[b]
	3	54.3
Granite	1	83.9
	2	79.5
	3	68.2
Traprock	1	56.8
	2	59.8
	3	62.4

[a] σ_{PL} = proportional limit stress

[b] proportional limit not obtained

AD-A126 442 BEHAVIOR OF A HIGH STRENGTH CONCRETE MODEL SUBJECTED TO BIAXIAL COMPRESSION(U) TEXAS UNIV AT AUSTIN DEPT OF CIVIL ENGINEERING J C HERRIN ET AL. DEC 82 2/2

UNCLASSIFIED AFOSR-TR-83-0137 AFOSR-81-0202 F/G 11/2 NL

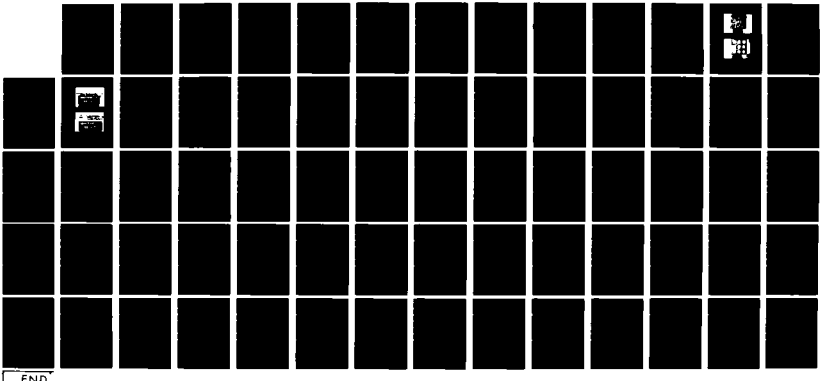

END

FILMED

DTIC

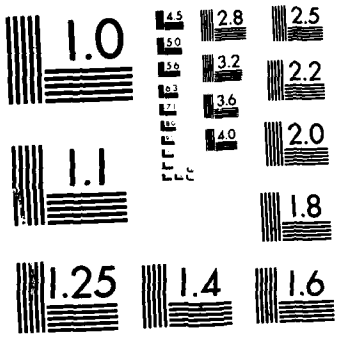

high-strength concrete is steeper and more linear to a higher stress-strength ratio."

6.2.4 Effect of Coarse Aggregate and Mortar Properties on the Proportional Limit

Under uniaxial loading the proportional limit, given as a percentage of the uniaxial strength, f'o, generally decreases as the coarse aggregate becomes stiffer relative to the mortar. Figure 6.17 shows the proportional limit, presented as a percentage of the uniaxial strength, f'o, versus the modulus of elasticity ratio of coarse aggregate to mortar. However, when considering specimens containing the same coarse aggregate, the proportional limit increases as the E_a/E_m ratio approaches unity for all types of coarse aggregate. This indicates that as the stiffness of the coarse aggregate inclusions approaches the stiffness of the mortar, the microcracking at the aggregate-mortar interface due to stress concentrations is reduced. The result is a stress-strain curve which is linear up to a higher stress-strength ratio.

No correlation was observed between the increase in proportional limit due to biaxial stress and the coarse aggregate or mortar elastic properties. In general, for all specimens tested, the higher the biaxial stress ratio, the larger the proportional limit stress to uniaxial strength ratio.

6.2.5 Discontinuity

The stage at which severe microcracking takes place in concrete has been termed the discontinuity point by Newman (34). The discontinuity point in brittle materials is analogous to the yield point in ductile materials. Many procedures have been used to calculate the discontinuity point. It has been defined as: a) the stage when there was a marked deviation from linearity of the load-pulse velocity curve, b) the point at which the volumetric strain begins to increase, and c) the point at which there is a significant deviation from linearity in the stress-strain behavior.

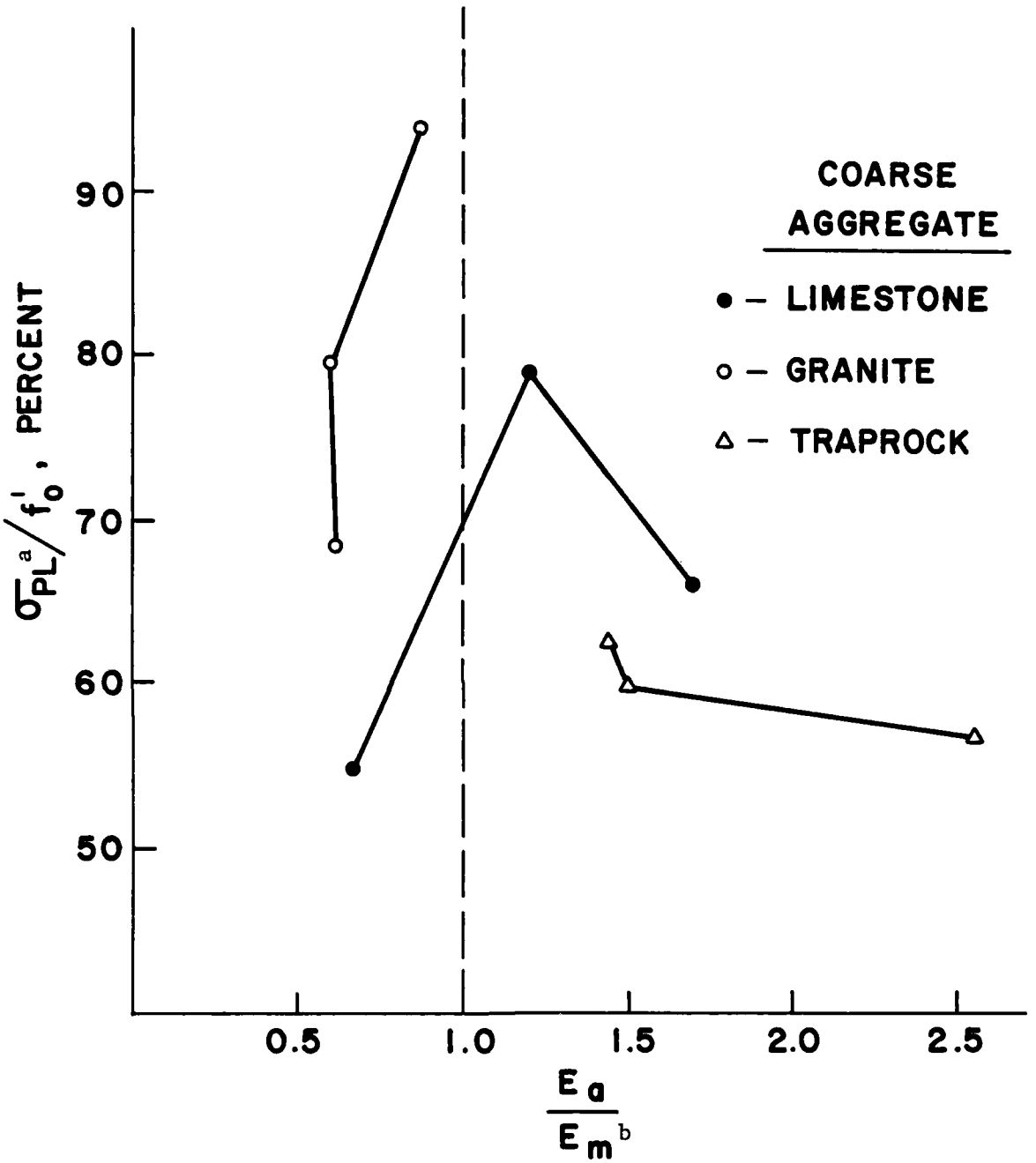

Figure 6.17 Average Proportional Limit as a Percent of the Uniaxial Strength versus Modulus of Elasticity Ratio of Coarse Aggregate to Mortar

[a] σ_{PL} = proportional limit stress

[b] E_a = modulus of elasticity of coarse aggregate

E_m = modulus of elasticity of mortar

A method similar to the latter was used to calculate the discontinuity point in the present study. It has been suggested that the discontinuity point in uniaxial compression occurs at the point at which Poisson's ratio begins to increase significantly (35, 36). This method has been used by previous investigators (24,25,28,29,30) and is used in this study to calculate the discontinuity point for specimens tested in uniaxial compression.

Typical Poisson's ratio versus applied stress, expressed as a percentage of the uniaxial compressive strength, are presented in Figs. 6.18 through 6.20 for all specimens tested in uniaxial compression. The average discontinuity point is given as a percentage of the uniaxial strength in Table 6.7 for all specimens tested. The discontinuity point for specimens tested under uniaxial compression was of the order of eighty to 87 percent of the uniaxial strength for specimens with limestone or granite coarse aggregate, and seventy to eighty percent for specimens with traprock.

Khana (28) and Liu (24) both performed tests on normal strength model specimens. The discontinuity point under uniaxial compression was found to be seventy and sixty percent, respectively. In tests on real normal strength concrete plate specimens, Tasuji (25) and Park (29) calculated discontinuity to occur at 74 and seventy percent of the uniaxial compressive strength, respectively.

It can be seen that in high-strength concrete models, the discontinuity point occurs at a higher percentage of the ultimate uniaxial compressive strength than normal strength concrete model specimens. This agrees with the findings of Carrasquillo, et al (35, 36).

The discontinuity point cannot be determined for the specimens tested under biaxial compression using the Poisson's ratio method. The principal strain ratio ($\varepsilon_2/\varepsilon_1$), which corresponds to the Poisson's ratio for the uniaxial case, remains constant throughout the tests under biaxial compression due to the application of the minor principal stress. However, it has been determined that the discontinuity point becomes larger under biaxial compression (25). The proportional limit

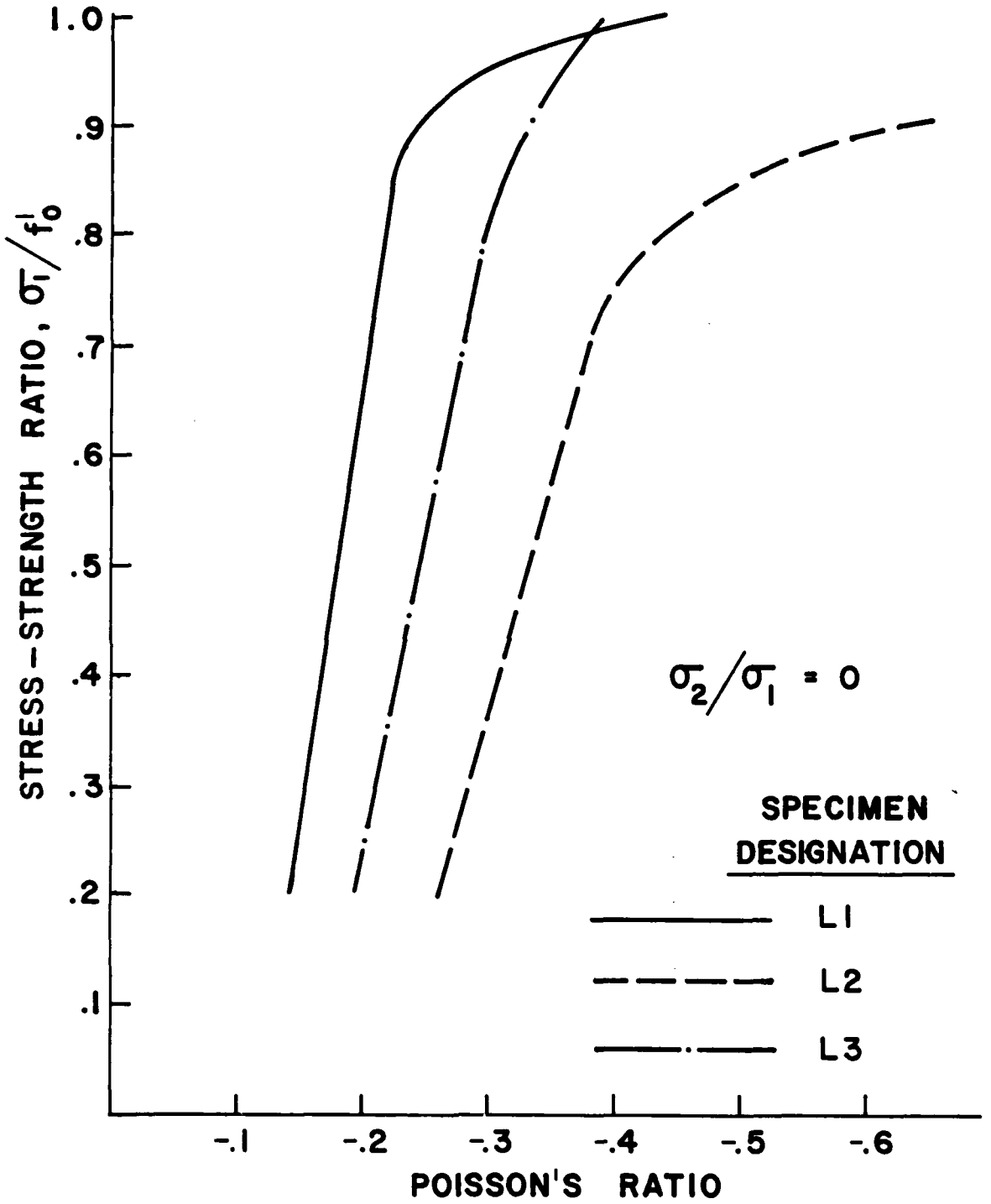

Figure 6.18 Typical Poisson's Ratio versus Applied Stress Expressed as a Percent of the Compressive Strength for Specimens with Limestone Coarse Aggregate Tested Under Uniaxial Compression

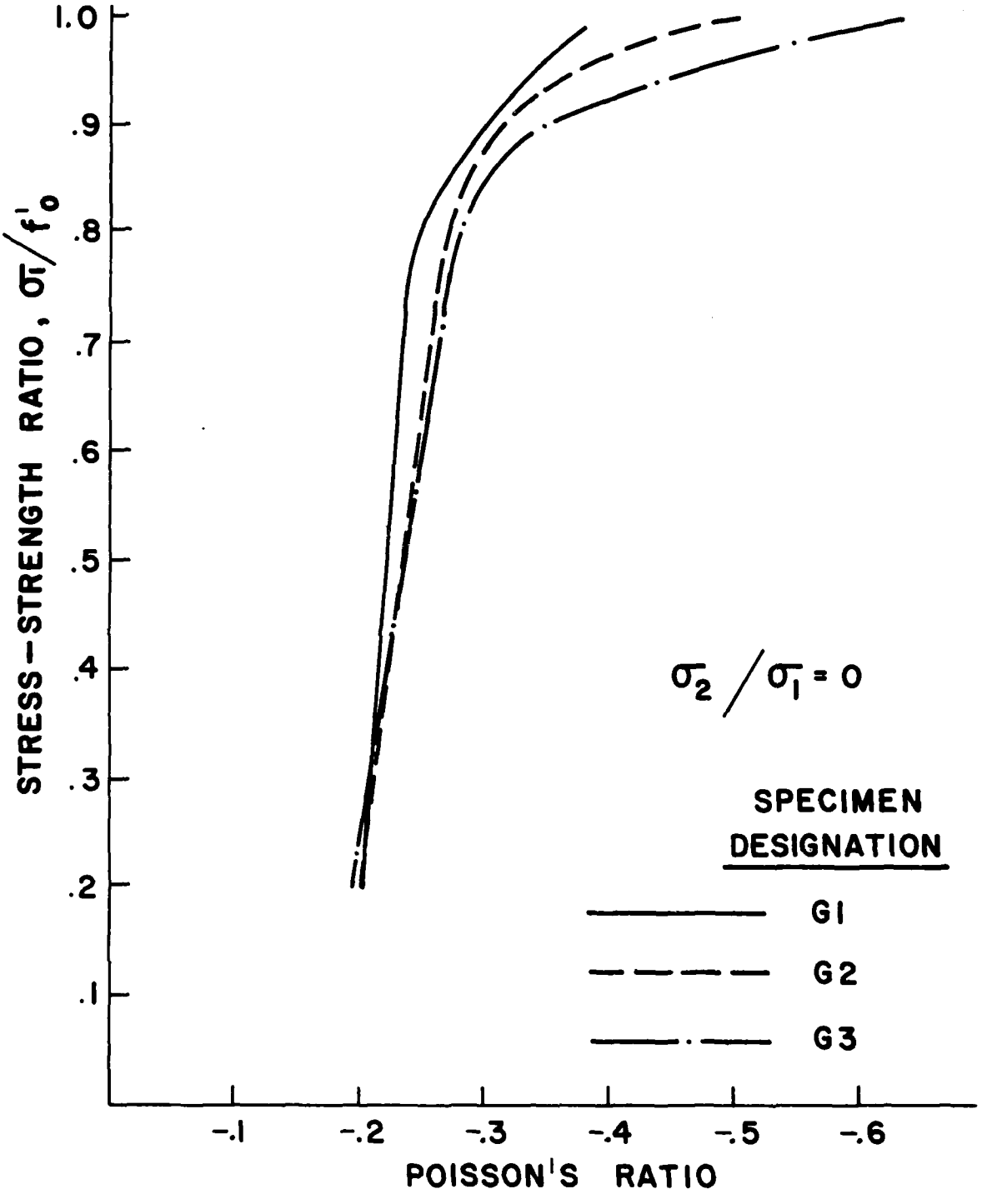

Figure 6.19 Typical Poisson's Ratio versus Applied Stress Expressed as a Percent of the Compressive Strength for Specimens with Granite Coarse Aggregate Tested Under Uniaxial Compression

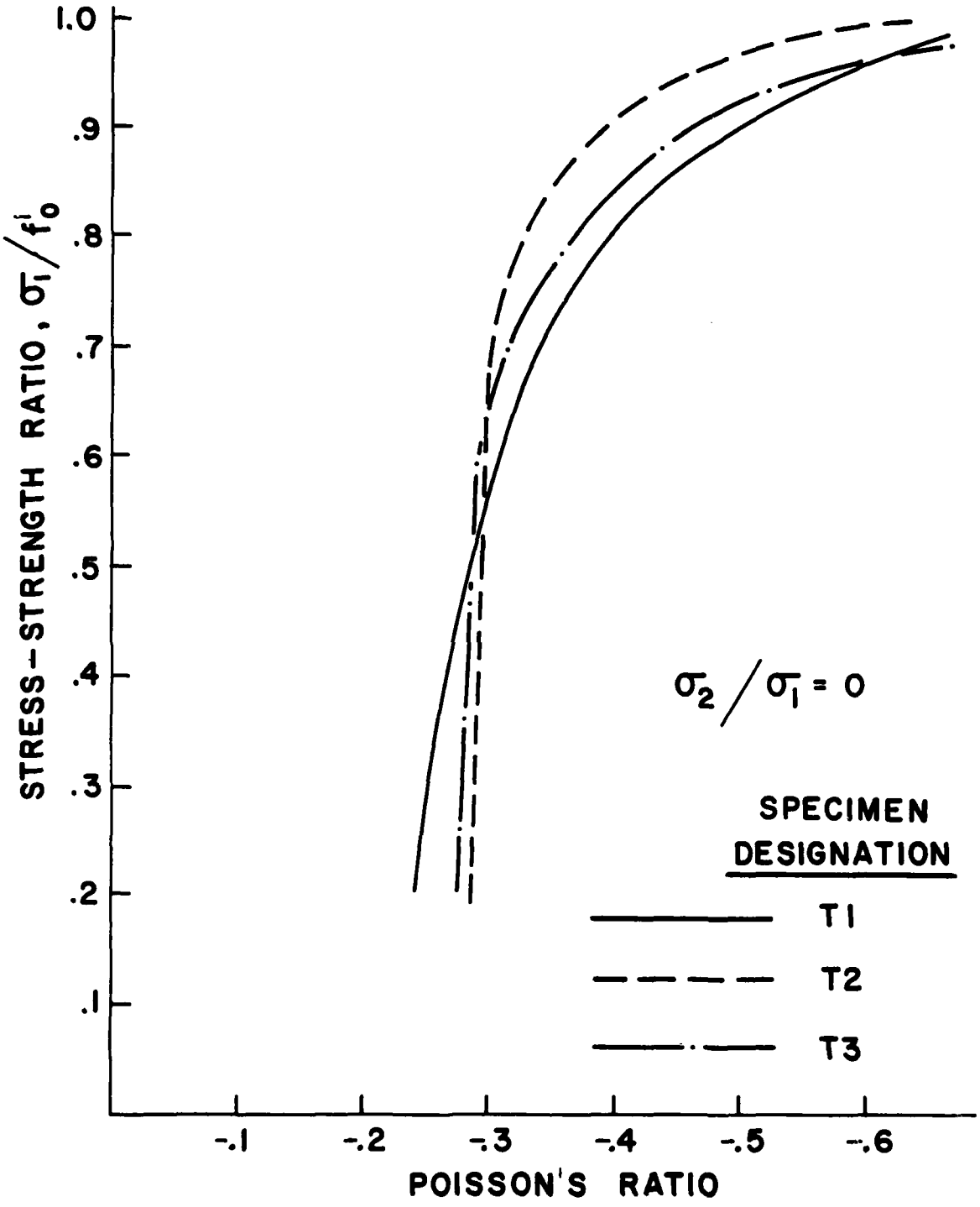

Figure 6.20 Typical Poisson's Ratio versus Applied Stress Expressed as a Percent of the Compressive Strength for Specimens with Traprock Coarse Aggregate Tested Under Uniaxial Compression

TABLE 6.7 AVERAGE DISCONTINUITY POINT FOR ALL SPECIMENS TESTED UNDER UNIAXIAL COMPRESSION ($\sigma_2/\sigma_1 = 0.0$)

Specimen Designation		$\sigma_D/f'o$,[a] percent
Coarse Aggregate	Mortar Mix	
Limestone	1	80
	2	87
	3	80
Granite	1	87
	2	80
	3	80
Traprock	1	70
	2	80
	3	70

[a] σ_D = stress at the discontinuity point

values, given in Table 6.5, increase as the biaxial stress ratio increases. This suggests that the discontinuity point also increases as the biaxial stress ratio increases.

6.2.6 Effect of Coarse Aggregate and Mortar Properties on the Discontinuity Point

Figure 6.21 shows a plot of the average discontinuity point for all specimens tested under uniaxial compression versus the modulus of elasticity ratio of coarse aggregate to mortar. The highest discontinuity point values occur as E_a/E_m approaches unity. The discontinuity point decreases as E_a/E_m deviates from unity.

Under uniaxial stress, microcracking initiates at the aggregate-mortar interface and propogates into the mortar matrix to cause failure (23, 24). It seems that as the stiffness of the coarse aggregate inclusions approaches the stiffness of the mortar the two materials behave more homogeneously. The stress concentrations caused by the coarse aggregate inclusions become smaller as the aggregate stiffness approaches the mortar stiffness. Therefore, the initial microcracks at the aggregate-mortar interface become less pronounced, resulting in a concrete model with a higher discontinuity point.

6.3 FAILURE MODES

The failure modes observed in this study agree with the observed failure modes in previous biaxial compression studies using plate specimens (22,23,24,25,28,29). Failure in uniaxial compression was due to cracks which formed parallel to the applied load and perpendicular to the face of the specimen, as illustrated in Fig. 6.22. Typical uniaxial failures are shown in Fig. 6.23. In general, the cracks propogated through the mortar and along the aggregate-mortar interface without breaking the aggregate discs. However, a few of the lower strength granite and limestone discs cracked at failure in uniaxial compression.

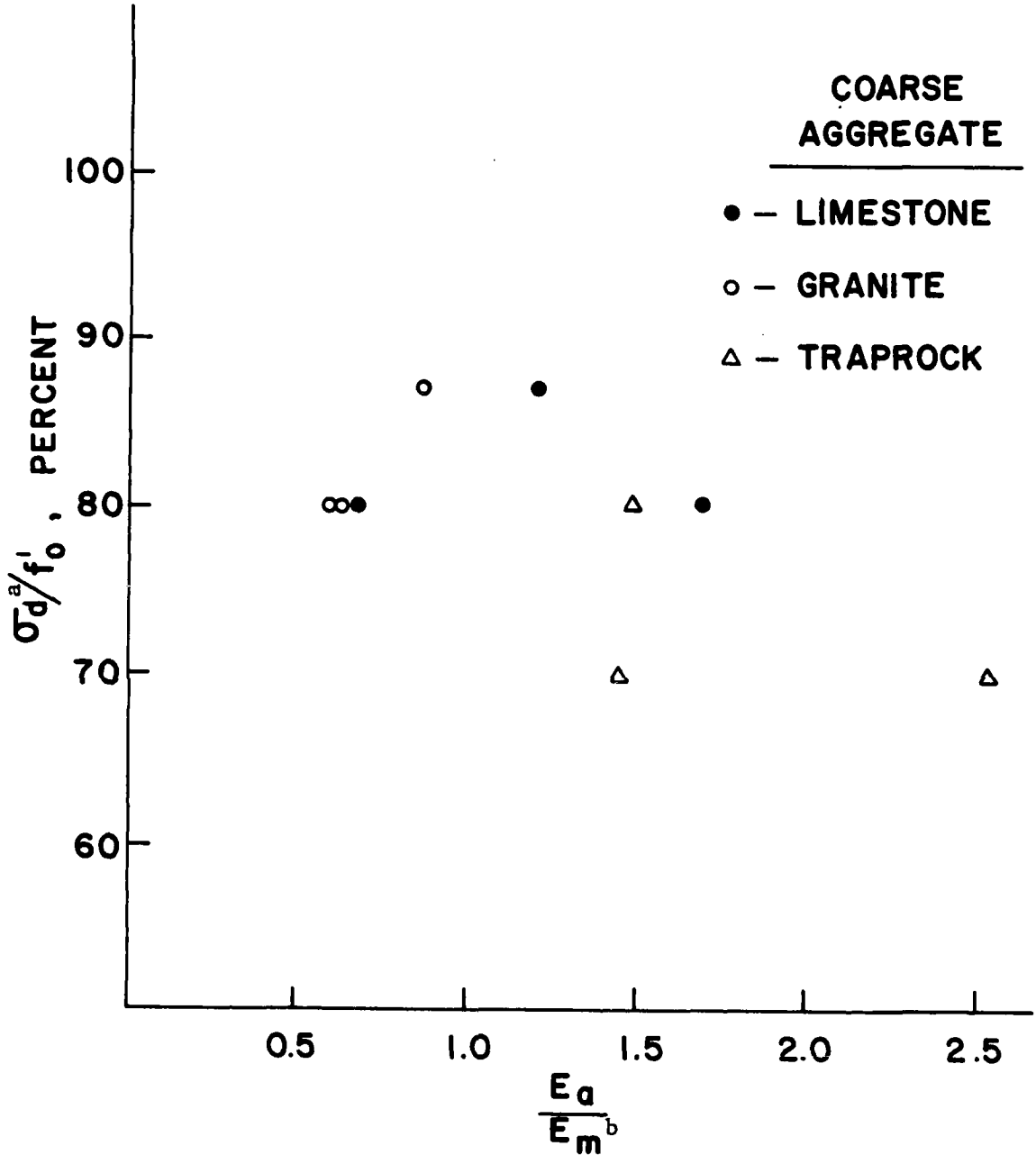

Figure 6.21 Average Discontinuity Point versus Modulus of Elasticity Ratio of Coarse Aggregate to Mortar

[a] σ_D = discontinuity point

[b] E_a = modulus of elasticity of coarse aggretate

E_m = modulus of elasticity of mortar

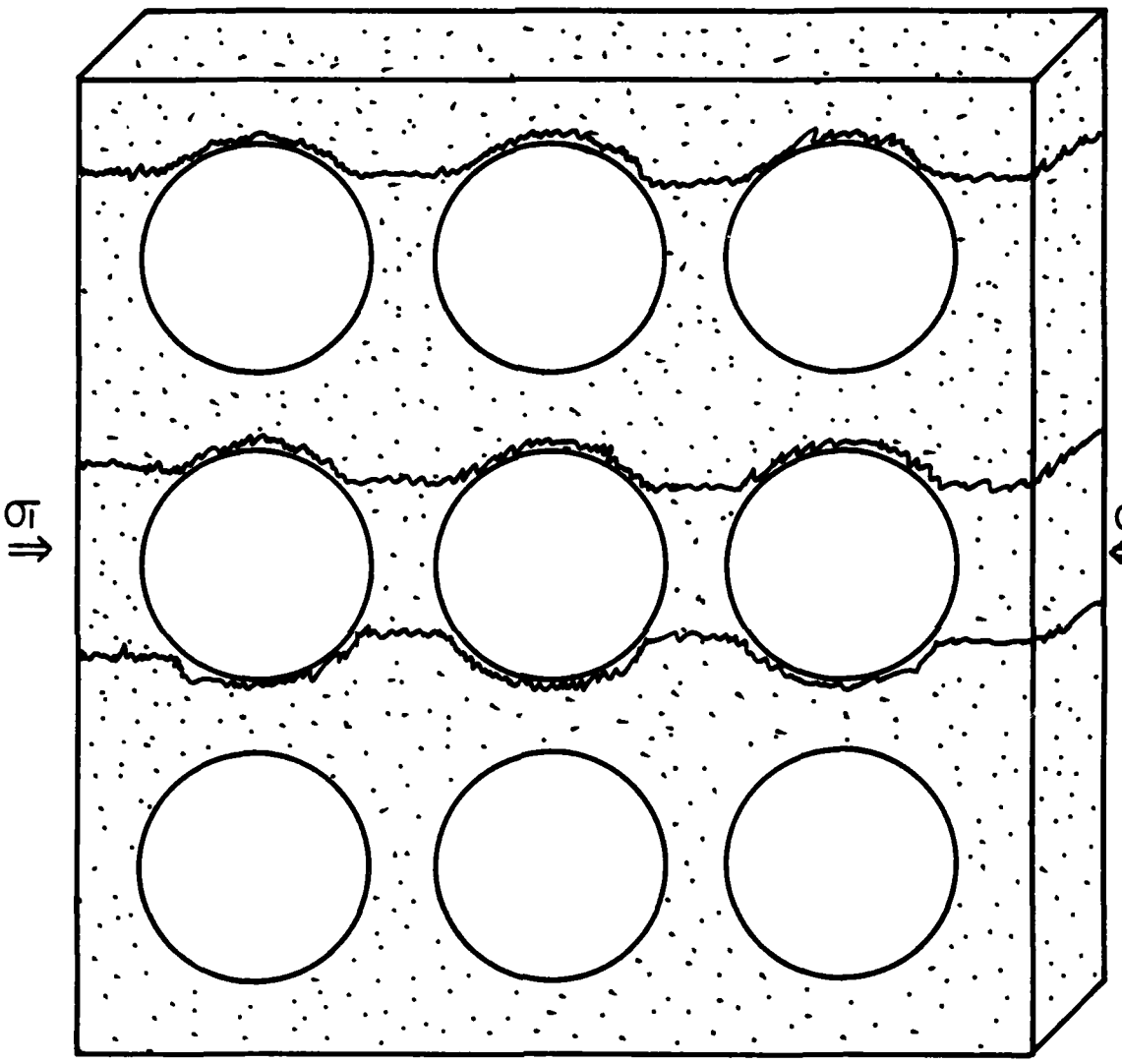

Figure 6.22 Typical Observed Failure Mode
in Uniaxial Compression

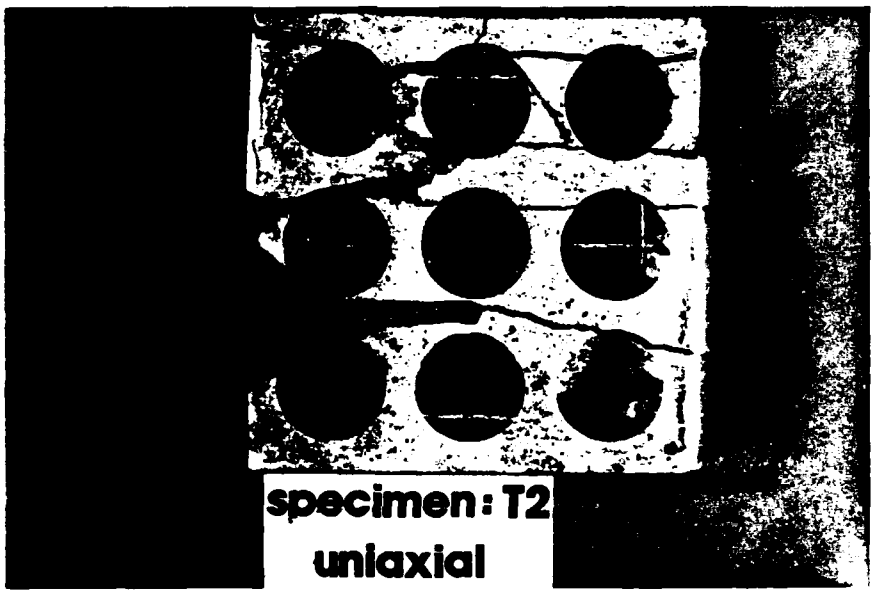

Fig 6.23. Typical Uniaxial Failure Mode.

The cracks described above are prevented from forming under biaxial compression due to the application of a minor principal stress, σ_2. Failure in biaxial compression was due to tensile splitting cracks which formed parallel to the unloaded face of the specimen for all biaxial stress ratios. This failure mode is illustrated in Fig. 6.24. Typical biaxial failures are shown in Fig. 6.25. In a few specimens subjected to a stress ratio of 1.0, a diagonal crack with an inclination of approximately 45 degrees occurred at failure in addition to the tensile splitting mechanism parallel to the unloaded face explained above. This diagonal crack occurred mostly in specimens with granite coarse aggregate discs, suggesting that the cause of the crack is related to the properties of the granite.

These modes of failure, which have been observed by previous investigators for normal strength concrete in biaxial compression studies, indicate that failure of concrete occurs whenever a certain tensile strain is reached in the unloaded direction. This limiting tensile strain criterion for the failure of concrete was proposed by Carino and Slate (30). It was concluded that the limiting tensile strain criterion is a promising tool, but more experimental data is needed to develop the criterion. The test set-up used in the present study did not allow for measurement of strains in the third direction, the unloaded direction out of the plane of the specimen. For this reason, no conclusion can be drawn as to the merits of a limiting tensile strain criterion in the present study.

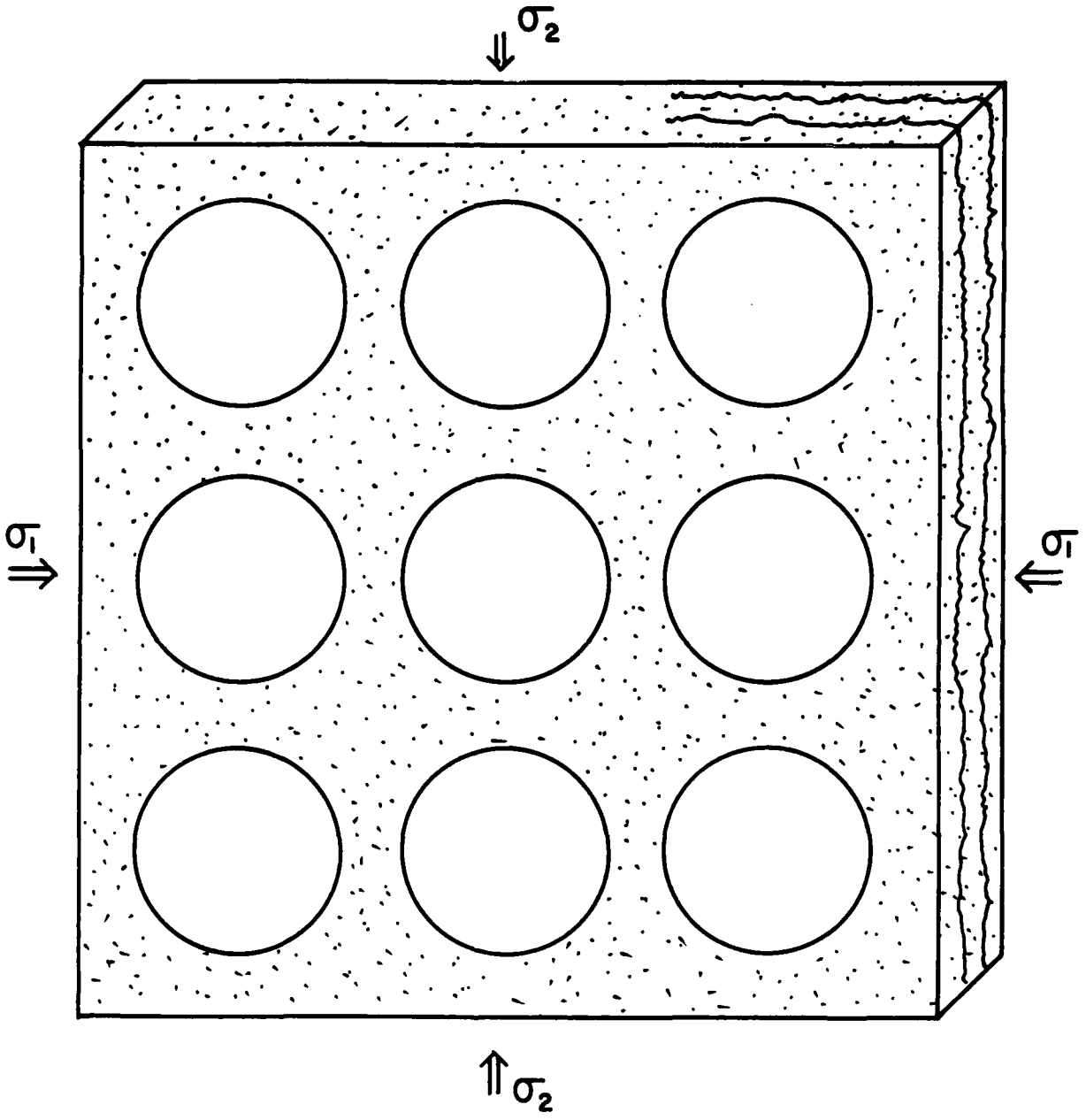

Figure 6.24 Typical Observed Failure Mode
Under Biaxial Compression

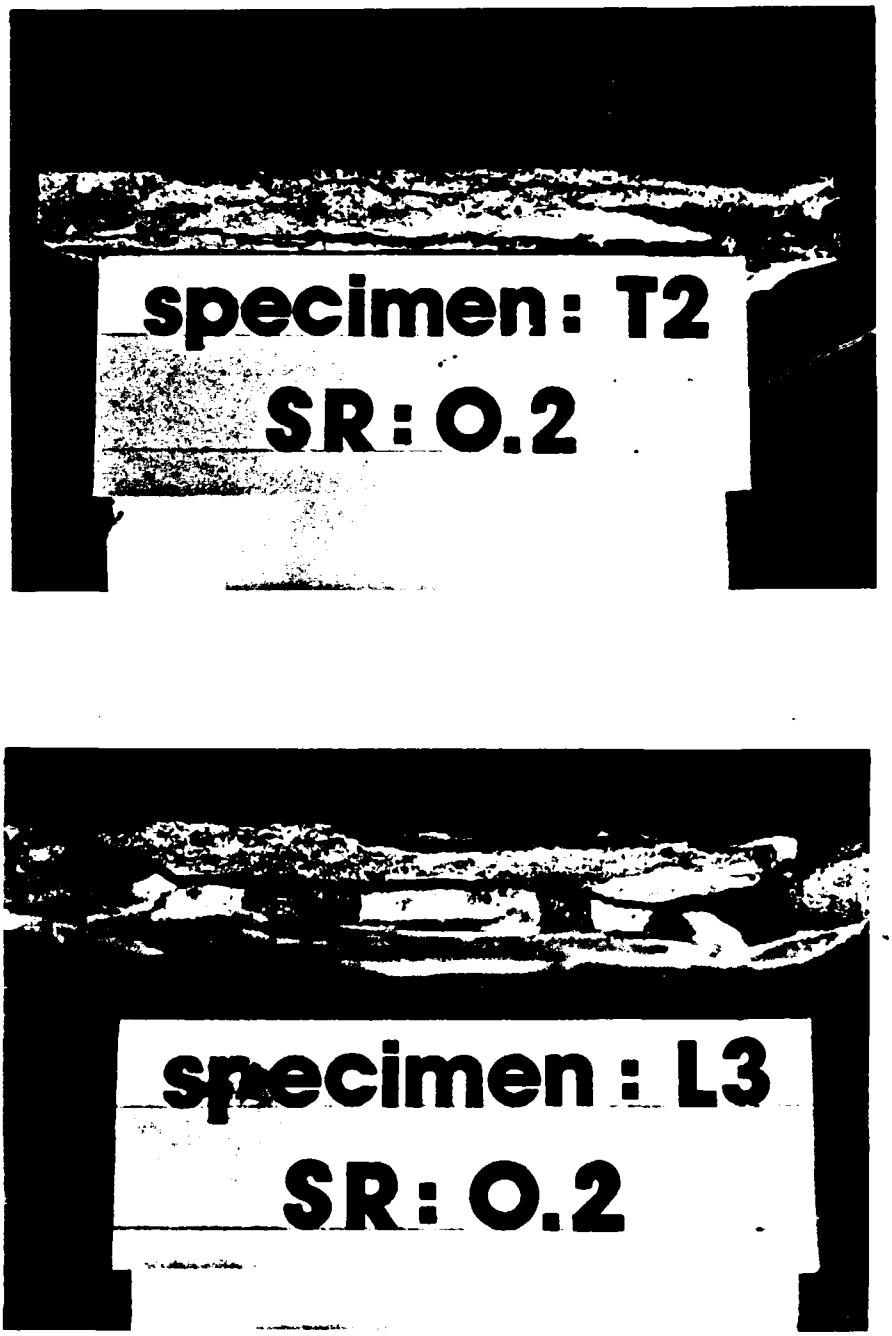

Fig 6.25. Typical Biaxial Failure Mode.

CHAPTER 7
CONCLUSIONS AND RECOMMENDATIONS

7.1 SUMMARY

The present study was conducted to determine the stress-strain behavior, strength characteristics, and failure mechanism of high-strength concrete subjected to biaxial compression. Model concrete plate specimens, composed of nine aggregate discs embedded in a mortar matrix, were used. Three types of coarse aggregate, limestone, granite, and traprock, were used together with three different high-strength mortar mixes in order to determine the effects of material properties on the biaxial behavior of high-strength concrete.

The plate specimens were loaded under four principal stress ratios: 0.0 (uniaxial), 0.2, 0.5, and 1.0. The load was applied to reduce frictional confining stresses. Data consisted of load-deflection curves in each of the principal stress directions.

7.2 CONCLUSIONS

Based on the results of the experimental investigation, the following general conclusions are drawn:

1) The ultimate strength in biaxial compression shows a significant increase over the uniaxial strength for all specimens tested.
2) Maximum biaxial strength occurs at a biaxial stress ratio (σ_2/σ_1) between 0.2 and 0.5 for all specimens tested.
3) The maximum biaxial strength showed an increase of 29 to 41 percent over the uniaxial strength for specimens using limestone coarse aggregate, 45 to 57 percent for specimens using granite coarse aggregate, and 31 to 43 percent for specimens using traprock coarse aggregate.

4) The ultimate strength under equal biaxial compression ($\sigma_2/\sigma_1 = 1.0$) showed an increase of eight to thirteen percent over the uniaxial strength for specimens using limestone coarse aggregate, seventeen to 26 percent for specimens using granite coarse aggregate, and two to sixteen percent for specimens using traprock coarse aggregate.
5) In general, the higher the modulus of elasticity of the aggregate, the higher the uniaxial strength that can be obtained.
6) The optimum modulus of elasticity ratio of coarse aggregate to mortar (E_a/E_m) for strength increases as the modulus of the coarse aggregate increases.
7) The maximum increase in strength under biaxial compression generally decreases as E_a/E_m ratio increases.
8) The maximum ultimate strength under biaxial stress was practically constant in the range of 8050 to 9125 psi (55.5 to 62.9 MN/m^2), with the exception of one mix with traprock aggregate.
9) In general, addition of a minor principal stress increases the stiffness of the model specimens in the major principal stress direction.
10) The increase in stiffness due to the minor principal stress was less for specimens using granite coarse aggregate due to the low modulus of elasticity and Poisson's ratio of the granite.
11) As the biaxial stress ratio (σ_2/σ_1) increases, the stress-strain curve becomes linear up to a higher stress-strength ratio.
12) The high-strength concrete model specimens behave elastically up to a higher stress-strength ratio than normal strength concrete model specimens.
13) The proportional limit increases as the E_a/E_m ratio approaches unity for specimens with the same type of coarse aggregate.

14) The discontinuity point occurs at 80 to 87 percent of the uniaxial strength for models using limestone or granite coarse aggregate, and seventy to eighty percent for trap-rock aggregate for all specimens tested under uniaxial compression.
15) The discontinuity point occurs at a higher stress-strength ratio for high-strength concrete models than for normal strength concrete model specimens.
16) The discontinuity point occurs at a higher stress-strength ratio as the E_a/E_m ratio approaches unity for all specimens tested under uniaxial compression.
17) Failure in uniaxial compression was due to splitting cracks which formed parallel to the applied load and perpendicular to the face of the specimen.
18) Failure under biaxial compression was due to tensile splitting cracks which formed parallel to the unloaded face of the specimen.
19) The observed failure modes indicate that failure occurs whenever a certain tensile strain is reached in the unloaded direction.

7.3 RECOMMENDATIONS

The following recommendations are made for further research:

1) Real concrete plate specimens should be tested in the same manner as the model specimens to determine if the model actually exhibits the same properties as real concrete.
2) To complete the biaxial data, high-strength concrete plate specimens should be tested in biaxial tension and compression-tension, as well as under cyclic loading.
3) An attempt should be made to measure the deformation in the unloaded third direction in order to provide more information to evalute the potential of the limiting tensile strain failure criterion for concrete.

APPENDIX

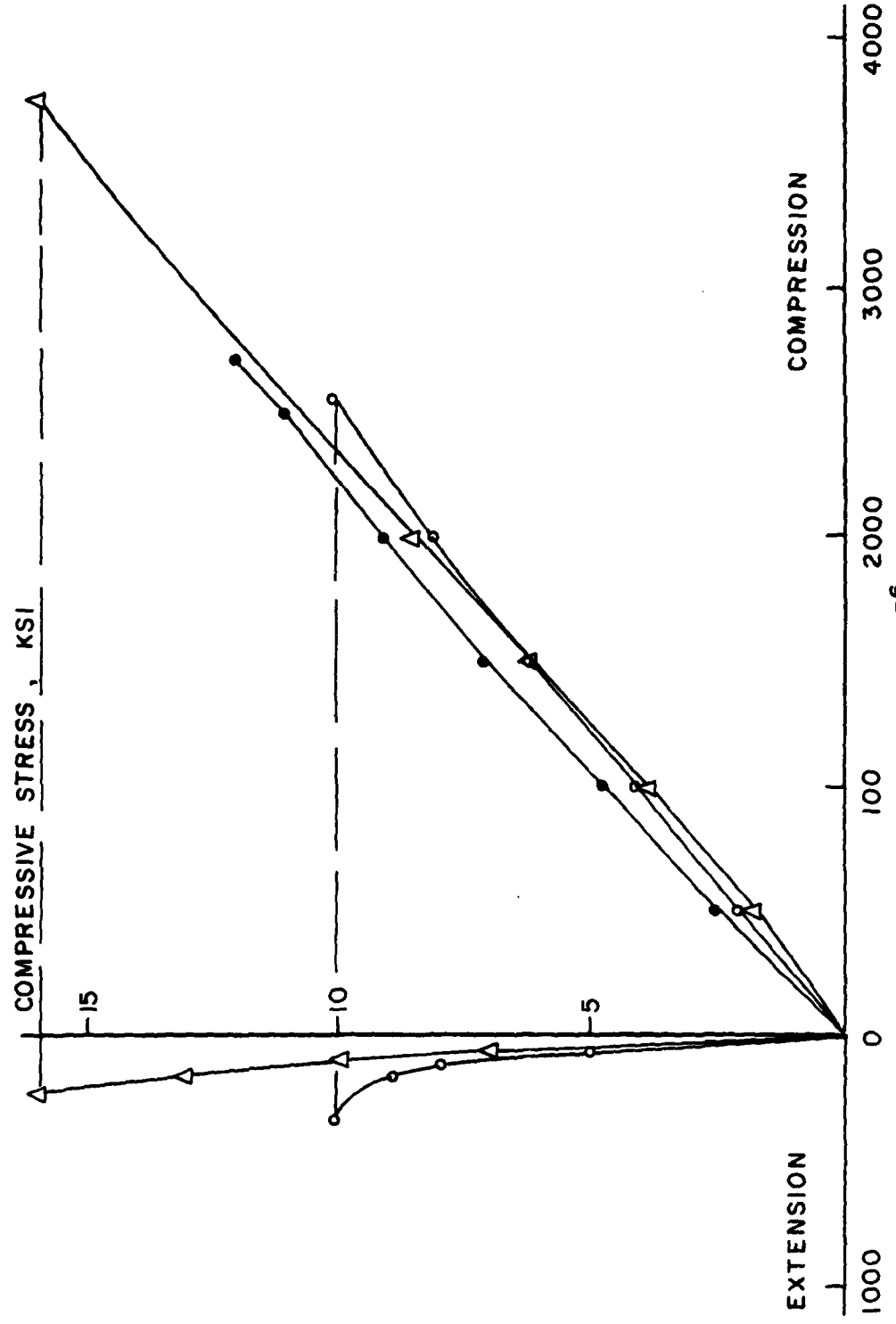

Figure A.1 Longitudinal and Transverse Stress-Strain Curves for Limestone

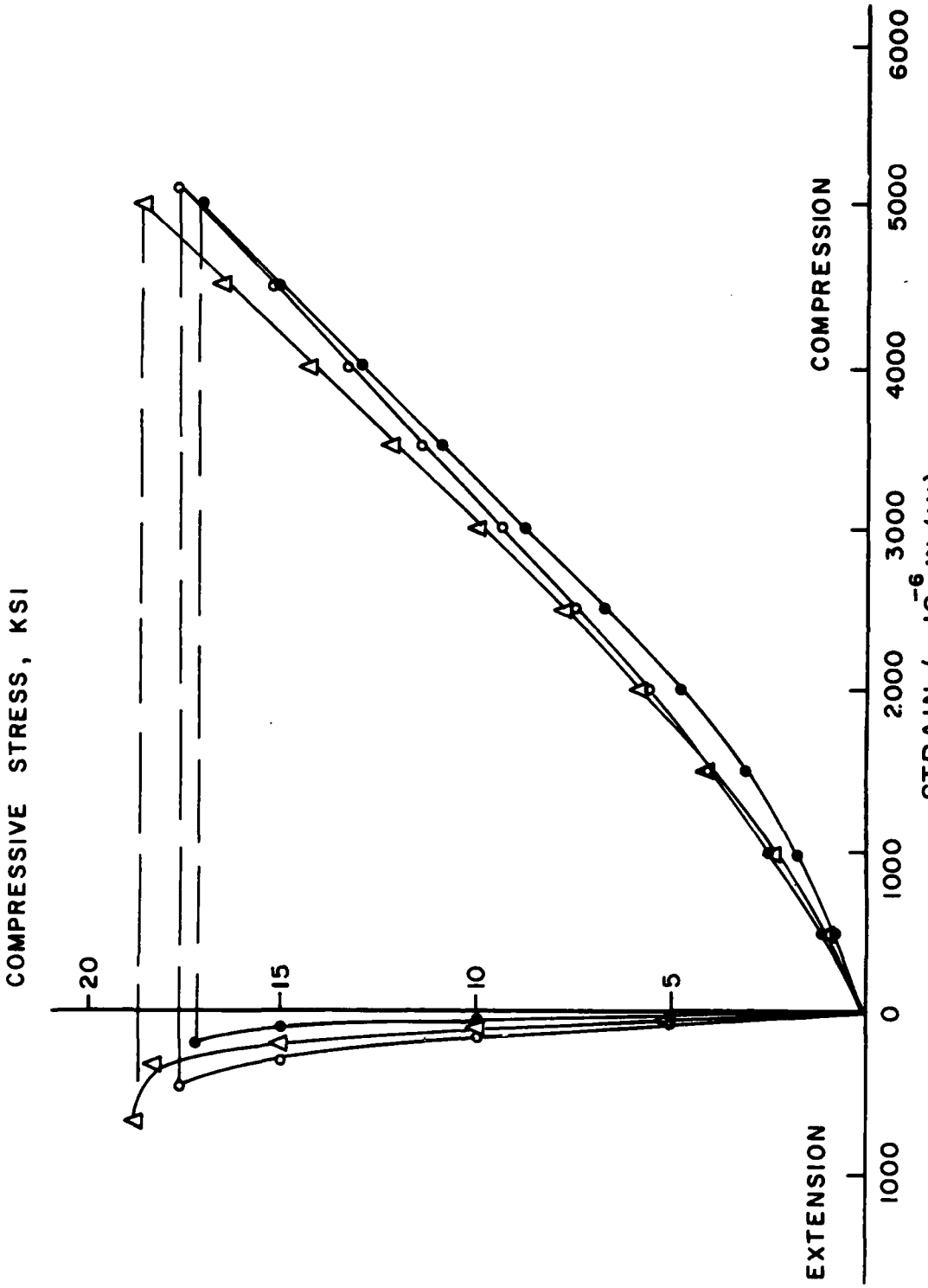

Figure A.2 Longitudinal and Transverse Stress-Strain Curves for Granite

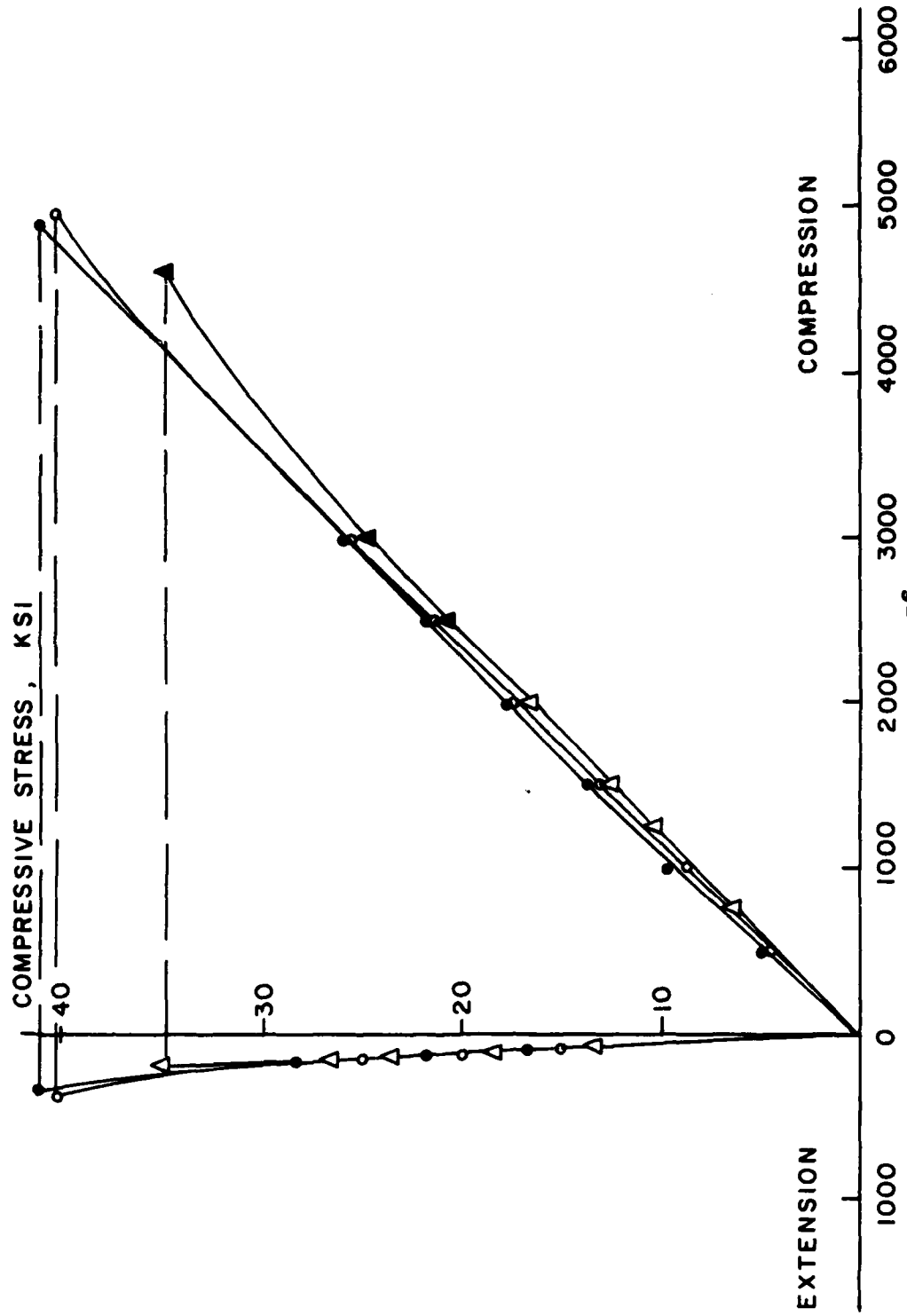

Figure A.3 Longitudinal and Transverse Stress-Strain Curves for Traprock

TABLE A-1 COMPRESSIVE STRENGTH AND MODULUS OF ELASTICITY VALUES FOR MORTAR CYLINDERS USING BRAND A CEMENT AND W/C RATIO OF 0.40

Sand/ Cement	Water/ Cement Ratio	Type of Cement	Type of Sand	Average f'c (psi)	Average Modulus of Elasticity (psi)
			F.B.	7,900	3.1×10^6
0.2	0.40	Brand A	Local	8,710	3.2×10^6
			Cemix	7,800	3.1×10^6
			F.B.	8,700	3.5×10^6
0.5	0.40	Brand A	Local	10,710	3.7×10^6
			Cemix	7,840	3.3×10^6
			F.B.	8,730	3.7×10^6
1.0	0.40	Brand A	Local	11,460	4.4×10^6
			Cemix	10,100	3.7×10^6
			F.B.	9,450	4.0×10^6
1.5	0.40	Brand A	Local	11,600	4.7×10^6
			Cemix	10,030	4.1×10^6
			F.B.	7,690	4.7×10^6
2.0	0.40	Brand A	Local	11,200	4.8×10^6
			Cemix	8,900	4.7×10^6
			F.B.	-	-
2.5	0.40	Brand A	Local	9.820	4.9×10^6
			Cemix	-	-
			F.B.	-	-
3.0	0.40	Brand A	Local	-	-
			Cemix	-	-

TABLE A-2 COMPRESSIVE STRENGTH AND MODULUS OF ELASTICITY VALUES FOR MORTAR CYLINDERS USING BRAND A CEMENT AND A W/C RATIO OF 0.35

Sand/ Cement	Water/ Cement Ratio	Type of Cement	Type of Sand	Average f'c (psi)	Average Modulus of Elasticity (psi)
			F.B.	10,500	3.6×10^6
0.2	0.35	Brand A	Local	12,040	3.8×10^6
			Cemix	10,010	3.5×10^6
			F.B.	10,100	3.6×10^6
0.5	0.35	Brand A	Local	12,480	4.1×10^6
			Cemix	10,300	3.6×10^6
			F.B.	10,600	4.5×10^6
1.0	0.35	Brand A	Local	12,040	4.8×10^6
			Cemix	10,250	4.2×10^6
			F.B.	10,440	4.8×10^6
1.5	0.35	Brand A	Local	11,730	5.3×10^6
			Cemix	10,000	4.1×10^6
			F.B.	7,870	5.0×10^6
2.0	0.35	Brand A	Local	11,320	5.9×10^6
			Cemix	9,100	4.6×10^6
			F.B.	-	-
2.5	0.35	Brand A	Local	5,000	4.4×10^6
			Cemix	-	-
			F.B.	-	-
3.0	0.35	Brand A	Local	-	-
			Cemix	-	-

TABLE A-3 COMPRESSIVE STRENGTH AND MODULUS OF ELASTICITY VALUES FOR MORTAR CYLINDERS USING BRAND A CEMENT AND A W/C RATIO OF 0.30

Sand/ Cement	Water/ Cement Ratio	Type of Cement	Type of Sand	Average f'c (psi)	Average Modulus of Elasticity (psi)
0.0	0.30	Brand A	-	11,860	3.7×10^6
			F.B.	13,000	4.2×10^6
0.2	0.30	Brand A	Local	13,990	4.5×10^6
			Cemix	11,510	3.8×10^6
			F.B.	13,000	4.4×10^6
0.5	0.30	Brand A	Local	12,830	4.3×10^6
			Cemix	11,420	3.9×10^6
			F.B.	12,170	4.8×10^6
1.0	0.30	Brand A	Local	12,340	4.8×10^6
			Cemix	10,540	4.2×10^6
			F.B.	9,590	5.8×10^6
1.5	0.30	Brand A	Local	11,700	5.4×10^6
			Cemix	10,200	4.8×10^6
			F.B.	8.200	5.3×10^6
2.0	0.30	Brand A	Local	10,160	4.9×10^6
			Cemix	10,020	4.5×10^6
			F.B.	-	-
2.5	0.30	Brand A	Local	3,400	-
			Cemix	-	-
			F.B.	-	-
3.0	0.30	Brand A	Local	-	-
			Cemix	-	-

TABLE A-4 COMPRESSIVE STRENGTH AND MODULUS OF ELASTICITY VALUES FOR MORTAR CYLINDERS USING BRAND B CEMENT AND A W/C RATIO OF 0.40

Sand/ Cement	Water/ Cement Ratio	Type of Cement	Type of Sand	Average f'c (psi)	Average Modulus of Elasticity (psi)
			F.B.	-	-
0.2	0.40	Brand B	Local	-	-
			Cemix	-	-
			F.B.	-	-
0.5	0.40	Brand B	Local	-	-
			Cemix	-	-
			F.B.	7,630	4.5×10^6
1.0	0.39	Brand B	Local	7,380	4.4×10^6
			Cemix	8.550	4.2×10^6
	0.38		F.B.	8,260	5.1×10^6
1.5	0.39	Brand B	Local	8,070	4.6×10^6
	0.39		Cemix	8,400	4.5×10^6
	0.38		F.B.	6,370	4.3×10^6
2.0	0.39	Brand B	Local	8,200	4.8×10^6
	0.39		Cemix	7,825	4.7×10^6
	0.37		F.B.	4,410	3.2×10^6
2.5	0.38	Brand B	Local	5,020	3.8×10^6
	0.38		Cemix	4,250	3.8×10^6
	0.36		F.B.	3,410	3.4×10^6
3.0	0.38	Brand B	Local	3,820	3.7×10^6
	0.38		Cemix	3,380	3.6×10^6

TABLE A-5 COMPRESSIVE STRENGTH AND MODULUS OF ELASTICITY VALUES FOR MORTAR CYLINDERS USING BRAND B CEMENT AND A W/C RATIO OF 0.35

Sand/ Cement	Water/ Cement Ratio	Type of Cement	Type of Sand	Average f'c (psi)	Average Modulus of Elasticity (psi)
			F.B.	-	-
0.2	0.35	Brand B	Local	-	-
			Cemix	-	-
			F.B.	-	-
0.5	0.35	Brand B	Local	-	-
			Cemix	-	-
			F.B.	10,040	5.0×10^6
1.0	0.34	Brand B	Local	10,240	4.6×10^6
			Cemix	9,000	4.2×10^6
	0.33		F.B.	8,970	5.2×10^6
1.5	0.34	Brand B	Local	9,460	4.9×10^6
	0.34		Cemix	8,760	4.8×10^6
	0.33		F.B.	7,650	4.7×10^6
2.0	0.34	Brand B	Local	9,200	4.8×10^6
	0.34		Cemix	8,080	4.4×10^6
	0.32		F.B.	4,740	3.4×10^6
2.5	0.33	Brand B	Local	5,420	3.9×10^6
	0.33		Cemix	4,540	3.7×10^6
	0.31		F.B.	3,650	3.2×10^6
3.0	0.33	Brand B	Local	4,120	3.7×10^6
	0.33		Cemix	3,500	3.3×10^6

TABLE A-6 COMPRESSIVE STRENGTH AND MODULUS OF ELASTICITY VALUES FOR MORTAR CYLINDERS USING BRAND B CEMENT AND A W/C RATIO OF 0.30

Sand/ Cement	Water/ Cement Ratio	Type of Cement	Type of Sand	Average f'c (psi)	Average Modulus of Elasticity (psi)
0.0	0.30	Brand B	-	11,920	3.6×10^6
			F.B.	12,080	3.9×10^6
0.2	0.30	Brand B	Local	12,210	4.3×10^6
			Cemix	11,610	3.6×10^6
			F.B.	12,000	4.4×10^6
0.5	0.30	Brand B	Local	13,290	4.5×10^6
			Cemix	12,340	4.0×10^6
			F.B.	11,370	5.2×10^6
1.0	0.30	Brand B	Local	12,000	5.1×10^6
			Cemix	11,620	4.6×10^6
			F.B.	10,810	5.3×10^6
1.5	0.30	Brand B	Local	10,700	5.1×10^6
			Cemix	10,560	5.0×10^6
			F.B.	8,930	5.3×10^6
2.0	0.30	Brand B	Local	10,230	4.7×10^6
			Cemix	8,200	4.4×10^6
			F.B.	-	-
2.5	0.30	Brand B	Local	-	-
			Cemix	-	-
			F.B.	-	-
3.0	0.30	Brand B	Local	-	-
			Cemix	-	-

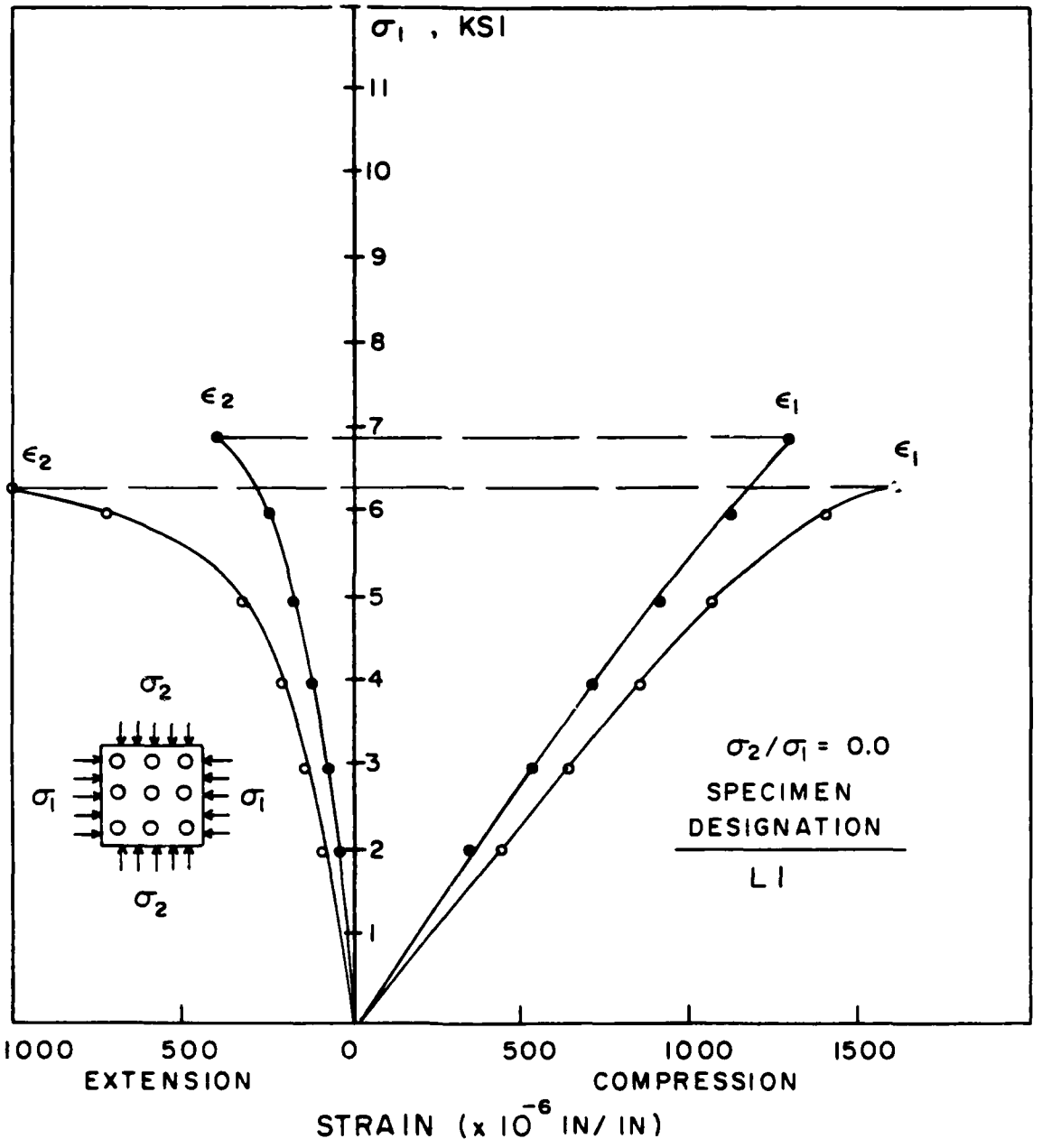

Figure B.1 Stress-Strain Curves for Model Specimens L1 with a Stress Ratio of 0.0 (Uniaxial)

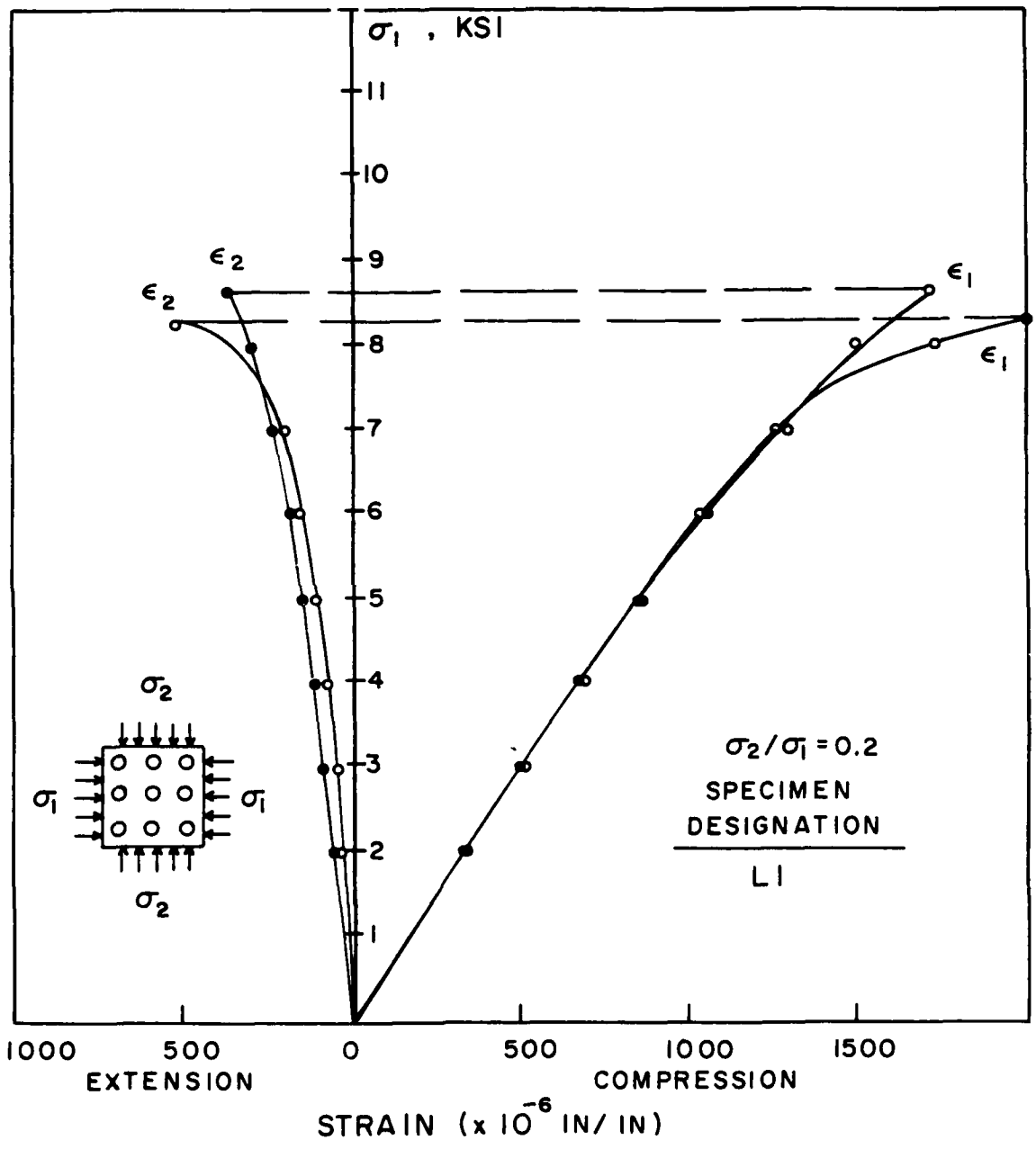

Figure B.2 Stress-Strain Curves for Model Specimens L1 with a Stress Ratio of 0.2

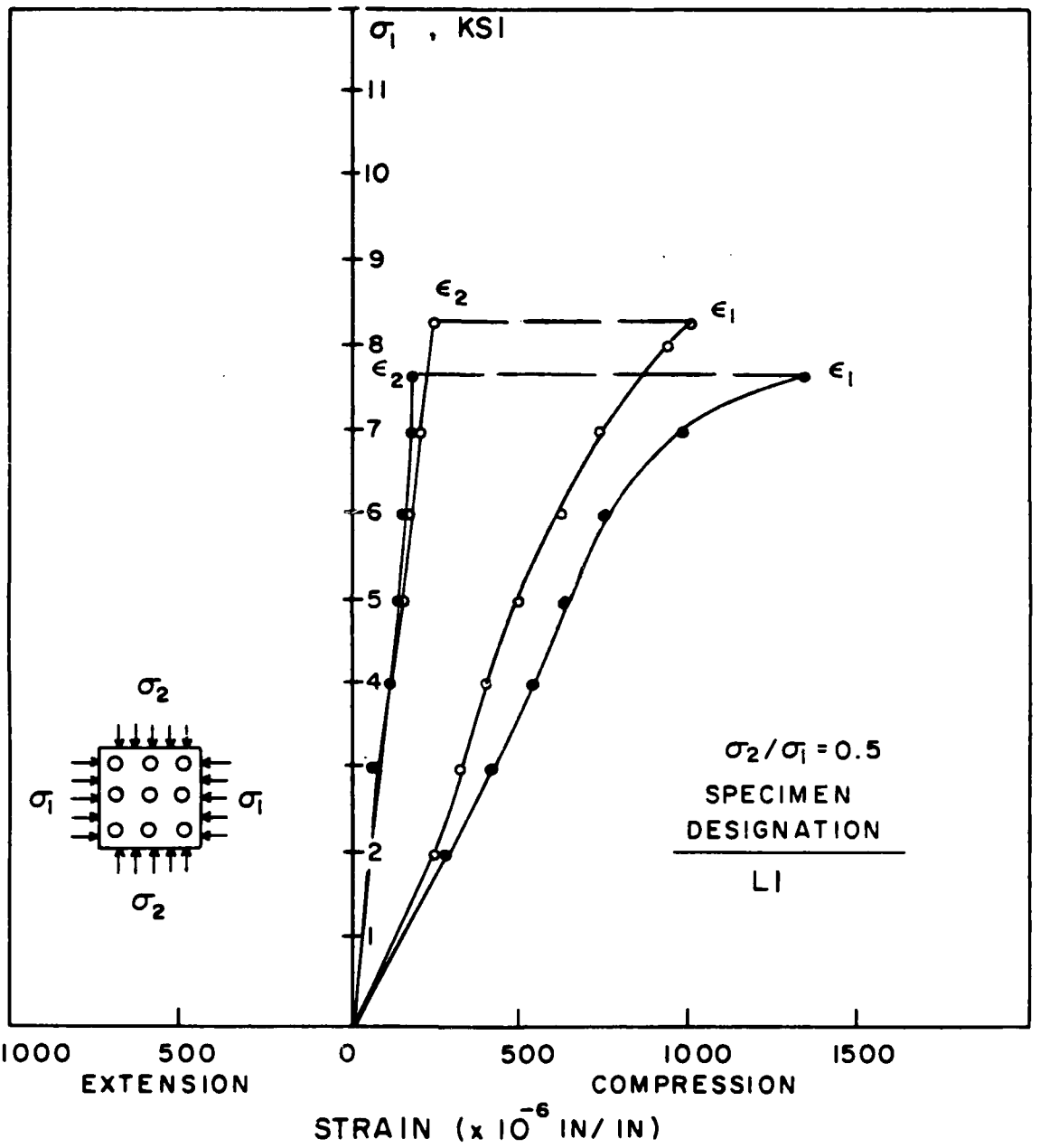

Figure B.3 Stress-Strain Curves for Model Specimens L1 with a Stress Ratio of 0.5

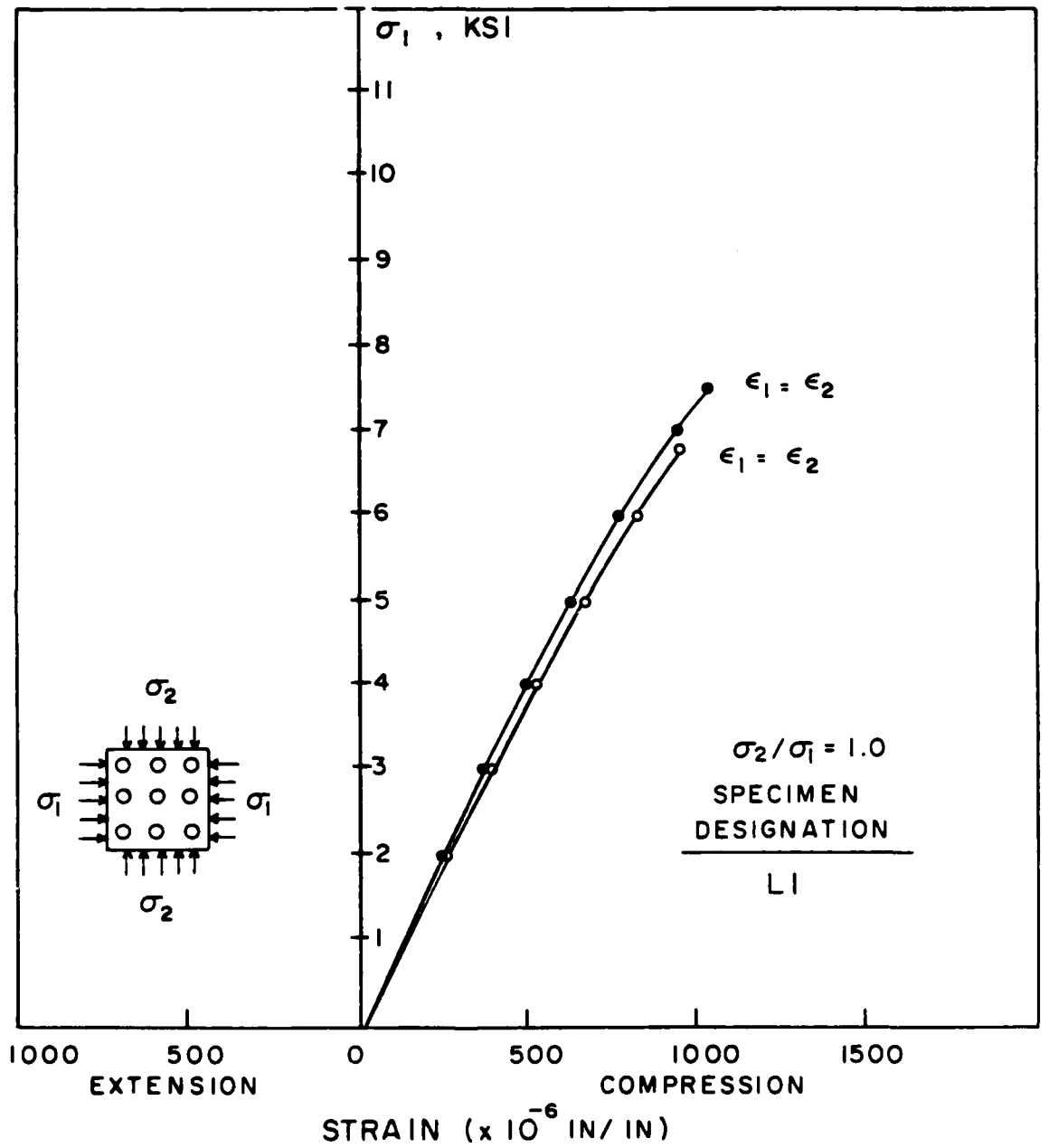

Figure B.4 Stress-Strain Curves for Model Specimens L1 with a Stress Ratio of 1.0

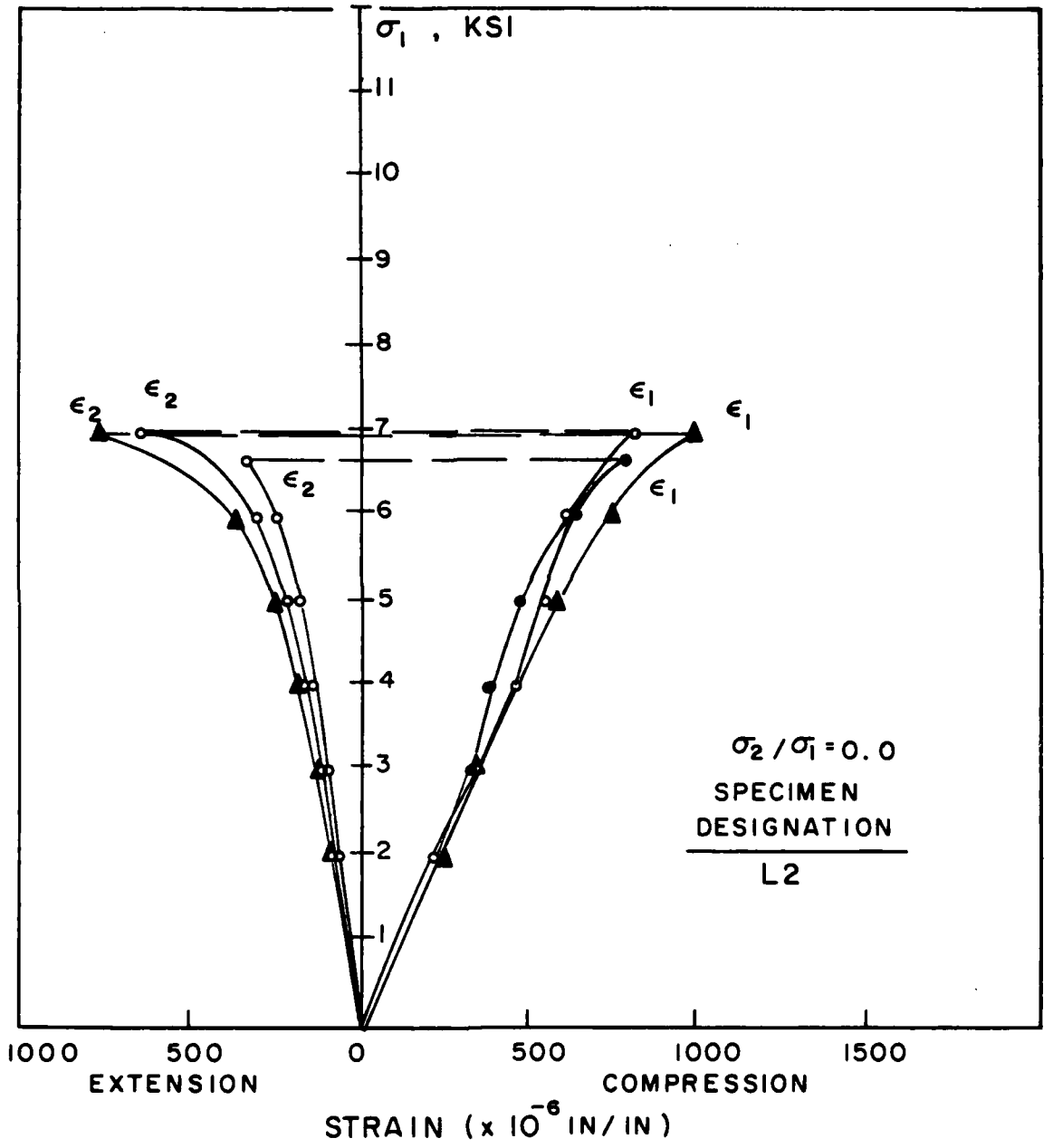

Figure B.5 Stress-Strain Curves for Model Specimens L2 with a Stress Ratio of 0.0 (Uniaxial)

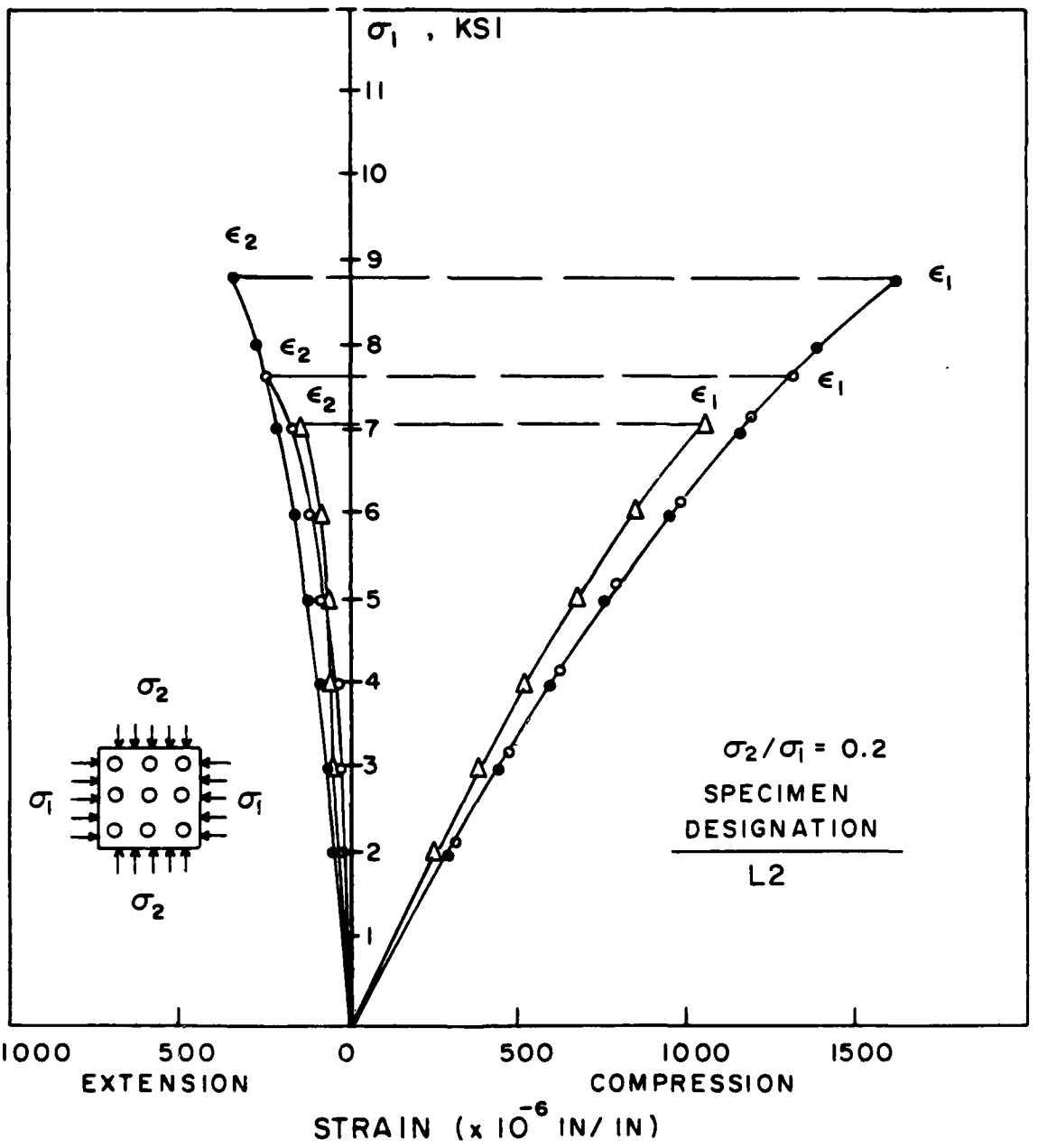

Figure B.6 Stress-Strain Curves for Model Specimens L2 with a Stress Ratio of 0.2

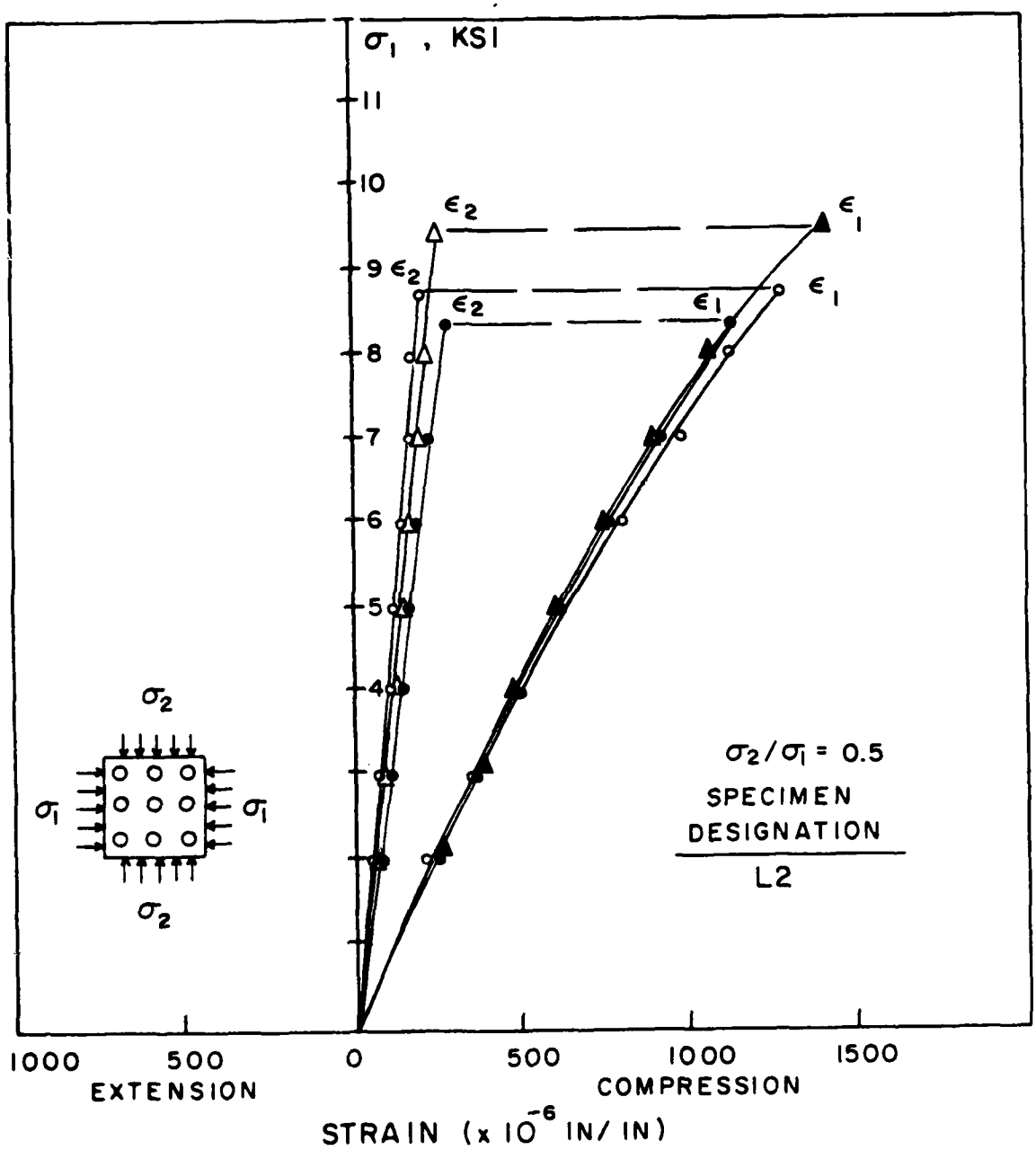

Figure B.7 Stress-Strain Curves for Model Specimens L2 with a Stress Ratio of 0.5

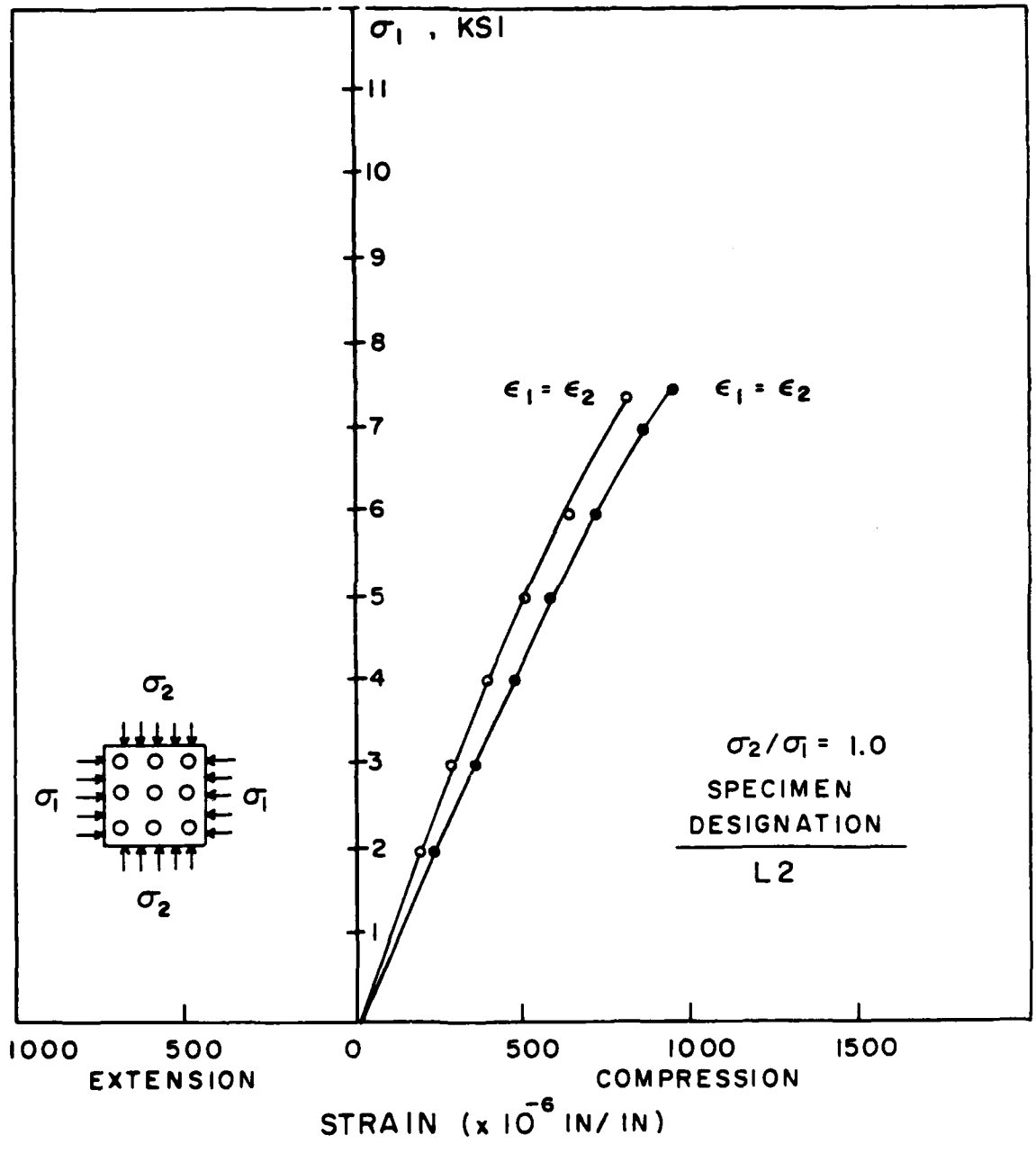

Figure B.8 Stress-Strain Curves for Model Specimens L2 with a Stress Ratio of 1.0

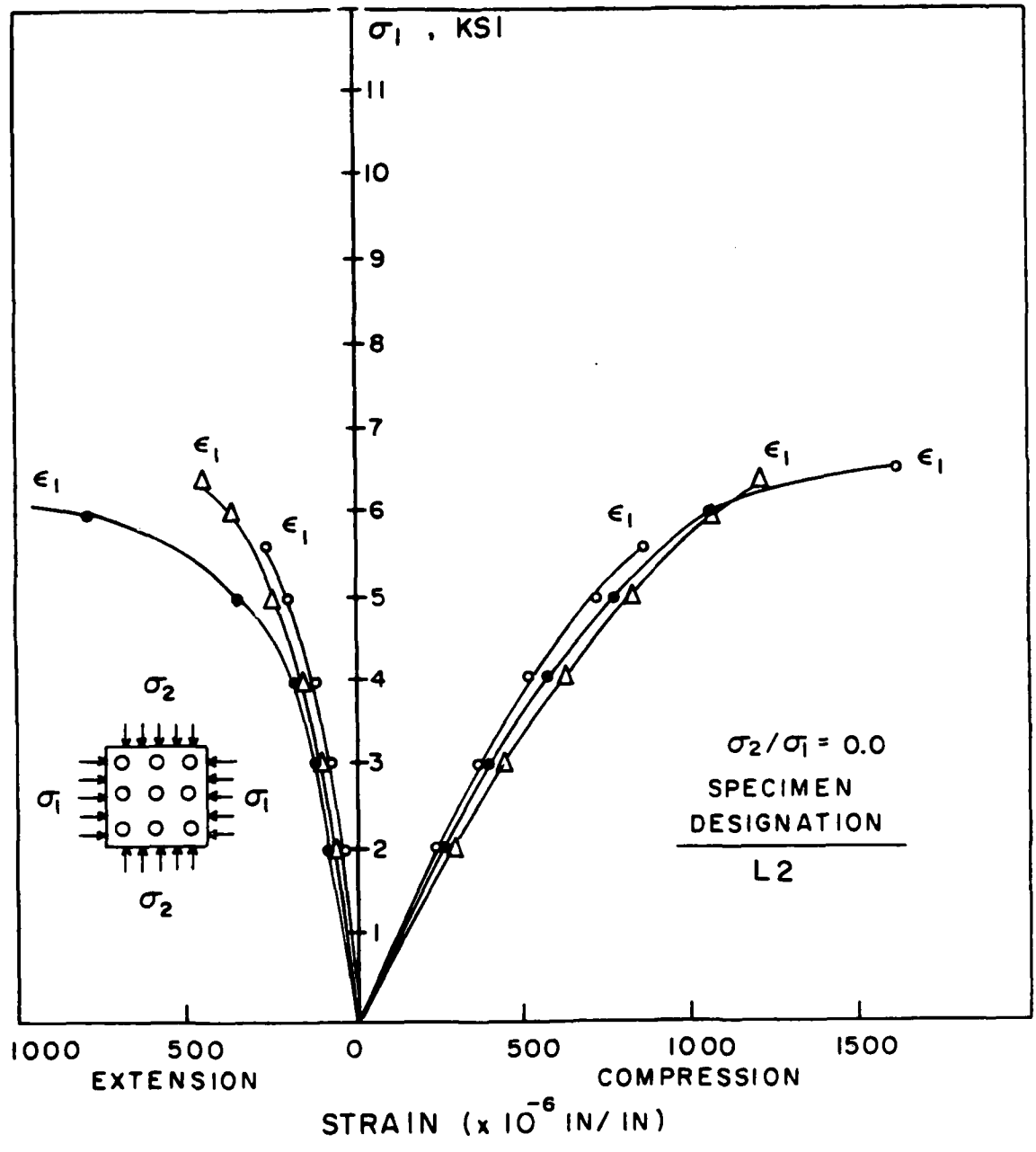

Figure B.9 Stress-Strain Curves for Model Specimens L3 with a Stress Ratio of 0.0 (Uniaxial)

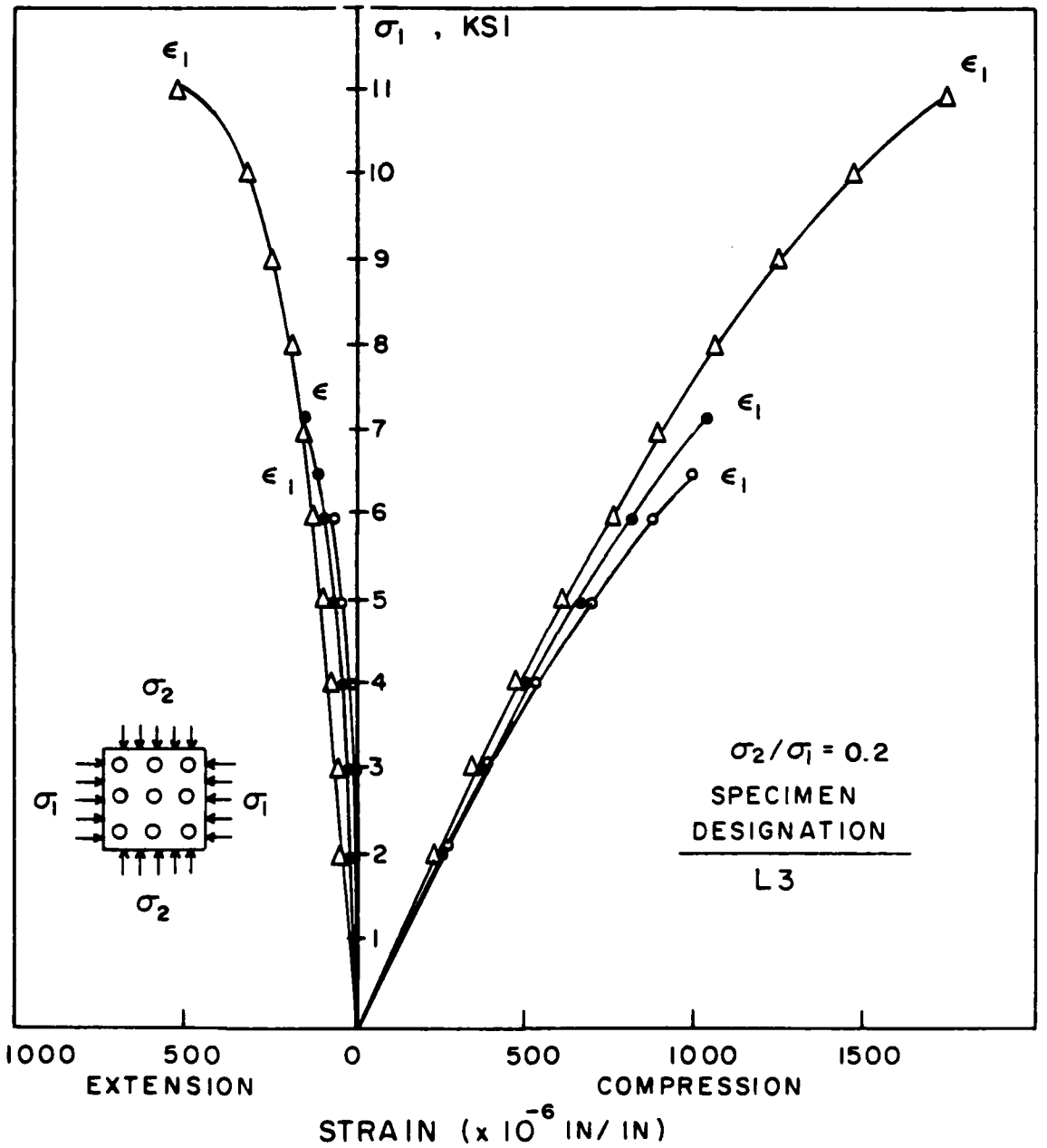

Figure B.10 Stress-Strain Curves for Model Specimens L3 with a Stress Ratio of 0.2

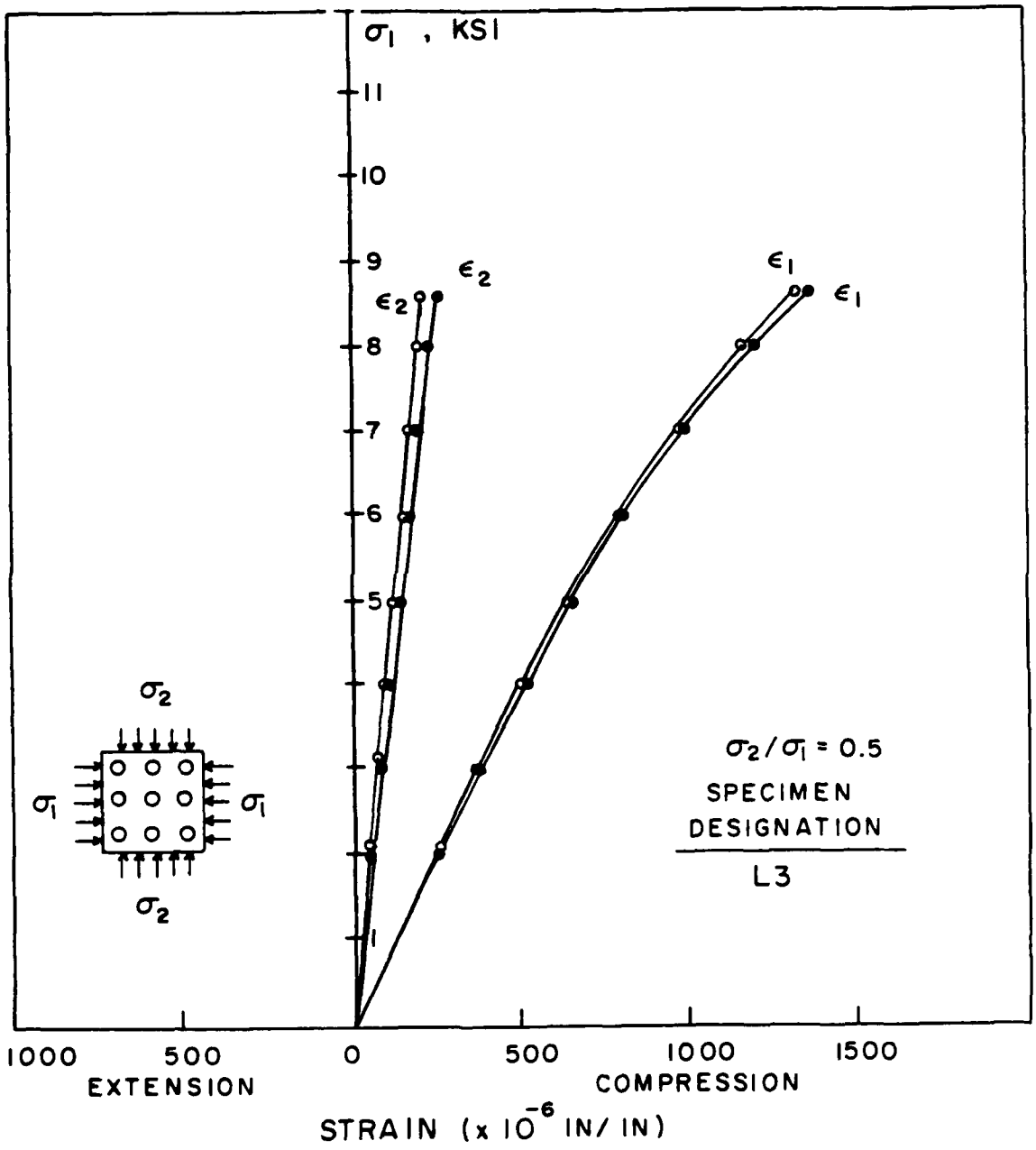

Figure B.11 Stress-Strain Curves for Model Specimens L3 with a Stress Ratio of 0.5

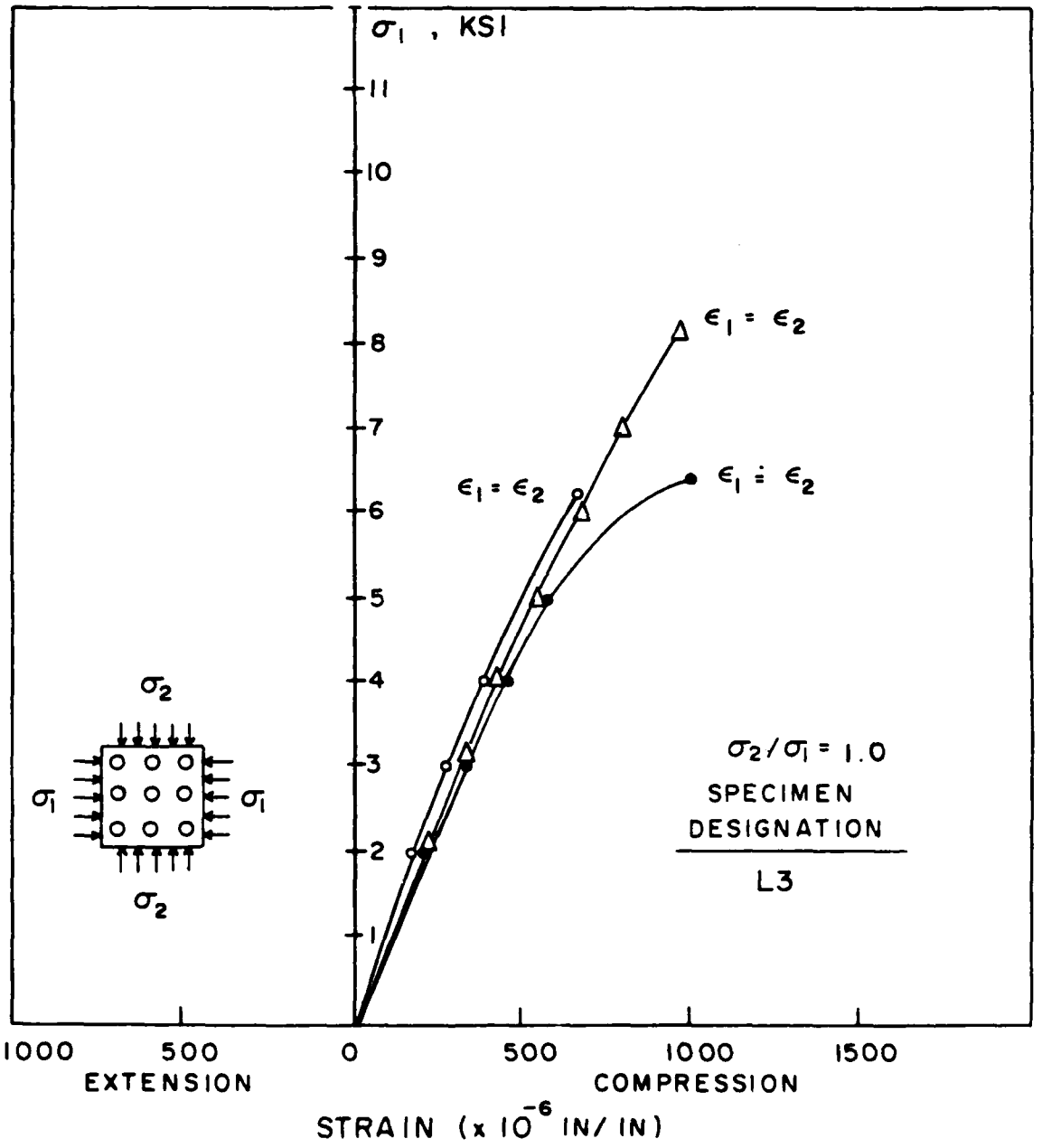

Figure B.12 Stress-Strain Curves for Model Specimens L3 with a Stress Ratio of 1.0

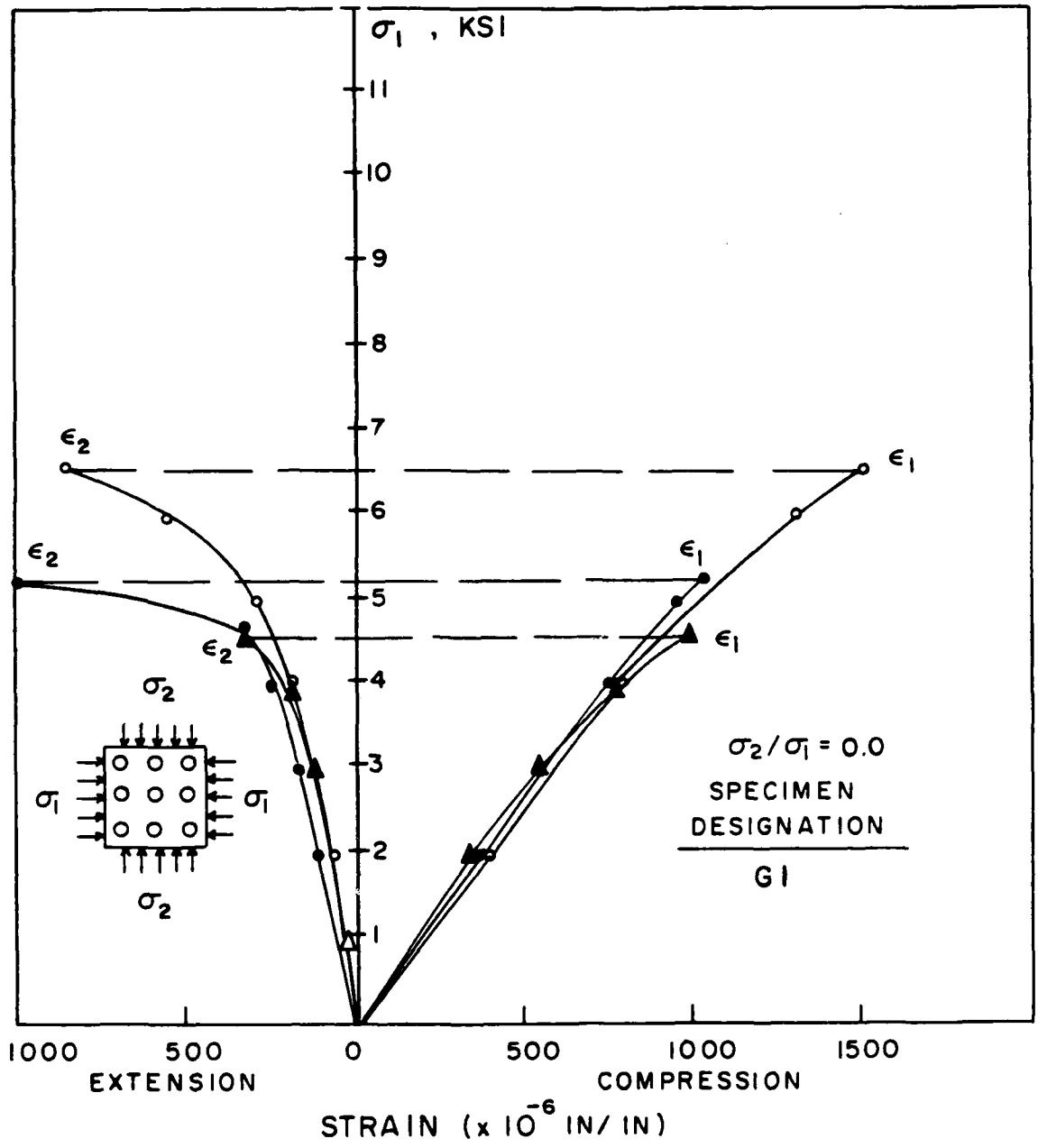

Figure B.13 Stress-Strain Curves for Model Specimens G1 with a Stress Ratio of 0.0 (Uniaxial)

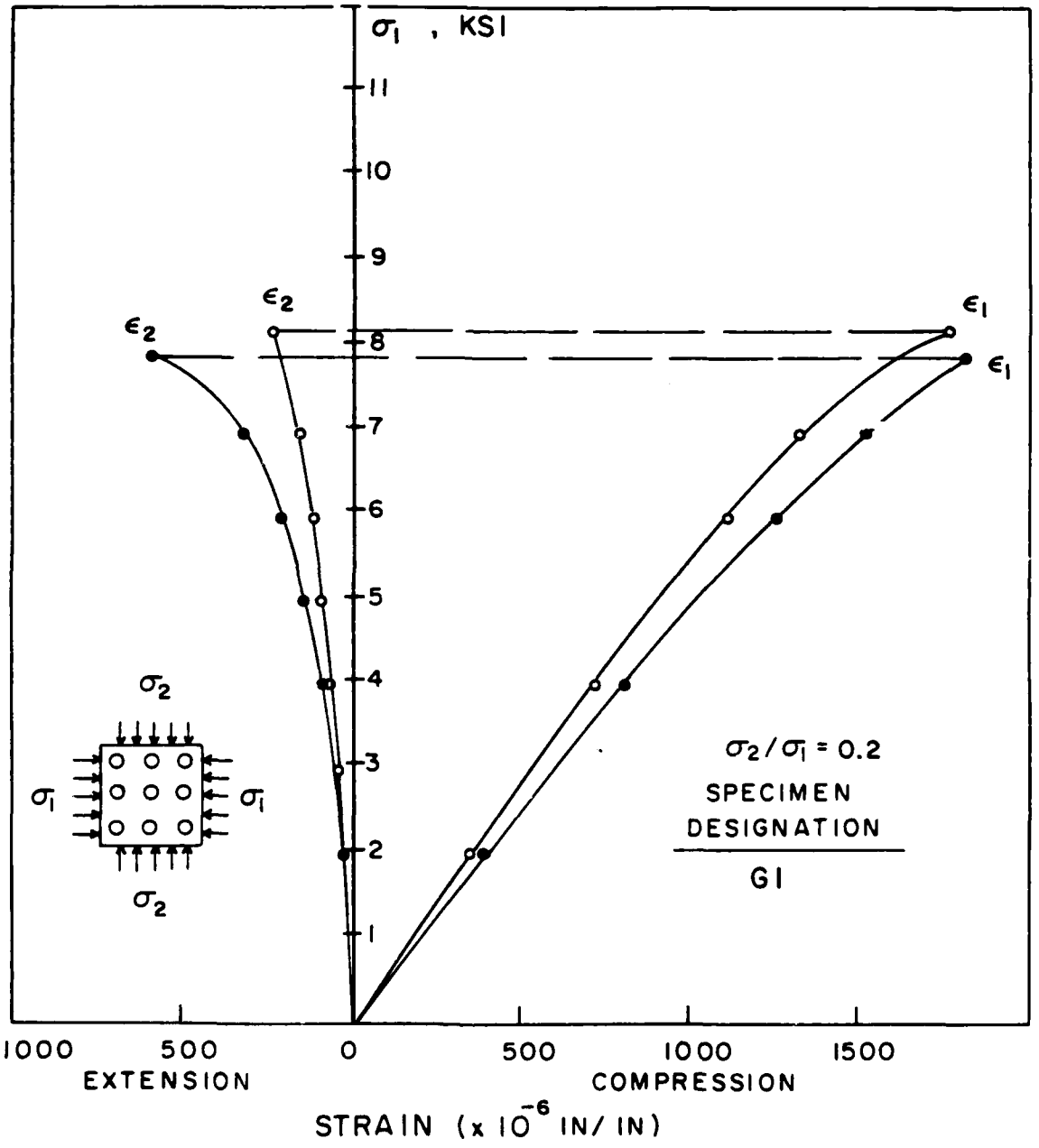

Figure B.14 Stress-Strain Curves for Model Specimens G1 with a Stress Ratio of 0.2

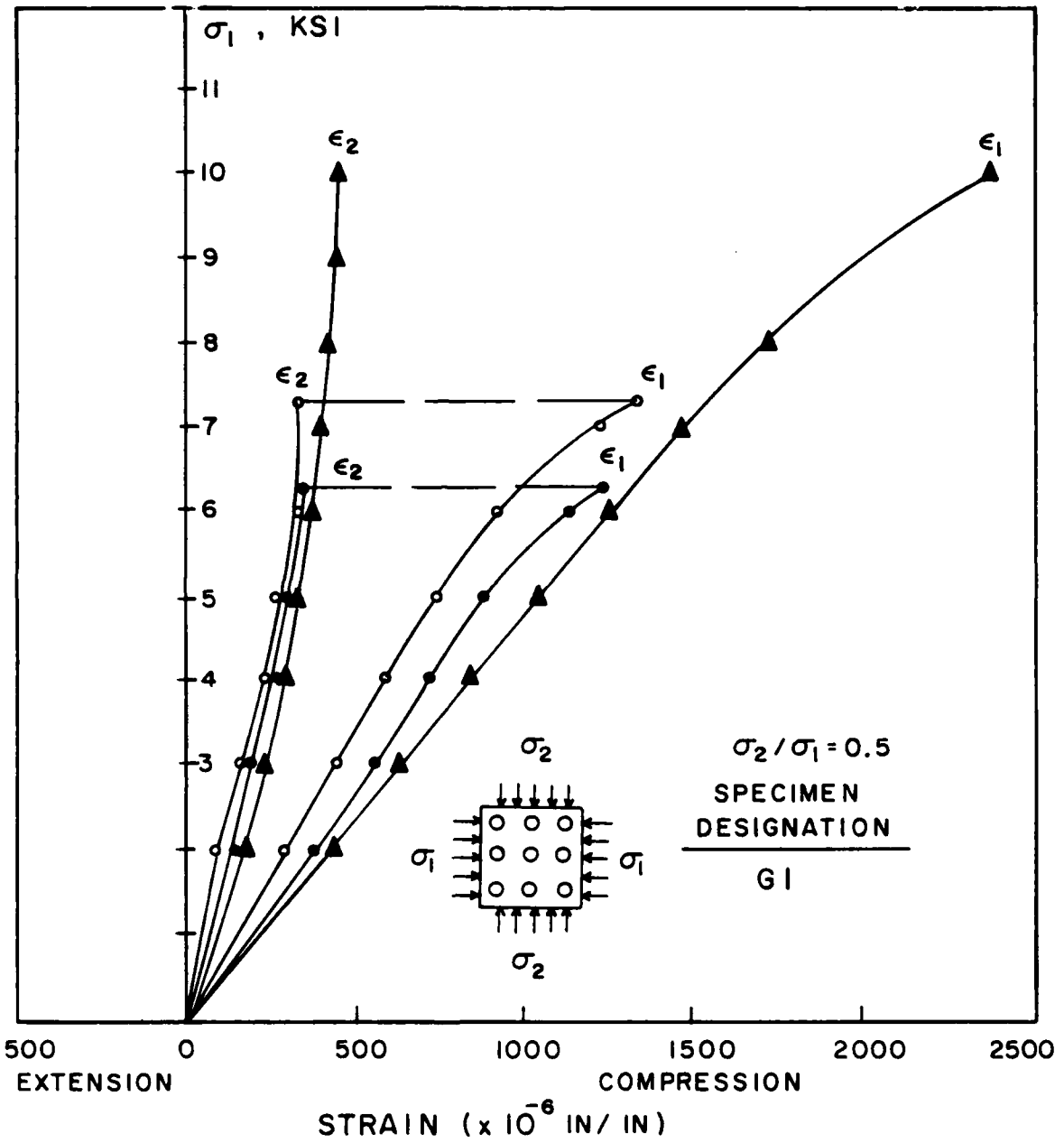

Figure B.15 Stress-Strain Curves for Model Specimens G1 with a Stress Ratio of 0.5

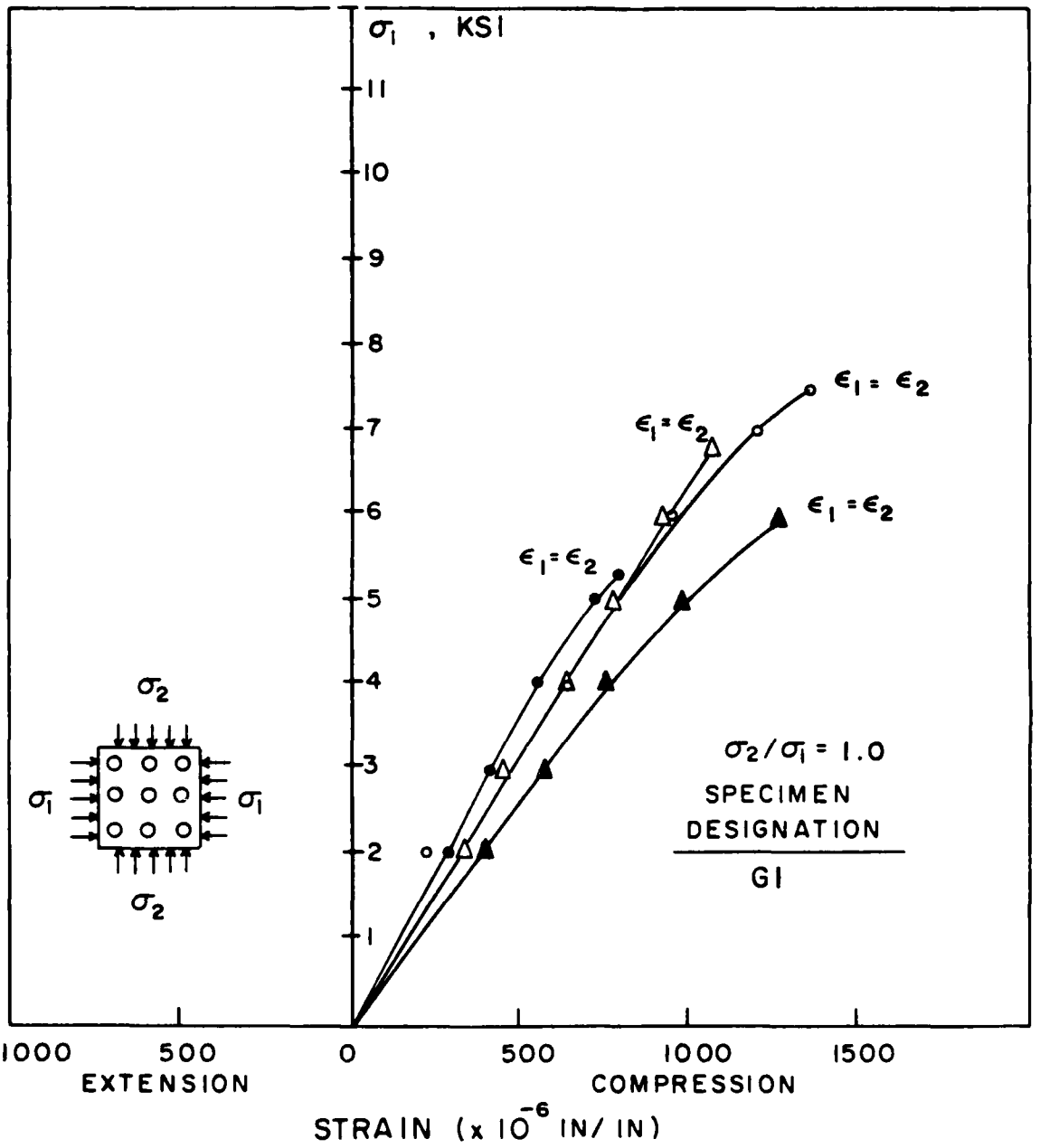

Figure B.16 Stress-Strain Curves for Model Specimens G1 with a Stress Ratio of 1.0

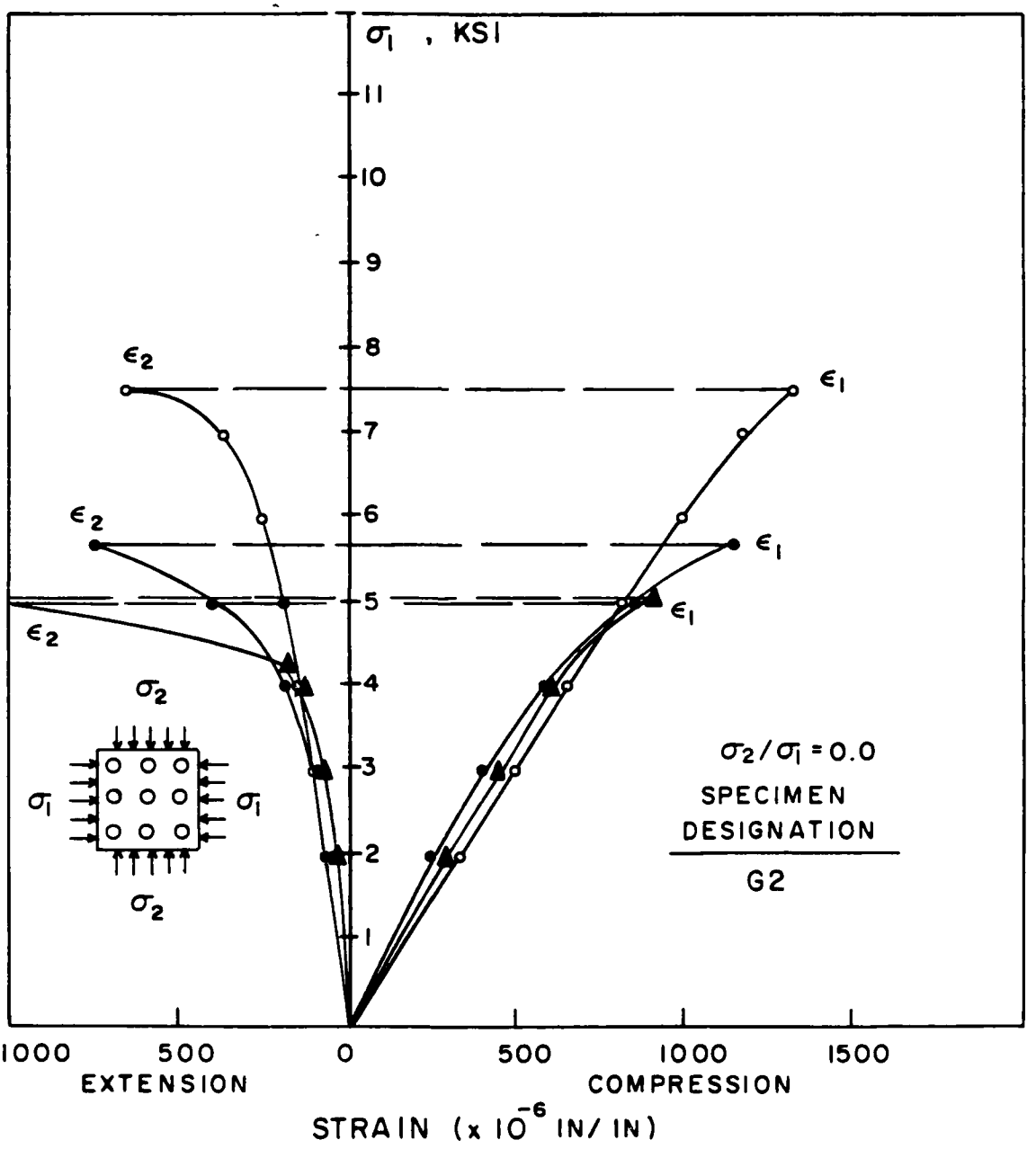

Figure B.17 Stress-Strain Curves for Model Specimens G2 with a Stress Ratio of 0.0 (Uniaxial)

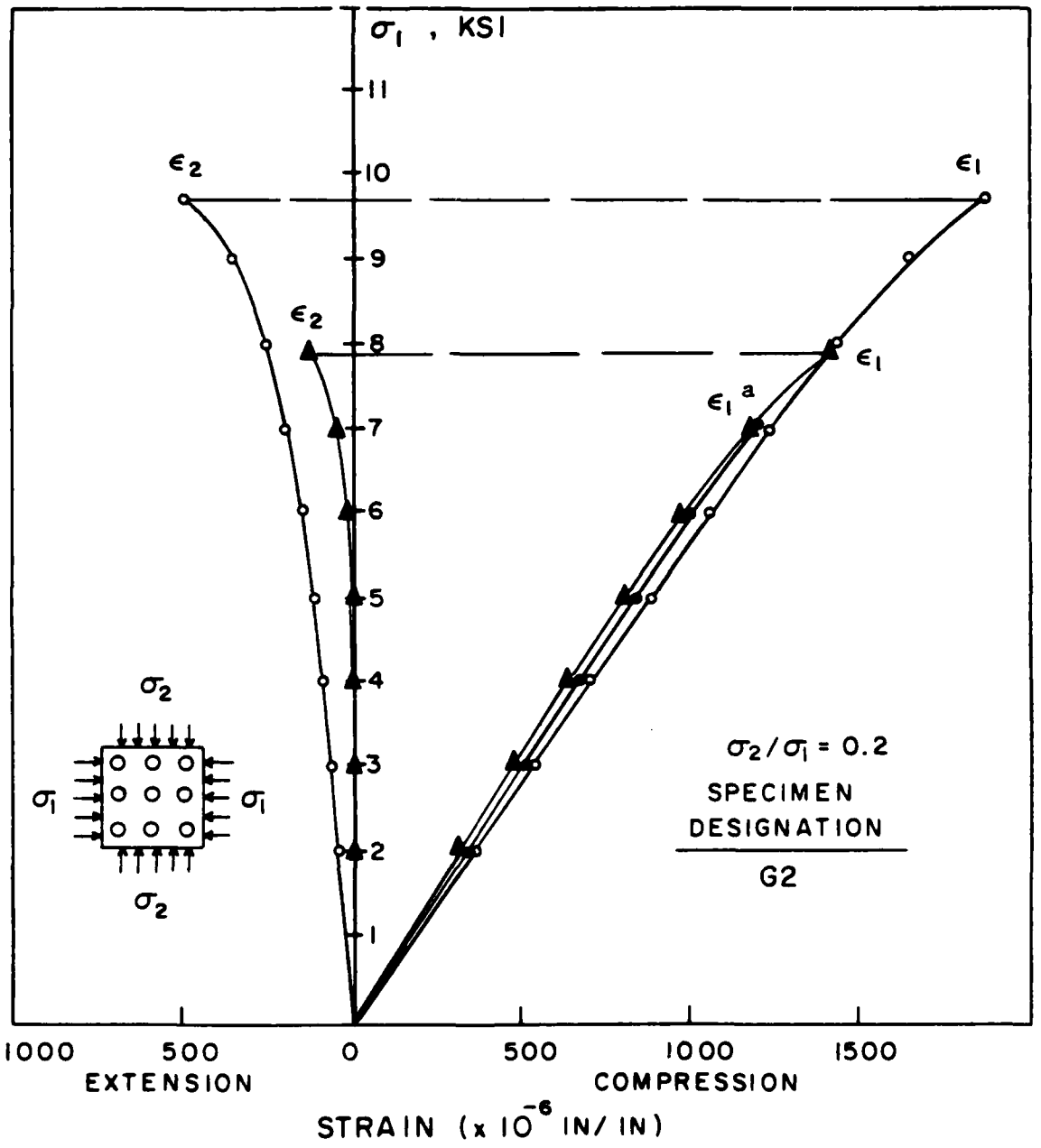

Figure B.18 Stress-Strain Curves for Model Specimens G2 with a Stress Ratio of 0.2

[a] ε_2 curve was not obtained for this specimen

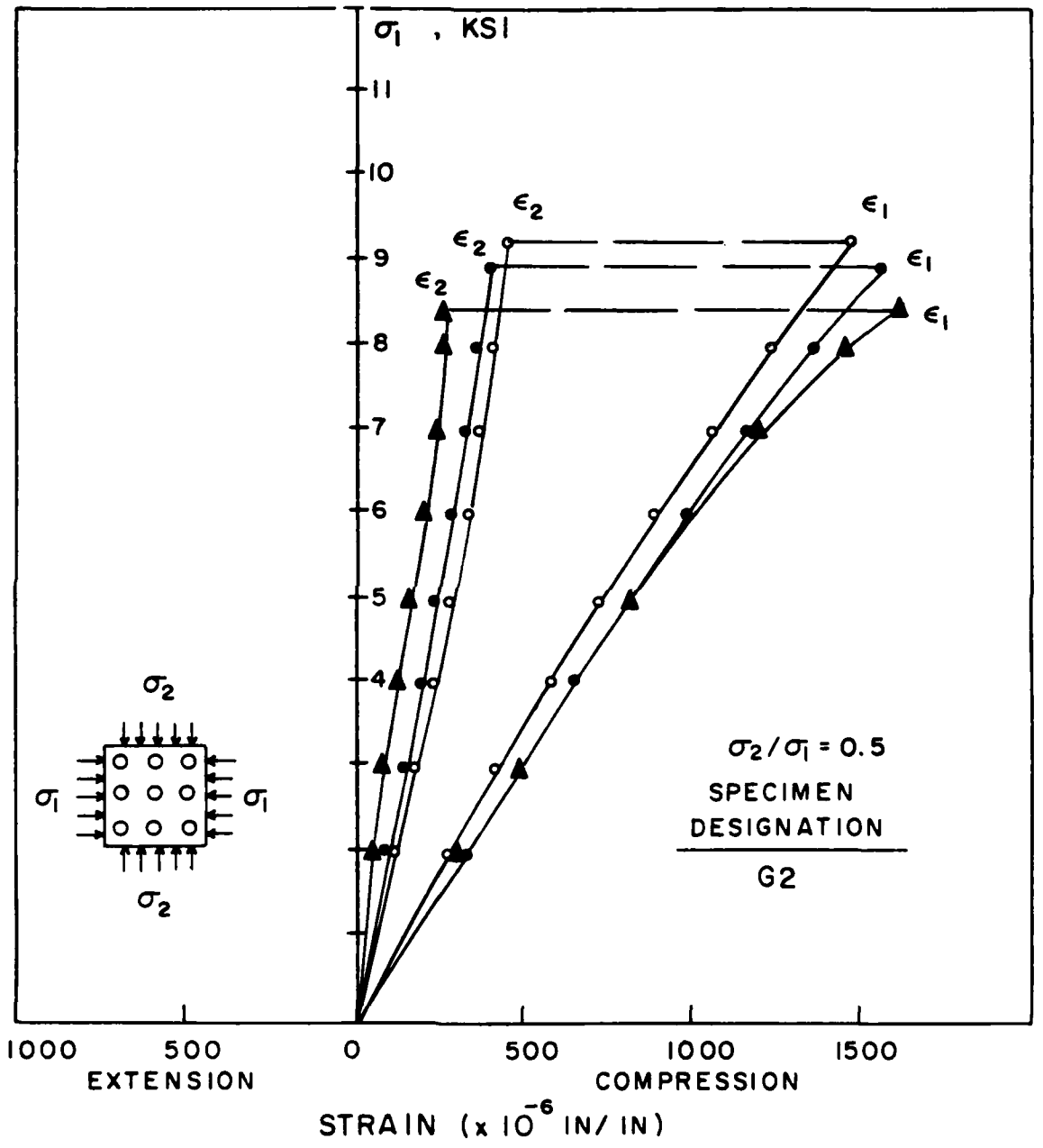

Figure B.19 Stress-Strain Curves for Model Specimens G2 with a Stress Ratio of 0.5

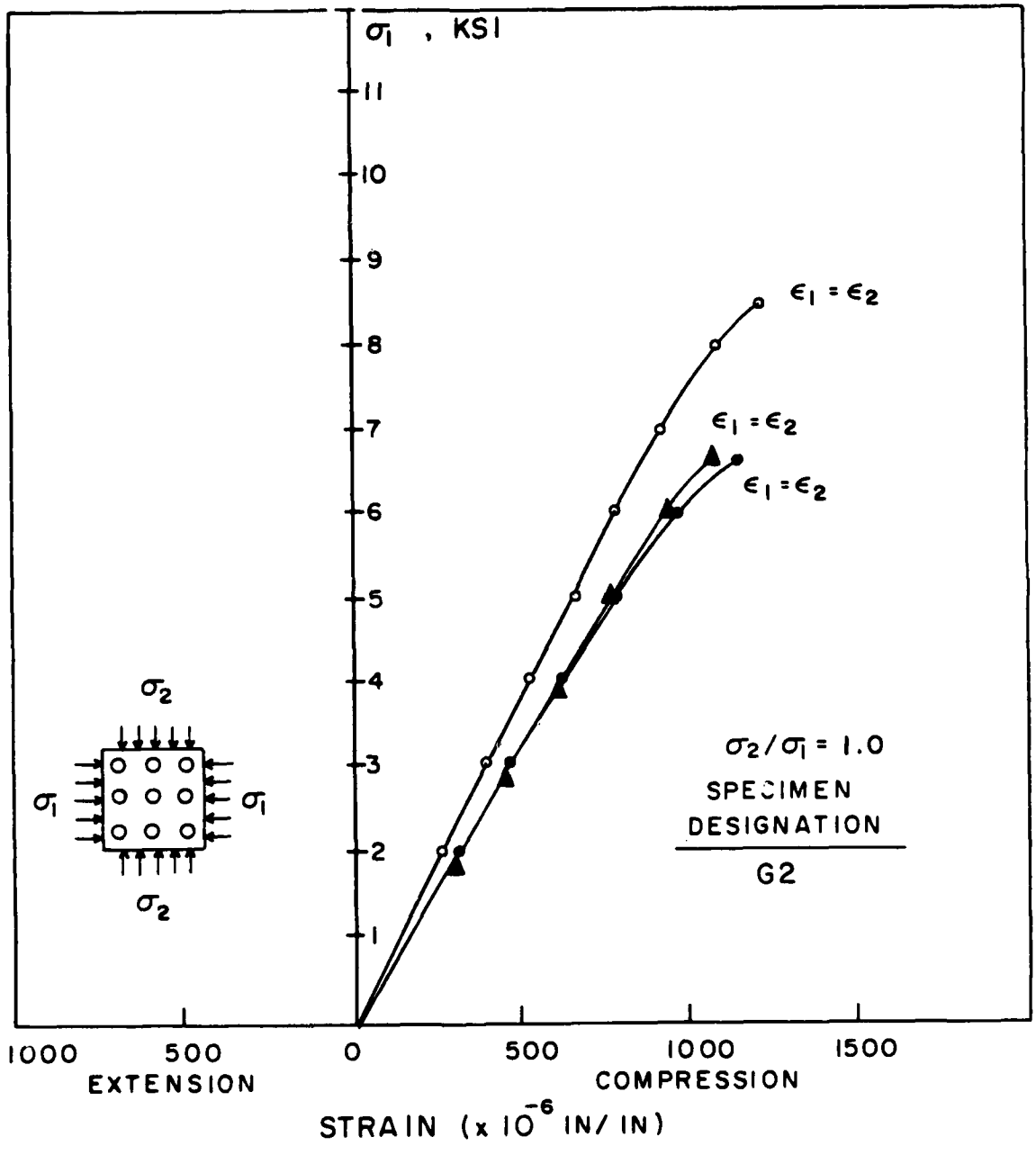

Figure B.20 Stress-Strain Curves for Model Specimens G2 with a Stress Ratio of 1.0

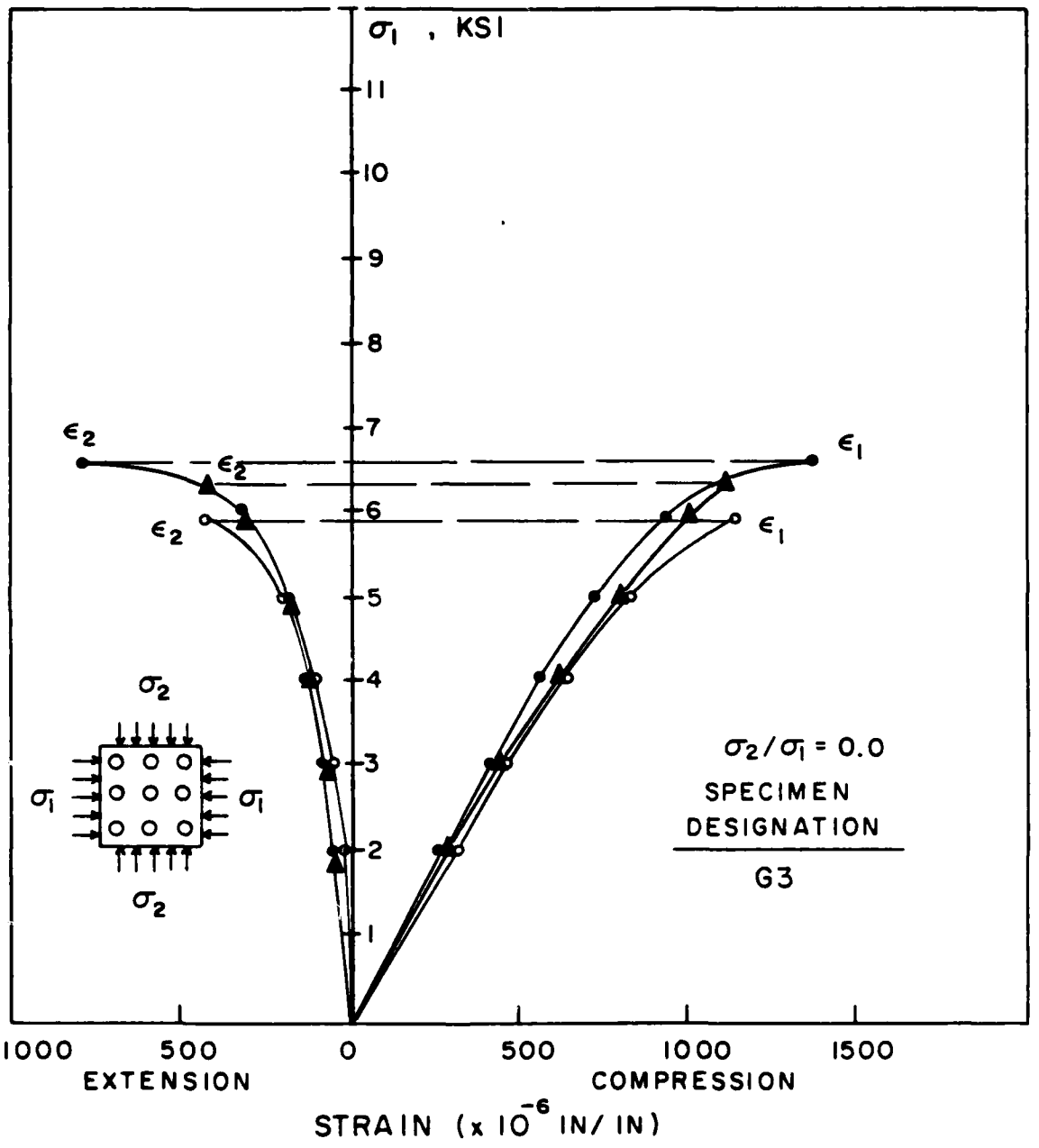

Figure B.21 Stress-Strain Curves for Model Specimens G3 with a Stress Ratio of 0.0 (Uniaxial)

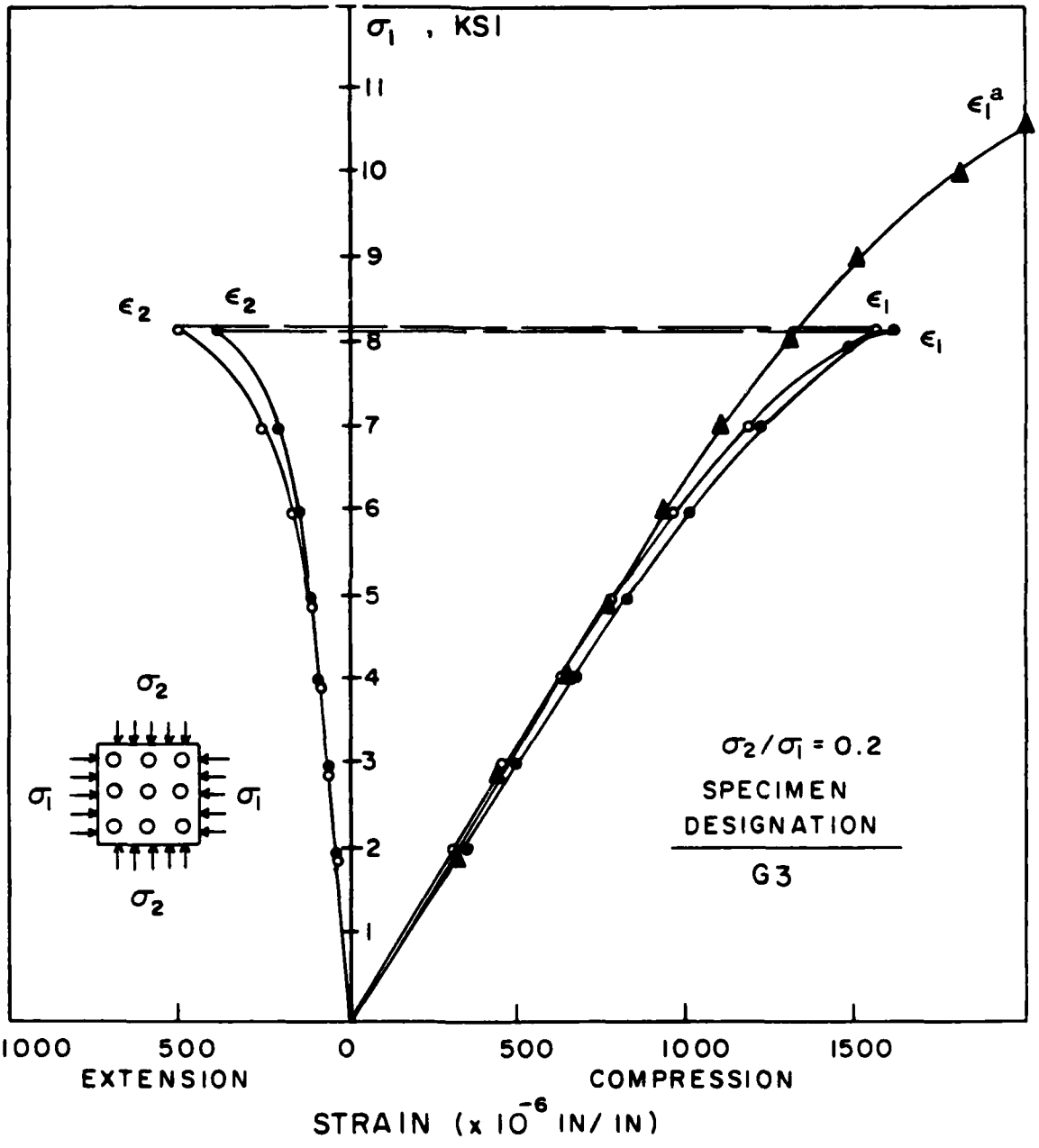

Figure B.22 Stress-Strain Curves for Model Specimens G3 with a Stress Ratio of 0.2

[a] ε_2 curve not obtained for this specimen

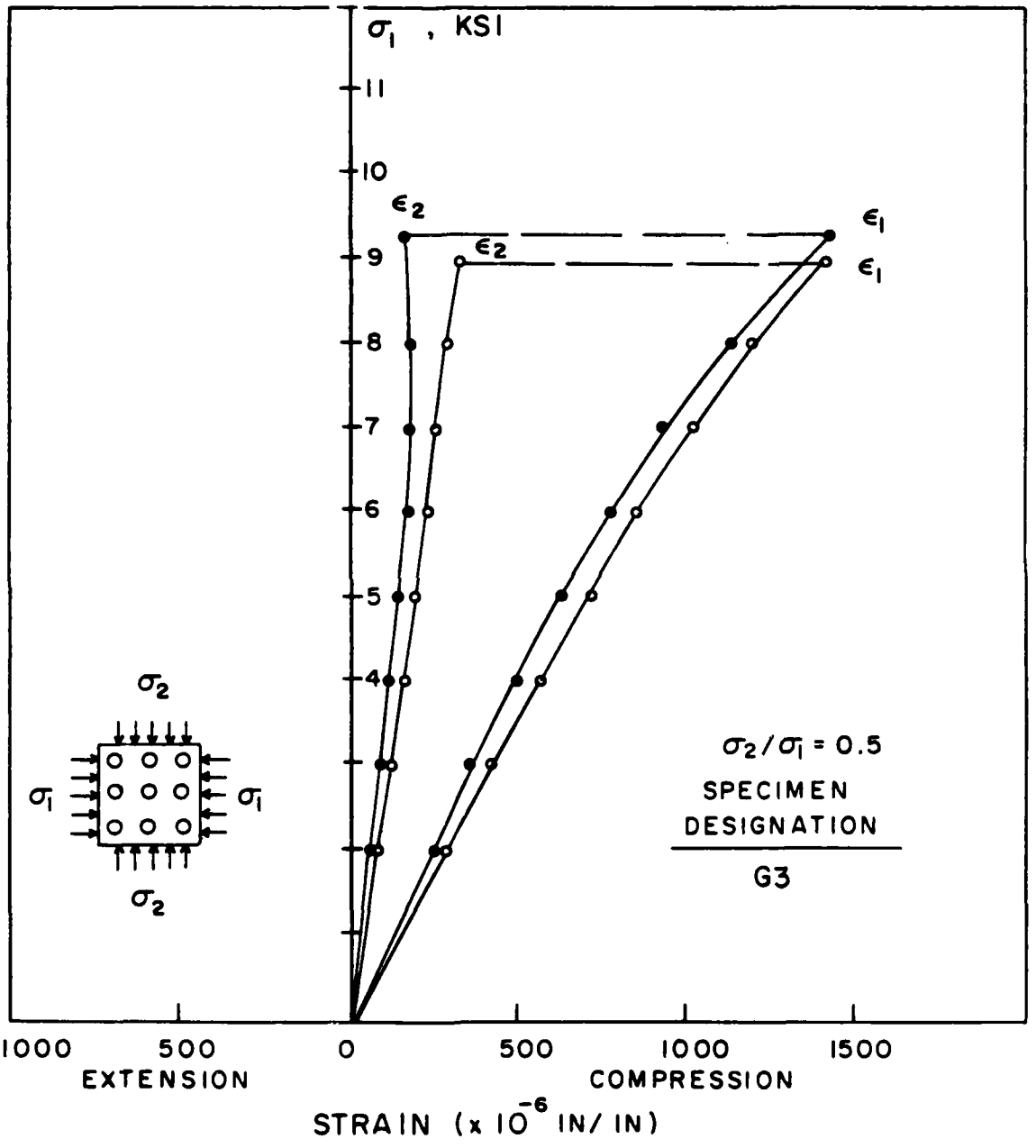

Figure B.23 Stress-Strain Curves for Model Specimens G3 with a Stress Ratio of 0.5

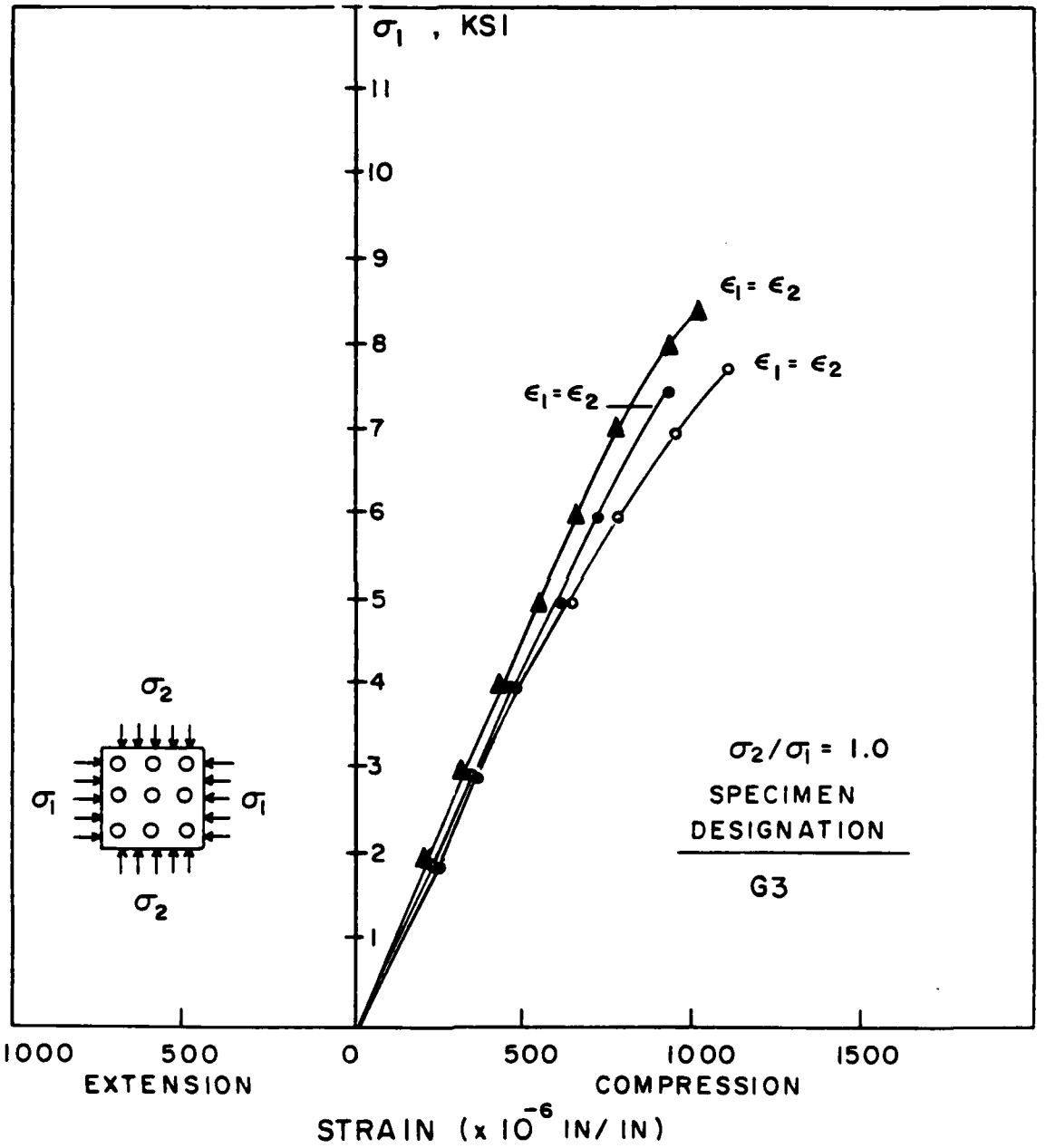

Figure B.24 Stress-Strain Curves for Model Specimens G3 with a Stress Ratio of 1.0

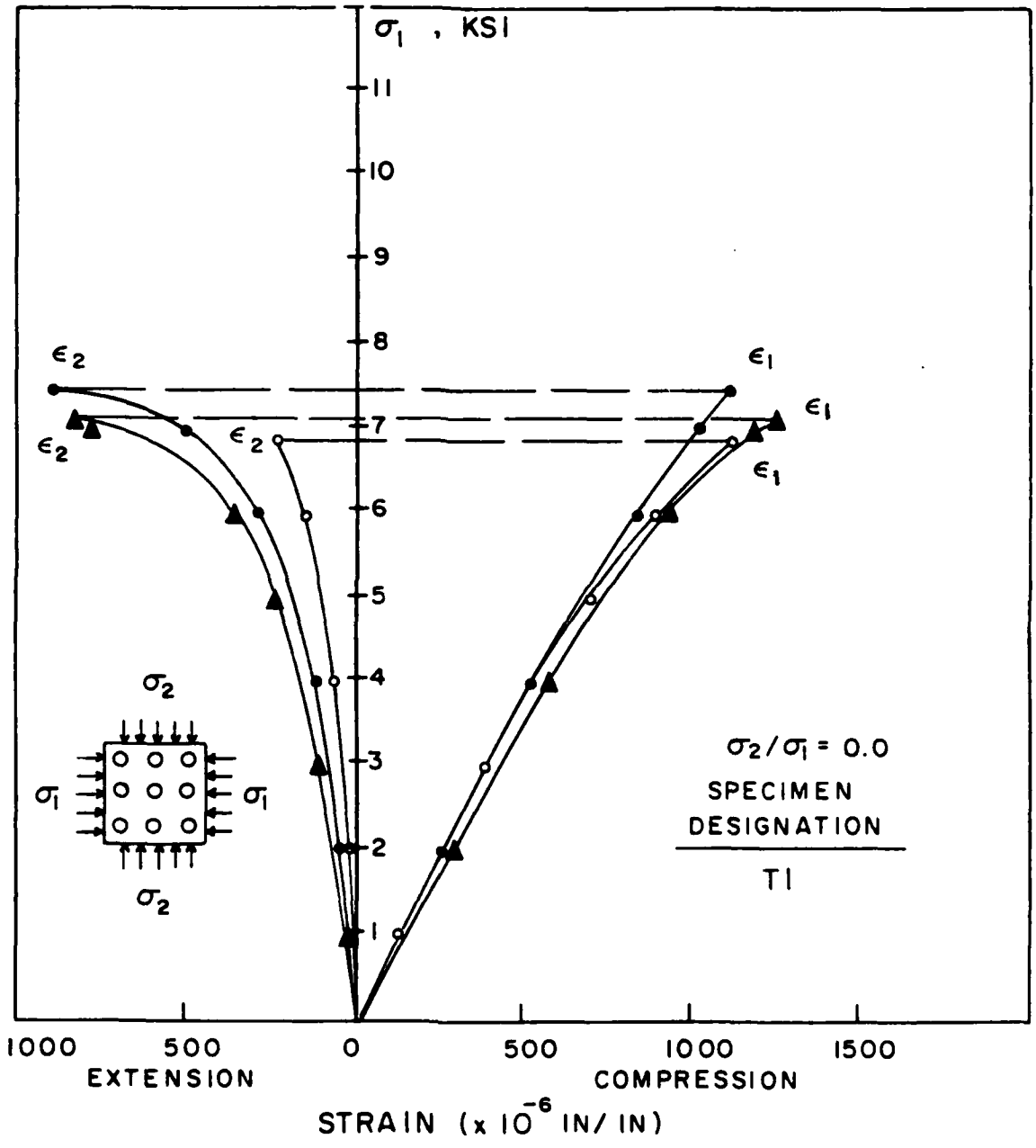

Figure B.25 Stress-Strain Curves for Model Specimens T1 with a Stress Ratio of 0.0 (Uniaxial)

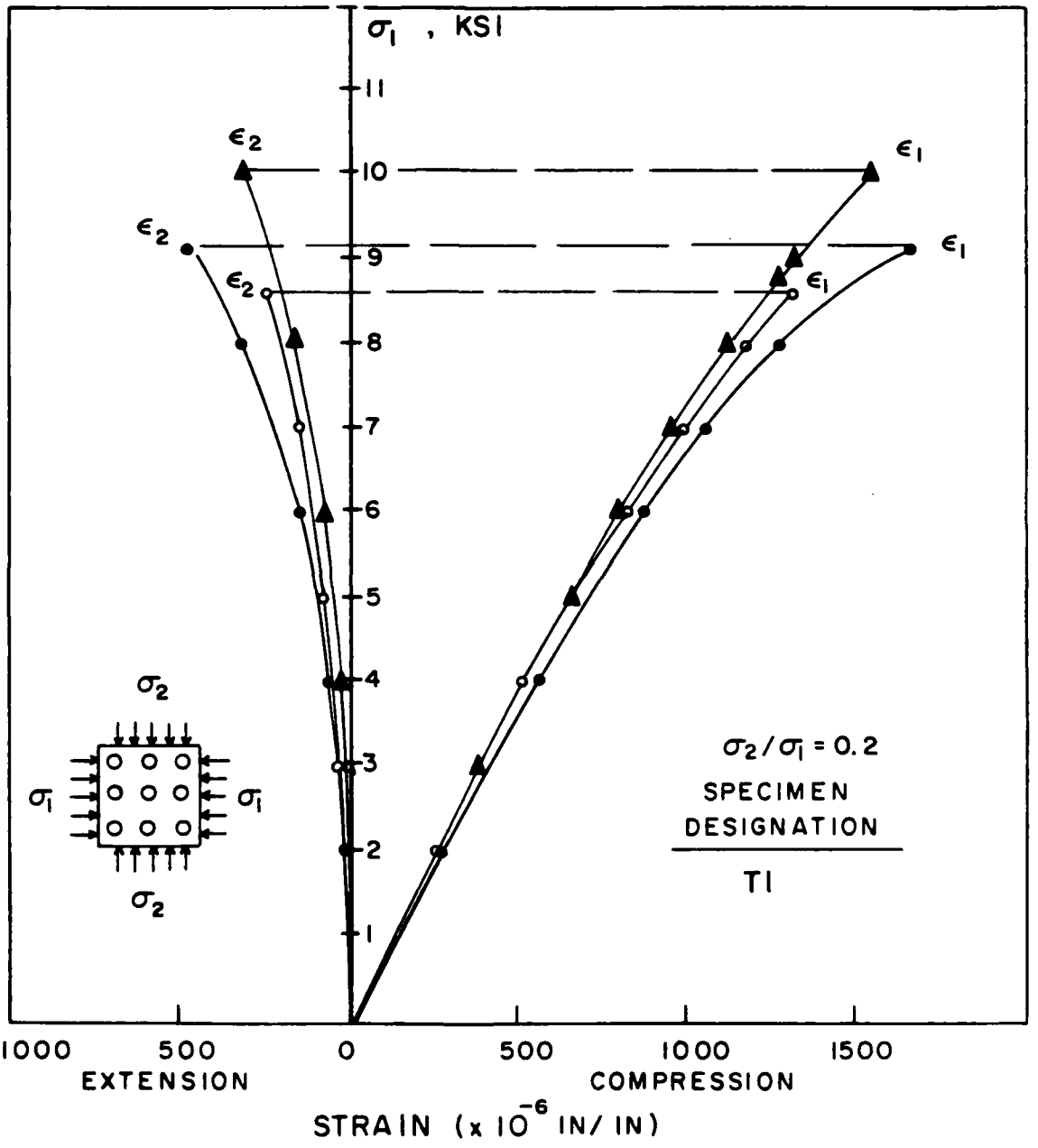

Figure B.26 Stress-Strain Curves for Model Specimens T1 with a Stress Ratio of 0.2

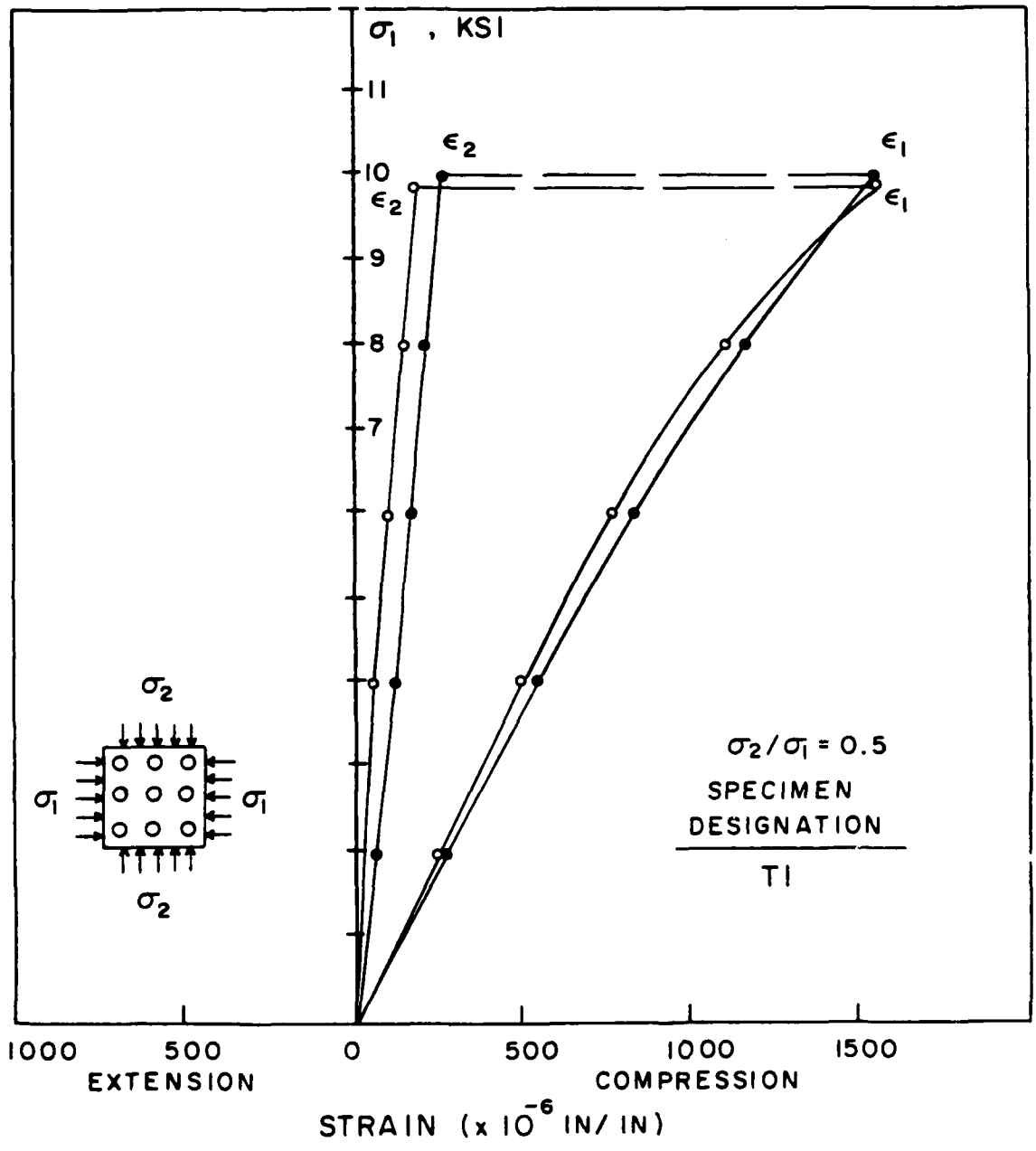

Figure B.27 Stress-Strain Curves for Model Specimens T1 with a Stress Ratio of 0.5

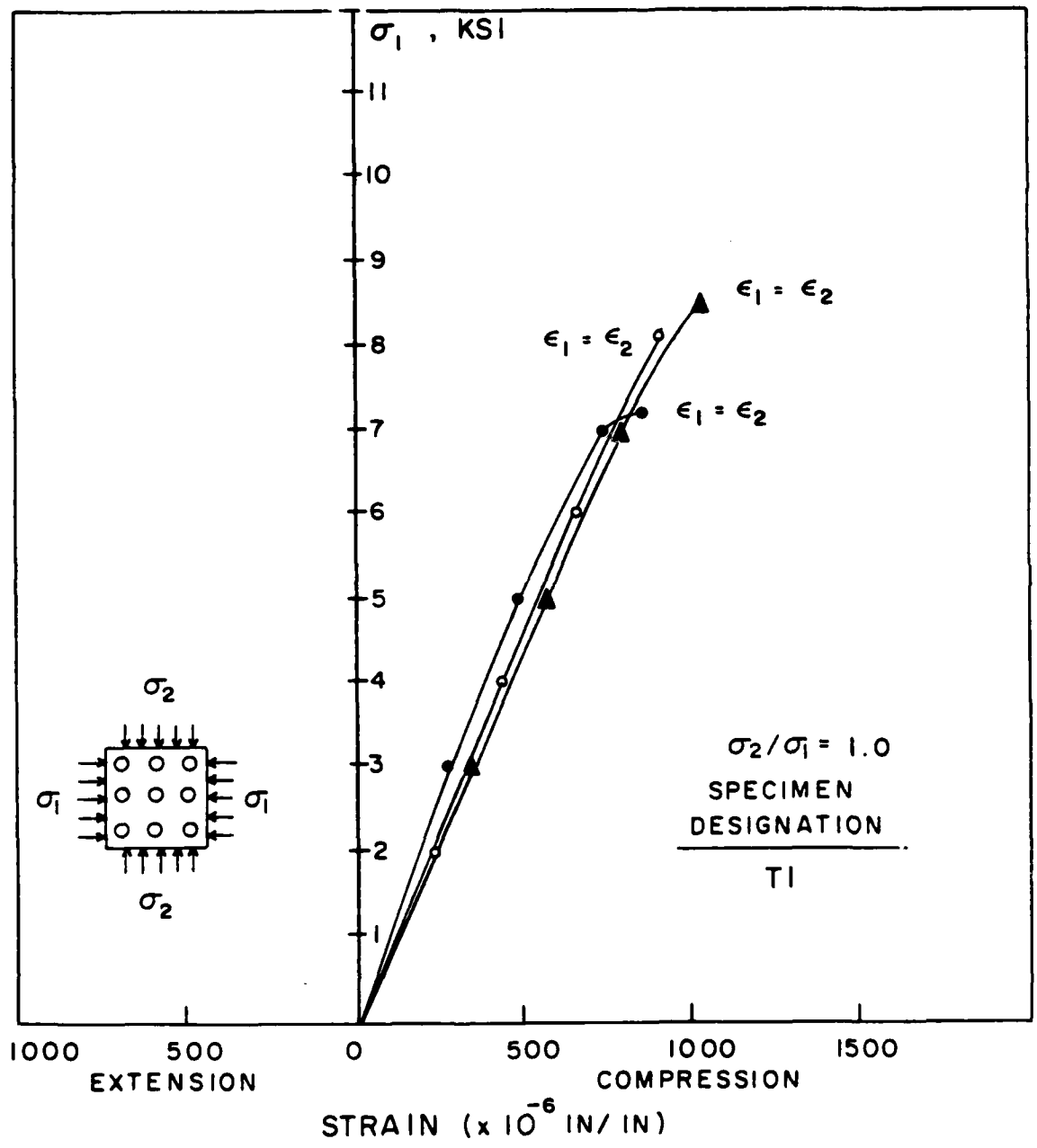

Figure B.28 Stress-Strain Curves for Model Specimens T1 with a Stress Ratio of 1.0

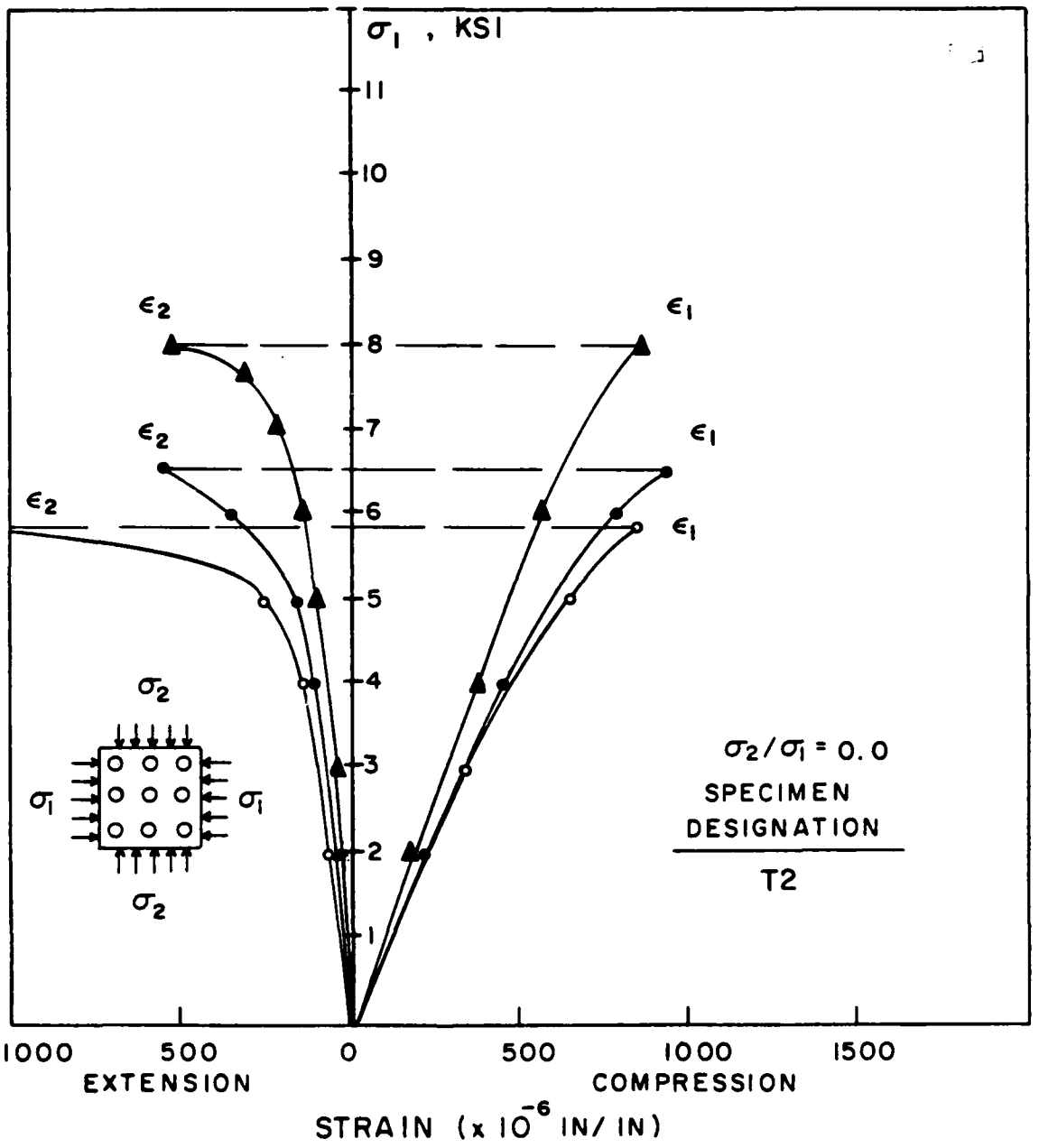

Figure B.29 Stress-Strain Curves for Model Specimens T2 with a Stress Ratio of 0.0 (Uniaxial)

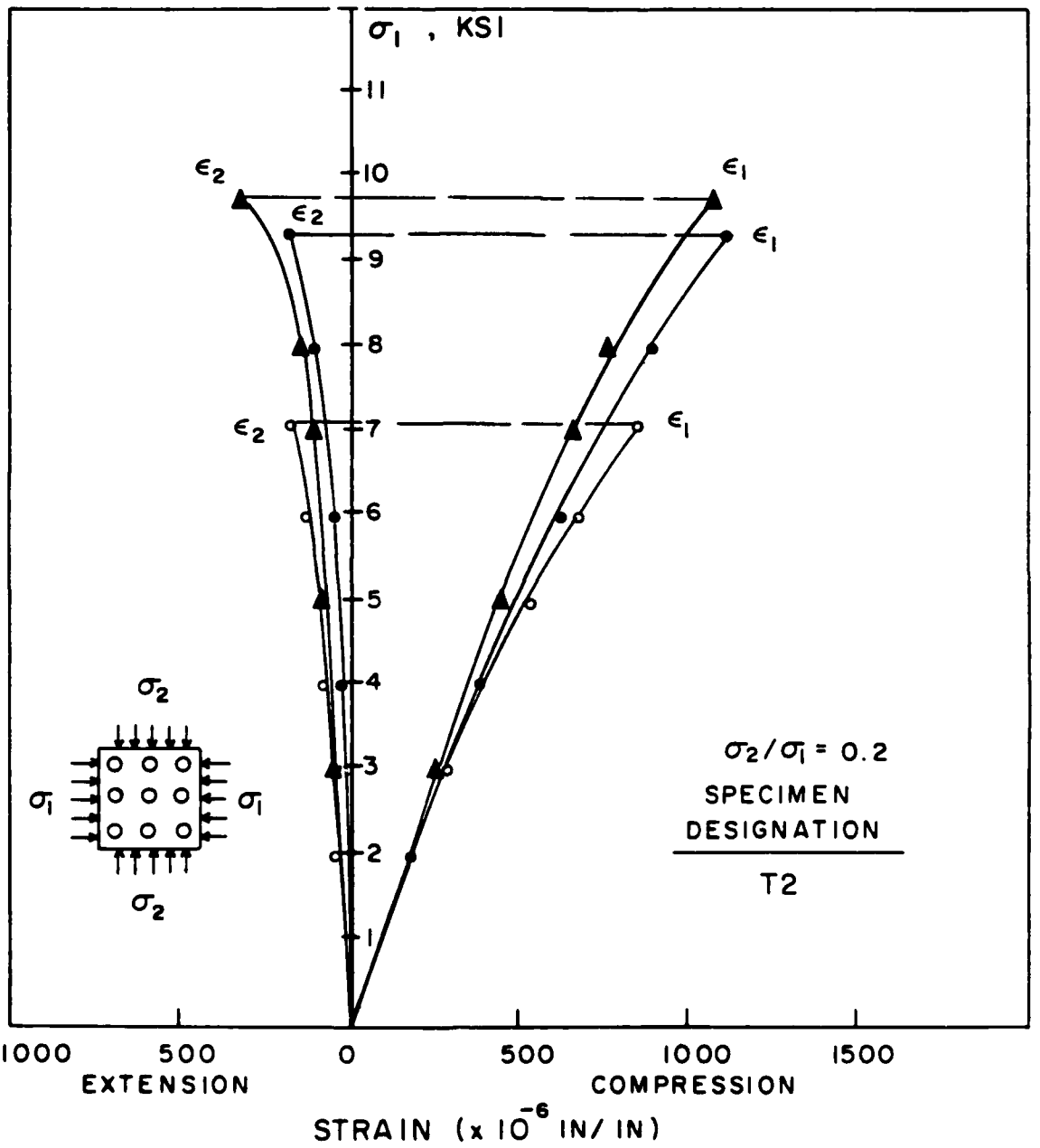

Figure B.30 Stress-Strain Curves for Model Specimens T2 with a Stress Ratio of 0.2

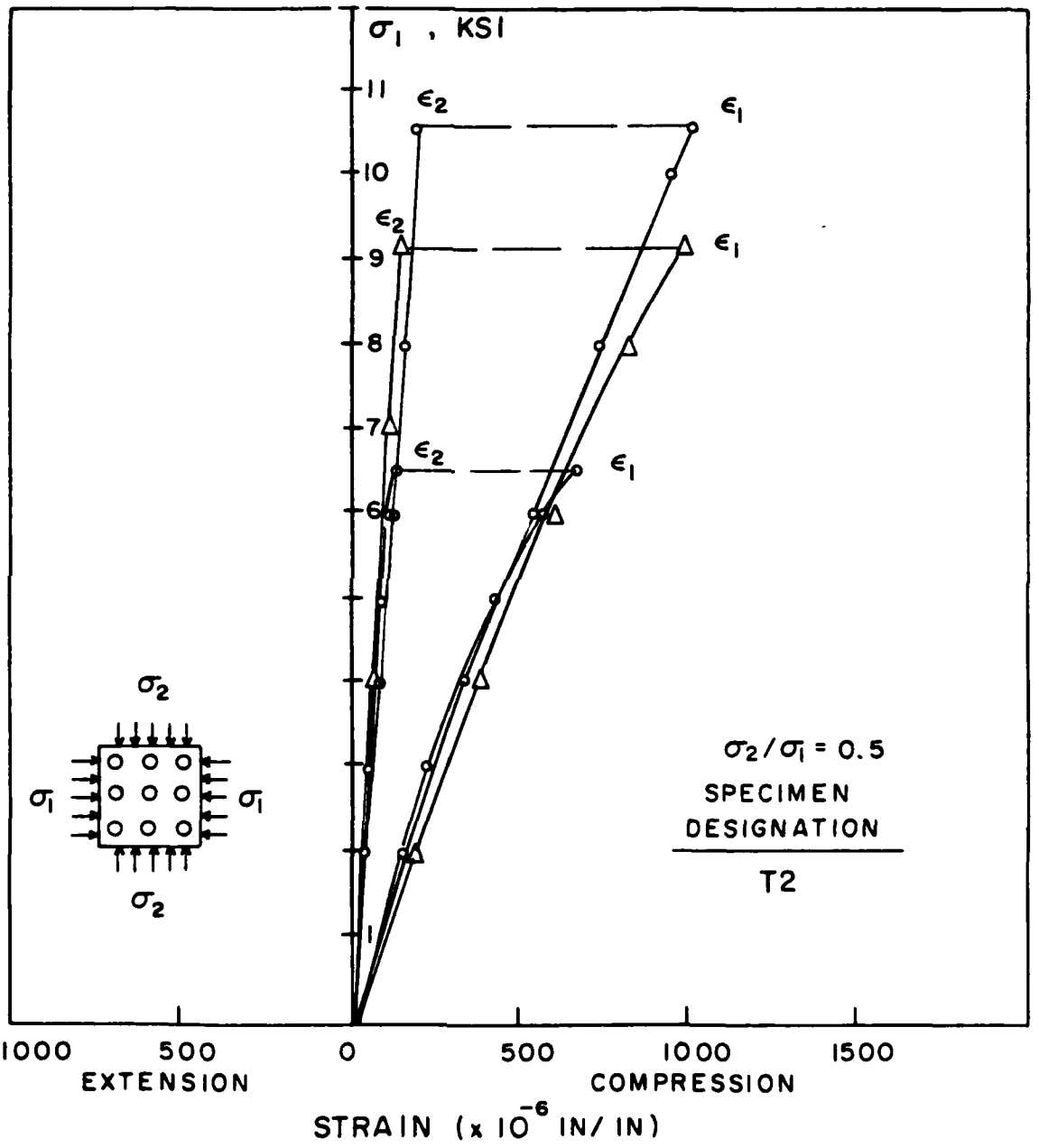

Figure B.31 Stress-Strain Curves for Model Specimens T2 with a Stress Ratio of 0.5

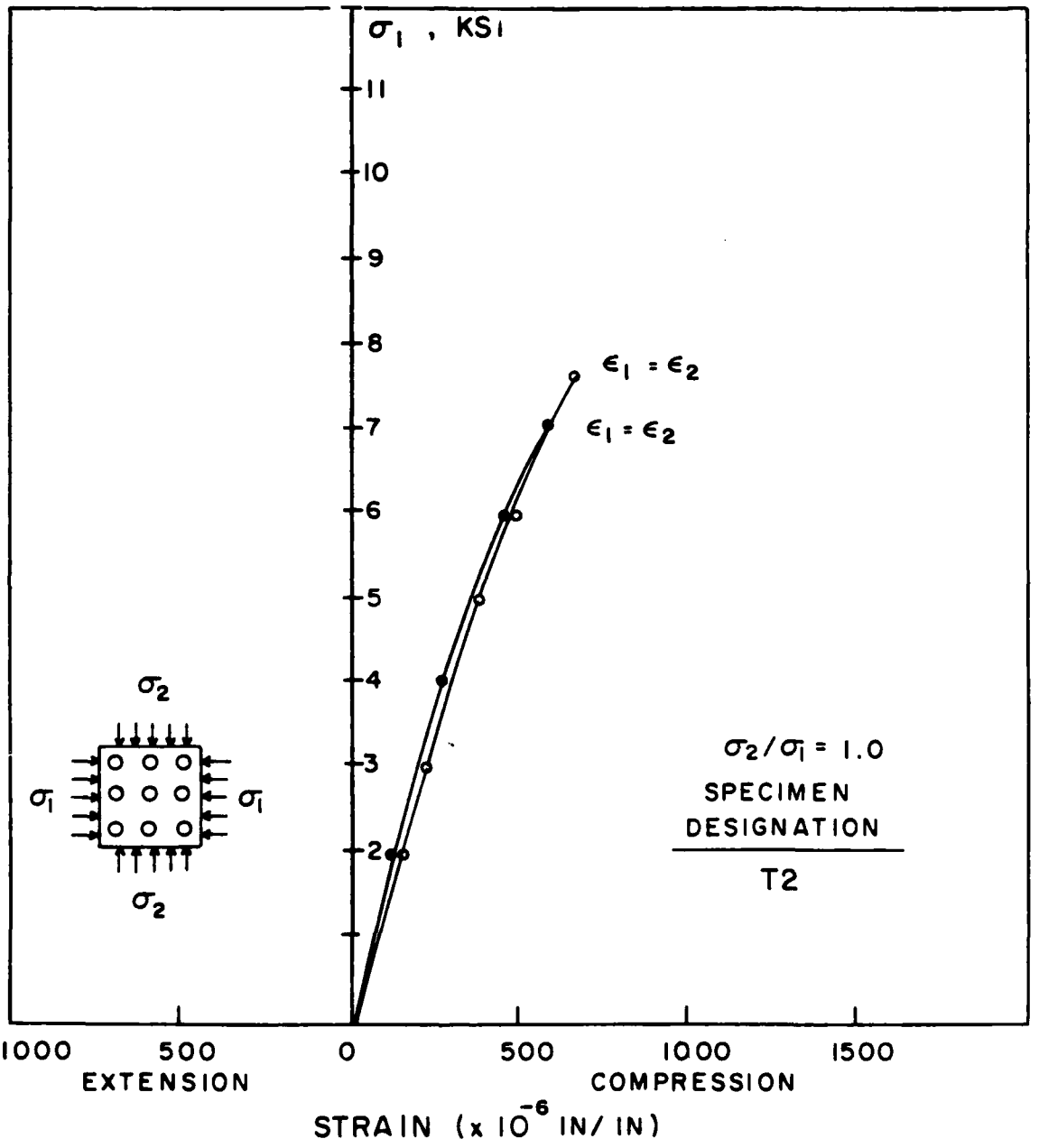

Figure B.32 Stress-Strain Curves for Model Specimens T2 with a Stress Ratio of 1.0

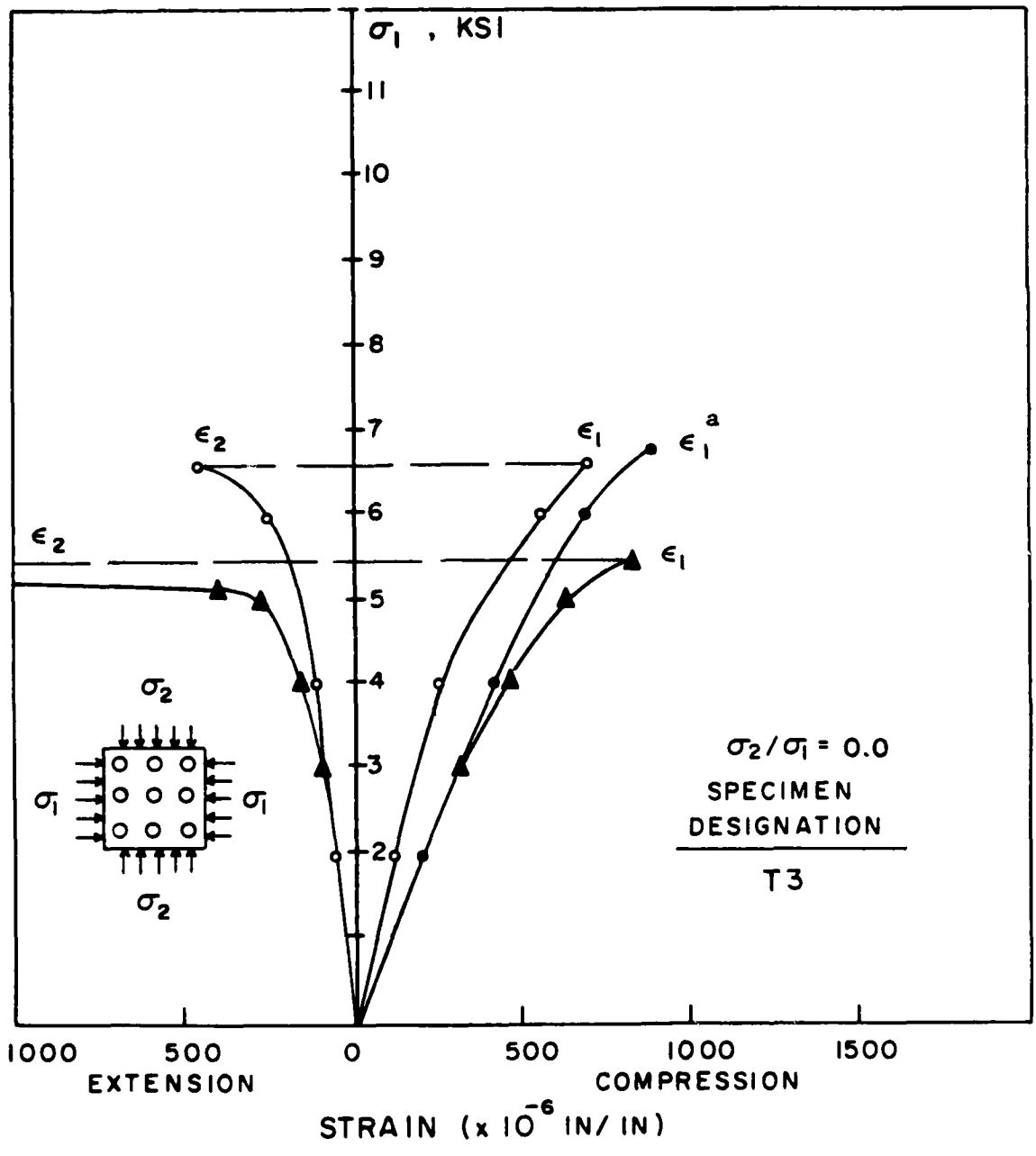

Figure B.33 Stress-Strain Curves for Model Specimens T3 with a Stress Ratio of 0.0 (Uniaxial)

[a] ε_2 curve not obtained for this specimen

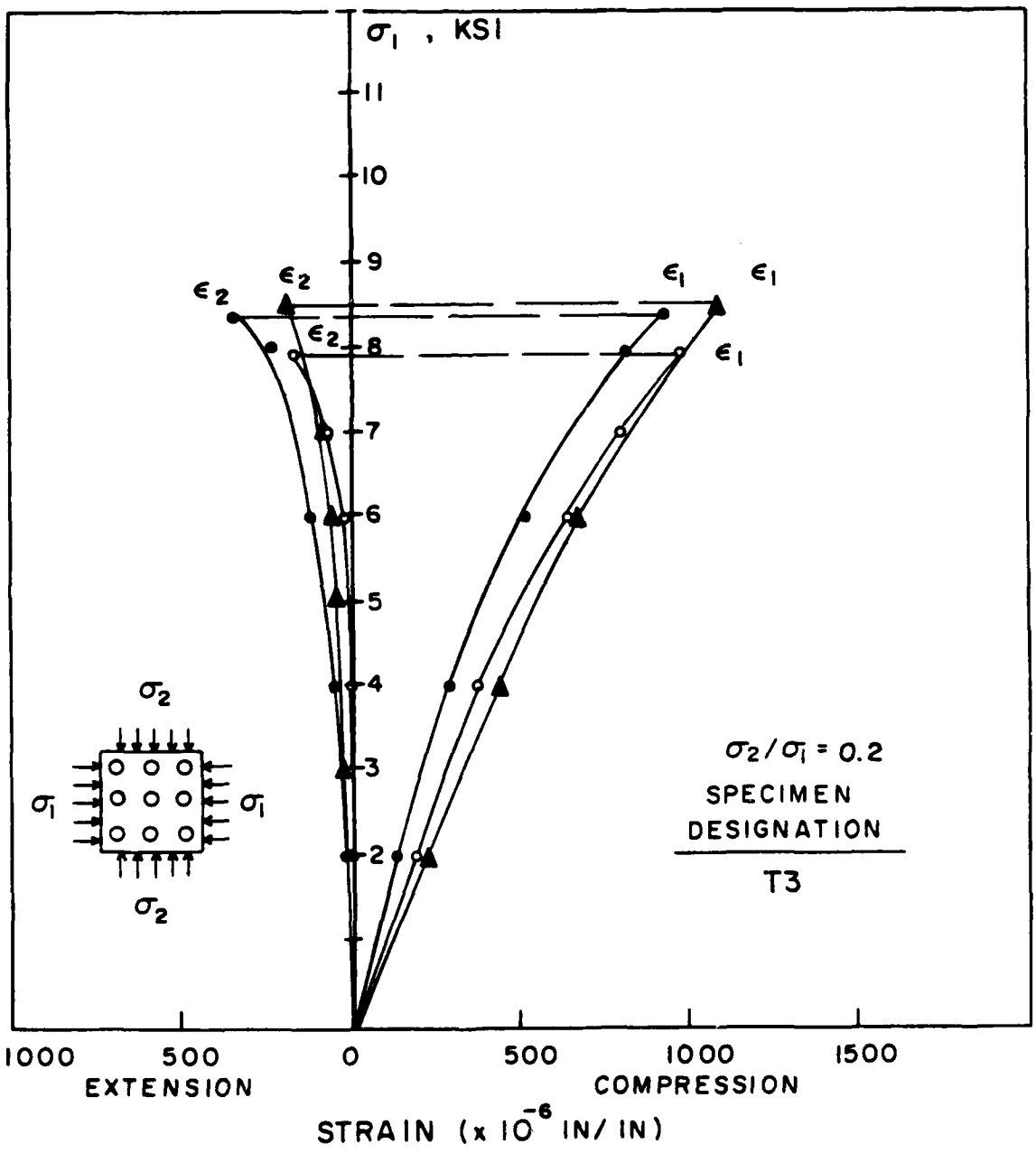

Figure B.34 Stress-Strain Curves for Model Specimens T3 with a Stress Ratio of 0.2

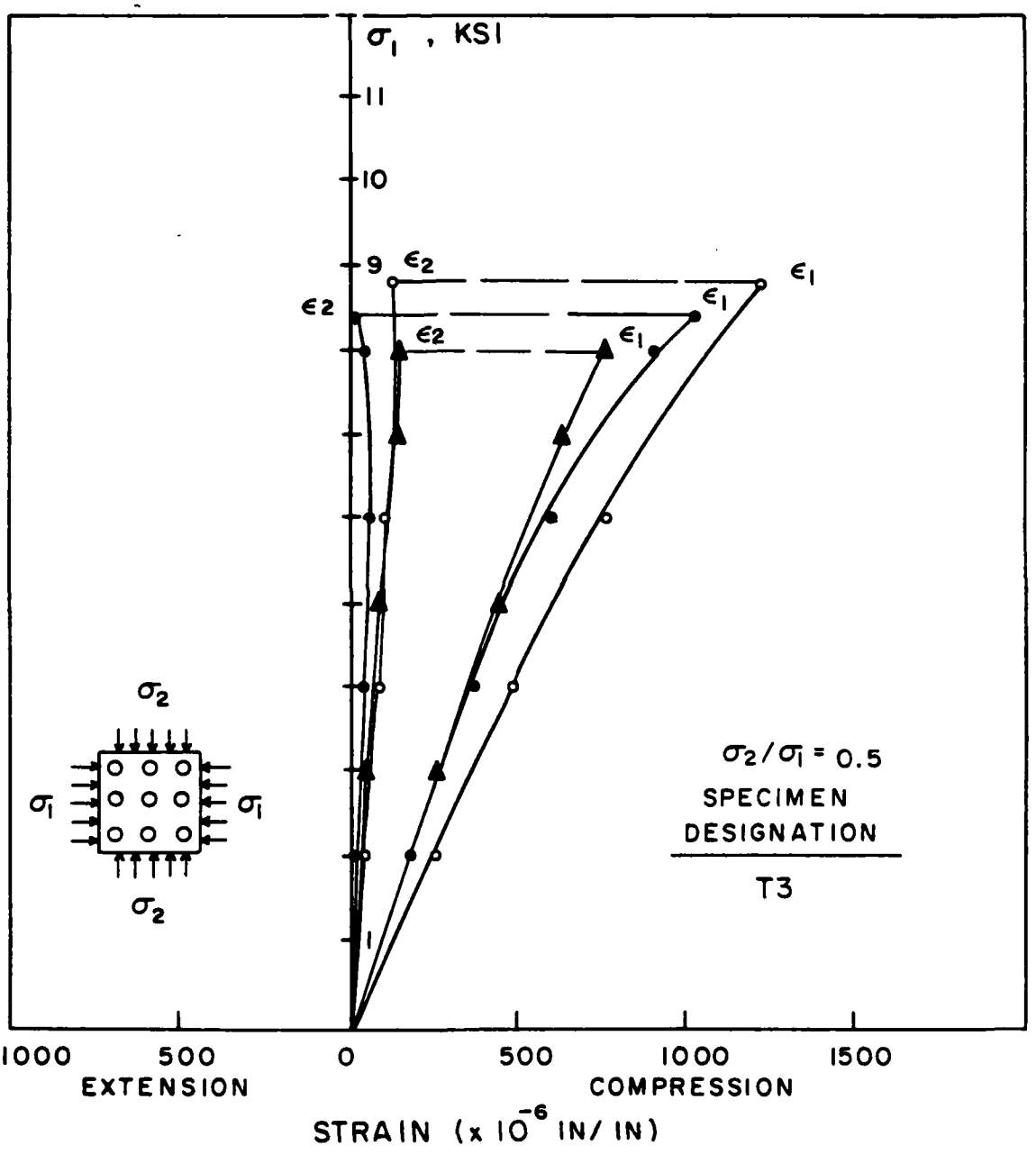

Figure B.35 Stress-Strain Curves for Model Specimens T3 with a Stress Ratio of 0.5

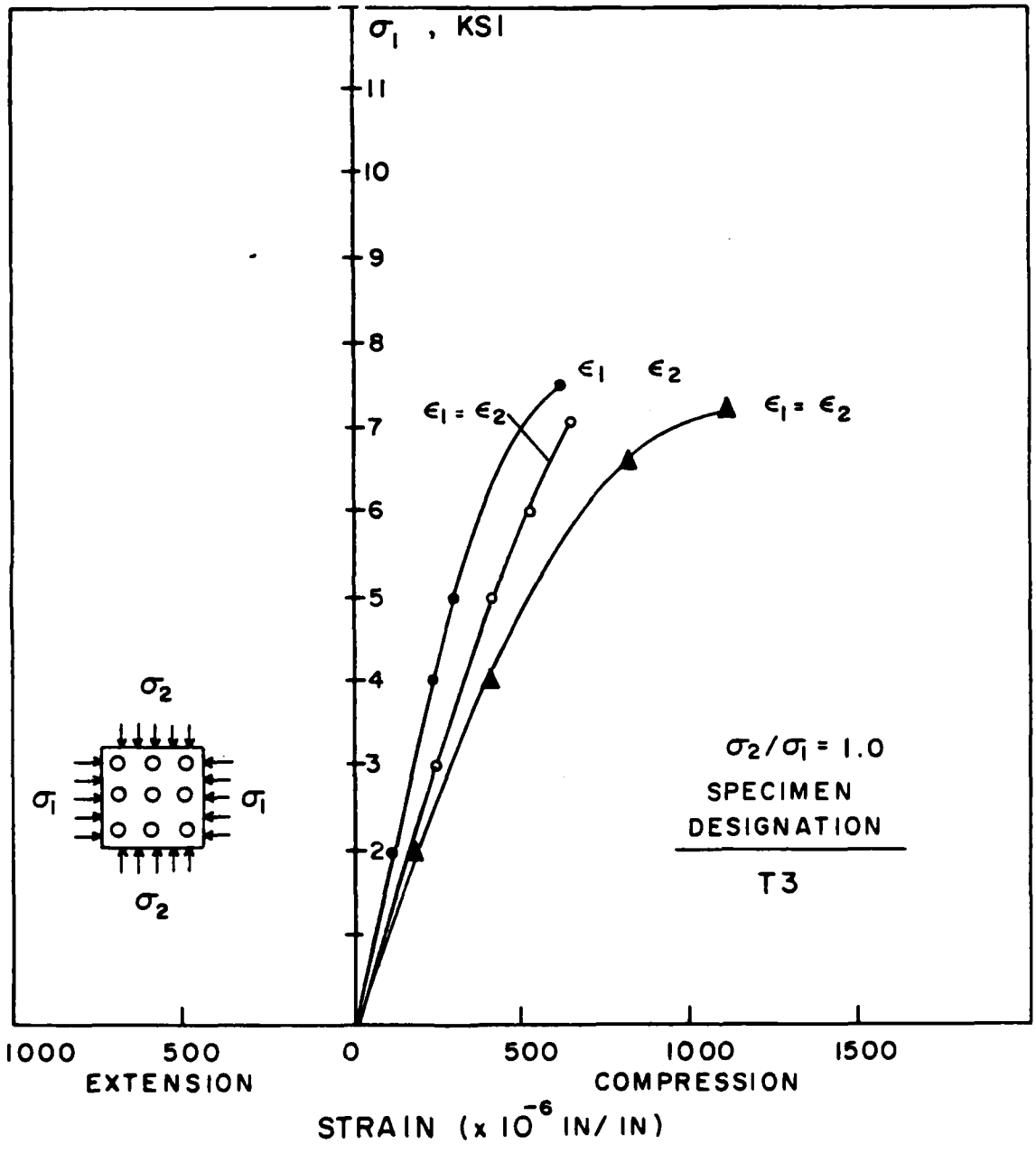

Figure B.36 Stress-Strain Curves for Model Specimens T3 with a Stress Ratio of 1.0

BIBLIOGRAPHY

BIBLIOGRAPHY

1. Karman, Th. V., "Festigkeitsversuche Unter Allseitigem Druck," Zeitschrift des Vereins Deutscher Ingenievre, Berun, No. 42, 1911.

2. Boker, R., "Die Mechanik der Bleibenden Formanderungen in Kristallinisch Aufgebauten Korpern," Mitteilungen Uber Forschungsarbeiten, Berlin, No. 175-176, 1915.

3. Richart, F.E., Brandtzaeg, A., and Brown, R.L., "A Study of the Failure of Concrete Under Combined Compressive Stresses," University of Illinois Engineering Experiment Station, Bulletin No. 185, November 1928.

4. Fumagalli, E., "Strength of Concrete Under Biaxial Compression," ACI Journal, Proceedings, Vol. 62, No. 2, February 1965, pp. 1187-1188.

5. Smith, F.C., and Brown, R.Q., "The Shearing Strength of Cement Mortar," University of Washington Engineering Experiment Station, Bulletin No. 106, February 1941.

6. Balmer, G.G., "Shearing Strength of Concrete Under High Triaxial Stress," U.S. Bureau of Reclamation, Structural Research Lab. Report SP-23, October 1949, pp. 1-26.

7. Akroyd, T.N.W., "Concrete Under Triaxial Stress," Magazine of Concrete Research, Vol. 13, No. 39, November 1961, pp. 111-118.

8. Cordon, W.A., and Gillespie, A.J., "Variables in Concrete Aggregates and Portland Cement Paste Which Influence the Strength of Concrete," ACI Journal, Proceedings, Vol. 60, No. 8, August 1968, pp. 1029-1052.

9. Hanson, J.A., "Strength of Structural Lightweight Concrete Under Combined Stress," PCA Journal, Research and Development Lab., Vol. 5, No. 1, January 1963, pp. 39-46.

10. Chinu, J., and Zimmerman, R.M., "Behavior of Plain Concrete Under Various High Triaxial Compression Loading Conditions," U.S. Air Force Weapons Lab. Report, WL-TR64-163, August 1965.

11. McCreath, D.R., Newman, J.B., and Newman, K., "The Influence of Aggregate Particles on tbe Local Strain Distribution and Fracture Mechanism of Cement Paste During Shrinkage and Loading to Failure," RILEM Bulletin, Vol. 2, No. 7, January-February 1969, pp. 73-84.

12. Palaniswamy, R., and Shah, S.P., "Fracture and Stress-Strain Relationship of Concrete Under Triaxial Compression," Journal of the Structural Division, Proceedings of the ASCE, Vol. 100, No. STS, May 1974, pp. 901-916.

13. Bellamy, C.J., "Strength of Concrete Under Combined Stress," ACI Journal, Proceedings, Vol. 58, No. 4, October 1961, pp. 367-381.

14. Campbell-Allen, D., "Strength of Concrete Under Combined Stresses," Construction Review, Vol. 35, No. 4, April 1962, pp. 29-37.

15. Rosenthal, I., and Glucklich, J., "Strength of Plain Concrete Under Biaxial Stress," ACI Journal, Proceedings, Vol. 67, No. 11, November 1970, pp. 903-913.

16. Foppl, A., "Mitteilungen Aus Dem Mechanisch-Technischen Lab.," Technischen Hockschule, Munchen, No. 27, 1900.

17. Mills, L.L., and Zimmerman, R.M., "Compressive Strength of Plain Concrete Under Multiaxial Loading Conditions," ACI Journal, Proceedings, Vol. 67, No. 10, October 1970, pp. 802-807.

18. Weigler, H., and Becker, G., "Untersuchungen Uber Das Bruch-Und Verformungsverhalten von Beton B21 Zweiachsiger Beanspruchung," Deutscher Ausschuss fur Stahlbeton, Berlin, Heft 157, 1963, pp. 1-66.

19. Robinson, G.S., "Behavior of Concrete in Biaxial Compression," Journal of the Structural Division, Proceedings of the ASCE, Vol. 93, No. ST1, February 1967, pp. 71-86.

20. Sundara Raja Iyengar, K.T., Chandrashekhara, K., and Krishnaswamy, K.T., "Strength of Concrete Under Biaxial Compression," ACI Journal, Proceedings, Vol. 62, No. 2, February 1965, pp. 239-250.

21. Hilsdorf, H.K., "Die Bestimmung Der Zweiachsigen Festigkeit von Beton," Deutscher Ausschuss fur Stahlbeton, Heft 173, Berlin, 1965.

22. Kupfer, H., Hilsdorf, H.K., and Rusch, H., "Behavior of Concrete Under Biaxial Stresses," ACI Journal, Proceedings, Vol. 66, No. 8, August 1969, pp. 656-666.

23. Buyukozturk, O., Nilsen, A.H., and Slate, F.O., "Stress-Strain Response and Fracture of a Concrete Model in Biaxial Loading," ACI Journal, Proceedings, Vol. 68, No. 8, August 1971, pp. 590-599.

24. Liu, T.C.Y., Nilsen, A.H., and Slate, F.O., "Stress-Strain Response and Fracture of Concrete in Uniaxial and Biaxial Compression," ACI Journal, Proceedings, Vol. 69, Vo. 5, May 1972, pp. 291-295.

25. Tasuji, M.E., Slate, F.O., and Nilsen, A.H., "Stress-Strain Response and Fracture of Concrete in Biaxial Loading," ACI Journal, Proceedings, Vol. 75, No. 7, July 1978, pp. 306-312.

26. Atan, Y., and Slate, F.O., "Structural Lightweight Concrete Under Biaxial Compression," ACI Journal, Proceedings, Vol. 70, No. 5, March 1973, pp. 182-186.

27. Taylor, M.A., Jain, A.K., and Ramey, M.R., "Path Dependent Biaxial Compressive Testing of an All-Lightweight Aggregate Concrete," ACI Journal, Proceedings, Vol. 69, No. 12, December 1972, pp. 758-764.

28. Khana, S., "Stress-Strain Characteristics and Failure Mechanisms of Polymer Impregnated Concrete," M.S. Thesis, The University of Texas at Austin, 1981.

29. Park, S., "Stress-Strain Response of Polymer Impregnated Concrete Under Biaxial Compressive Loading," M.S. Thesis, The University of Texas at Austin, 1982.

30. Carino, N.J., and Slate, F.O., "Limiting Tensile Strain Criterion for Failure of Concrete," ACI Journal, Proceedings, Vol. 73, No. 15, March 1976, pp. 160-165.

31. Kupfer, H.B., and Gerstle, K.N., "Behavior of Concrete Under Biaxial Stresses," Journal of the Engineering Mechanics Div., Proceedings of the ASCE, Vol. 99, No. EM4, August 1973, pp. 853-866.

32. Foster, Robert J., Geology, Columbus, Ohio, Charles E. Merrill Publishing Company, 1976.

33. Materials Task Force, "High-Strength Concrete in Chicago High-Rise Buildings," Task Force Report No. 5, Chicago Committee on High-Rise Buildings, February 1977, p. 63.

34. Newman, K., "Criteria for the Behavior of Plain Concrete Under Complex States of Stress," Proceedings, International Conference on the Structure of Concrete (London, September 1965), Cement and Concrete Association, London, 1968, pp. 255-274.

35. Carrasquillo, R.L., Slate, F.O., and Nilsen, A.H., "Microcracking and Behavior of High Strength Concrete Subject to Short-Term Loading," ACI Journal, Proceedings, Vol. 78, No. 3, May-June 1981, pp. 179-186.

36. Carrasquillo, R.L., Nilsen, A.H., and Slate, F.O., "Microcracking and Engineering Properties of High-Strength Concrete," Research Report No. 80-1, Department of Structural Engineering, Cornell University, Ithaca, February 1980, p. 254.

37. Parrot, L.J., "The Selection of Constituents and Proportions for Producing Workable Concrete with a Compressive Cube Strength of 80 to 110 N/MM^2 (11,600 to 15,900 psi)," Technical Report No. 416, Cement and Concrete Association, May 1969, p. 12.

38. Taylor, M.A., and Patel, B.K., "The Influence of Path Dependency and Moisture Conditions on the Biaxial Compression Envelope for Normal Weight Concrete," ACI Journal, Proceedings, December 1974, pp. 627-633.

39. Gerstle, K.H., "Simple Formulation of Biaxial Concrete Behavior," ACI Journal, Proceedings, Vol. 78, No. 5, January-February 1981, pp. 62-28.

40. Santiago, S.D., and Hilsdorf, H.K., "Fracture Mechanisms of Concrete Under Compressive Loads," Cement and Concrete Research, Vol. 3, 1973, pp. 363-388.

41. Andenaes, E., Gerstle, K.H., and Ko, H.K., "Response of Mortar and Concrete to Biaxial Compression," Journal of the Engineering Mechanics Division, Proceedings of the ASCE, No. EM4, August 1977, pp. 515-525.

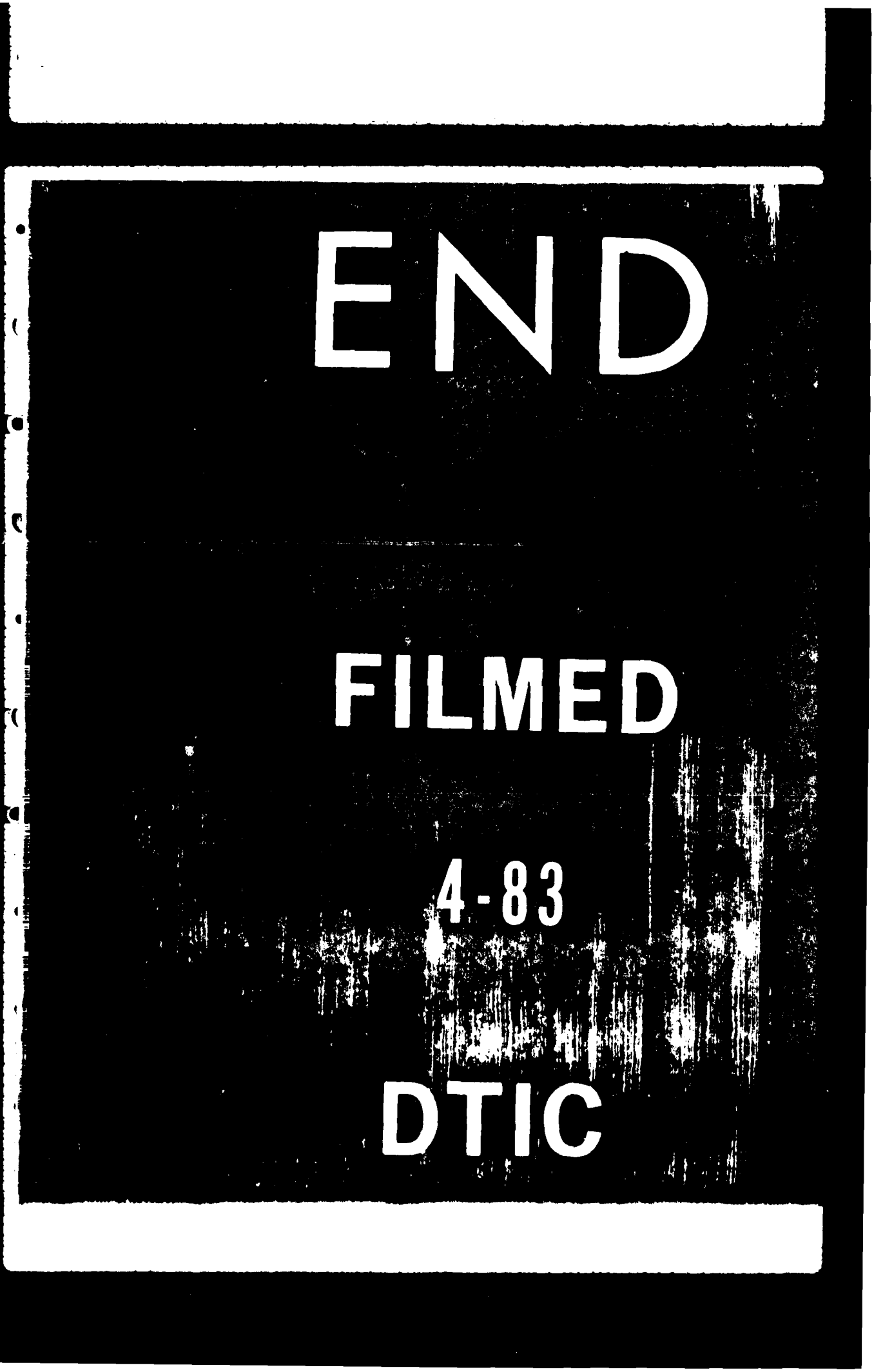
END
FILMED
4-83
DTIC